**CAPITAL UNIVERSITY OF SCIENCE AND
TECHNOLOGY, ISLAMABAD**

High Gain Antennas for Millimeter-wave 5G Applications

by

Muhammad Usman Tahir

A dissertation submitted in partial fulfillment for the
degree of Doctor of Philosophy

in the

Faculty of Engineering
Department of Electrical Engineering

2024

High Gain Antennas for Millimeter-wave 5G Applications

By

Muhammad Usman Tahir

(DEE151001)

Dr. Debabrata Karmokar, Lecturer/Program Director

University of South Australia, Australia

(Foreign Evaluator 1)

Dr. Peiyuan Qin, Associate Professor

University of Technology, Sydney, Australia

(Foreign Evaluator 2)

Dr. Muhammad Mansoor Ahmed

(Research Supervisor)

Dr. Noor Muhammad Khan

(Head, Department of Electrical Engineering)

Dr. Imtiaz Ahmad Taj

(Dean, Faculty of Engineering)

DEPARTMENT OF ELECTRICAL ENGINEERING

CAPITAL UNIVERSITY OF SCIENCE AND TECHNOLOGY

ISLAMABAD

2024

Dedicated to my family

CERTIFICATE OF APPROVAL

This is to certify that the research work presented in the dissertation, entitled "**High Gain Antennas for Millimeter-wave 5G Applications**" was conducted under the supervision of **Dr. Muhammad Mansoor Ahmed**. No part of this dissertation has been submitted anywhere else for any other degree. This dissertation is submitted to the **Department of Electrical Engineering, Capital University of Science and Technology** in partial fulfillment of the requirements for the degree of Doctor in Philosophy in the field of **Electrical Engineering**. The open defence of the dissertation was conducted on **November 22, 2023**.

Student Name :   Muhammad Usman Tahir
                       (DEE151001)

The Examination Committee unanimously agrees to award PhD degree in the mentioned field.

Examination Committee :

(a)	External Examiner 1:	Dr. Muhammad Farhan Shafique Professor COMSATS University, Islamabad
(b)	External Examiner 2:	Dr. Aamir Rashid Assistant Professor UET Taxila
(c)	Internal Examiner :	Dr. Noor Muhammad Khan Professor CUST, Islamabad

Supervisor Name :   Dr. Muhammad Mansoor Ahmed
                          Professor
                          CUST, Islamabad

Name of HoD :   Dr. Noor Muhammad Khan
                      Professor
                      CUST, Islamabad

Name of Dean :   Dr. Imtiaz Ahmad Taj
                       Professor
                       CUST, Islamabad

AUTHOR'S DECLARATION

I, **Muhammad Usman Tahir (Registration No. DEE151001)**, hereby state that my dissertation titled, **"High Gain Antennas for Millimeter-wave 5G Applications"** is my own work and has not been submitted previously by me for taking any degree from Capital University of Science and Technology, Islamabad or anywhere else in the country/ world.

At any time, if my statement is found to be incorrect even after my graduation, the University has the right to withdraw my PhD Degree.

22/11/2023

(Muhammad Usman Tahir)

Dated: 22 November, 2023

Registration No : DEE151001

PLAGIARISM UNDERTAKING

I solemnly declare that research work presented in the dissertation titled **"High Gain Antennas for Millimeter-wave 5G Applications"** is solely my research work with no significant contribution from any other person. Small contribution/ help wherever taken has been duly acknowledged and that complete dissertation has been written by me.

I understand the zero-tolerance policy of the HEC and Capital University of Science and Technology towards plagiarism. Therefore, I as an author of the above titled dissertation declare that no portion of my dissertation has been plagiarized and any material used as reference is properly referred/ cited.

I undertake that if I am found guilty of any formal plagiarism in the above titled dissertation even after award of PhD Degree, the University reserves the right to withdraw/ revoke my PhD degree and that HEC and the University have the right to publish my name on the HEC/ University Website on which names of students are placed who submitted plagiarized dissertation.

(Muhammad Usman Tahir)

Dated: 22 November, 2023

Registration No : DEE151001

List of Publications

It is certified that following publication(s) have been made out of the research work that has been carried out for this dissertation:-

1. **M. U. Tahir**, U. Rafique, and M. M. Ahmed, "Rhombus inscribed circular ring fractal array antenna for millimeter-wave 5G applications," *International Journal of Antennas and Propagation*, vol. 2022, pp. 1–10, 2022.

2. **M. U. Tahir**, U. Rafique, M. M. Ahmed, M. Alibakhshikenari, F. Arpanaei, and B. S. Virdee, "Equilateral triangular slot-based planar rectangular antenna for millimeter-wave applications," *International Conference on Electromagnetics in Advanced Applications (ICEAA) and IEEE-APS Topical Conference on Antennas and Propagation in Wireless Communications*, pp. 1–4, IEEE, 2022.

3. **M. U. Tahir**, U. Rafique, M. M. Ahmed, S. M. Abbas, S. Iqbal and S. Wong, "High gain metasurface integrated millimeter-wave planar antenna," *International Journal of Microwave and Wireless Technologies*, vol. 2023, pp. 1-12, 2023.

4. **M. U. Tahir**, U. Rafique, M. M. Ahmed, P. Dalal, S. Agarwal and S. M. Abbas, "Semi-ring patch array antenna for high gain 28 GHz applications," *Wireless Antenna and Microwave Symposium (WAMS)*, pp. 1-4, 2023.

(Muhammad Usman Tahir)

Registration No: DEE151001

Acknowledgement

I humbly praise and grateful to **ALMIGHTY ALLAH**, Who permits me to live and accomplish tasks, including the research work presented in this dissertation.

I would like to express my gratitude to my advisor **Prof. Dr. M. Mansoor Ahmed**, Vice Chancellor, Capital University of Science and Technology (CUST), Islamabad, for his support, encouragement, and mentorship. I would like to thank him because of the opportunity he has given me to follow and fulfill my research interests. I am so grateful for what I have learned from his gracious personality. Thanks to **Mr. Umair Rafique**, Doctoral Researcher, Center of Wireless Communications, Faculty of ITEE, University of Oulu, Oulu, Finland, for his good ideas, for developing the content, and for support in research work.

I am thankful to the administration of CUST for providing me with an excellent environment perfect for conducting research. I am also thankful to Dean, Faculty of Engineering, **Prof. Dr. Imtiaz Ahmad Taj**, and Head of Department, **Prof. Dr. Noor M. Khan**.

I also wish to express my feelings of gratitude to my family, who prayed for my health and brilliant future. I would not have achieved these goals without their sincere co-operation and love. I am also using this opportunity to thank all my friends who prayed for me and encouraged me through their love and sincerity.

(Muhammad Usman Tahir)

Abstract

5G is the latest mobile communication regime it utilizes wide range of frequency bands while the millimeter wave (mm-wave) band is the area of interest. Whereas antenna is the fundamental component for communication, to communicate in the band of interest patch antennas are the strong contender. There are couple of challenging task while designing patch antennas or antenna array for 5G communication that needs to be considered like size, efficiency, bandwidth and gain. In this dissertation all these issues are addressed while designing the elemental antenna or antenna array.

In the first part of the dissertation, a rectangular antenna based on equilateral triangular slots is presented for wideband mm-wave 5G applications. The front-side of the proposed antenna is composed of a rectangular patch radiator with an equilateral triangular slot fed using a 50Ω microstrip feed line, while the bottom face of the antenna consists of a partial ground plane. The overall antenna dimensions are 6.5×8.5mm^2. The simulation results showed 16.86 GHz impedance bandwidth when measured at -10 dB, while at -15 dB it is 12.82 GHz for the frequencies ranging from $22.28 - 39.14$ GHz and $24.18 - 37$ GHz respectively. The gain of the proposed antenna fluctuates between $3.89 - 6.86$ dBi with an antenna efficiency $>85\%$.

In the second part, patch antenna arrays are designed for two frequency bands $25.35 - 27.87$ GHz and $27.5 - 29.25$ GHz. The front-sides of the proposed designs are composed of a 1×2 array of half-ring radiating elements. The rear of the first array consists of a full ground plane with a rectangular slot, while the second design uses a full ground plane. The first proposed patch array exhibited a gain of 8.75 dBi with an antenna efficiency $>85\%$, while the second patch array exhibited a maximum gain of 10.6 dBi with an antenna efficiency $>90\%$ in operating bandwidths.

In the third part of this research work, a 1×4 planar fractal array antenna is designed and presented. The top face of the array consists of a rhombus-inscribed

circular ring fractal patch radiator, while the back face consists of a square notch loaded partial ground plane. To achieve high gain, a 1×4 corporate feed network is used to excite the array elements. The designed array has an overall size of 28×17.75 mm². The designed array offers a wide impedance bandwidth in the frequency range of $22.8 - 29.2$ GHz. In addition, a maximum gain of 10.7 dBi with a radiation efficiency >95% is observed in the operating bandwidth.

In the fourth and final part, a wideband planar antenna reinforced with a metasurface reflector is designed. A simple meandered structure is used for the design of the radiating elements, while the back side consists of a partial ground plane and parasitic elements. To obtain high gain and directional radiation characteristics, an array of metasurfaces is placed behind the radiating element and it is observed that the reflector tends to reach a maximum gain of ∼9 dBi in the band of interest.

Contents

List of Figures

List of Tables

Abbreviations

1G	First generation
2G	Second generation
2-D	Two-dimensional
3G	Third generation
3-D	Three-dimensional
4G	Fourth generation
5G	Fifth generation
AF	Array factor
ACMA	Aperture-coupled microstrip patch antenna
AMPS	Advanced Mobile Phone System
AVA	Antipodal Vivaldi antenna
BLC	Branch line coupler
BM	Butler matrix
CDMA	Code Division Multiple Access
CP	Circular polarization
CPS	Co-planar strips
CPW	Co-planar waveguide
CSD	Circuit-switched data
CSRR	Complementary split ring resonator
CST	Computer simulation technology
DD	Dense dielectric
DR	Dielectric resonator
DRAF	Dual-reverse-arrow fractal

DGS	Defected ground structure
EBG	Electromagnetic bandgap
EDGE	Enhanced Data rates for GSM Evolution
EM	Electromagnetic
ESIW	Empty substrate integrated waveguide
FBW	Fractional bandwidth
FCC	Federal communications commission
FSS	Frequency selective surface
GPRS	General Packet Radio Service
GSM	Global system for mobile communication
HSCSD	High-speed circuit-switched data
IoT	Internet of things
ITU	International telecommunication union
LHMs	Left-handed metamaterials
LP	Linear polarization
LTE	Long term evolution
MIMO	Multiple-input multiple-output
mm-wave	Millimeter-wave
MSA	Mobile station authentication
RF	Radio frequency
RFID	Radio frequency identification
RLSA	Radial line slot array
SDC	Signaling and data confidentially
SIC	Substrate integrated cavity
SIW	Substrate integrated waveguide
SLL	Sidelobe level
SMS	Short message service
TDM	Time division multiplexing
UHF	Ultra high frequency
UWB	Ultra wideband
WiMAX	Worldwide Interoperability for Microwave Access

WAP   Wireless Application Protocol

Wi-Fi   Wireless fidelity

WLAN   Wireless local area network

V2V   Vehicle-to-vehicle

Chapter 1

Introduction

1.1 Background

After every 10 years, a new generation comes after the deployment of the first generation (1G) mobile networks in 1982, and these generations grow over time to meet the needs of mobile users. These trends will continue to increase exponentially every year worldwide [1]. Table 1.1 lists the mobile communication generations created to date. It can be seen from the data in the table that each transmission generation has unique characteristics and they vary from each other in terms of data rate and frequency bands.

When it comes to mobile communication, it refers to the overall speed, technology, frequency, and system. Each generation has its unique characteristics. The 1G cellular communication network was introduced in the late 1970s and was fully implemented in the 1980s [2]. The 1G communication technology was based on analogue signals, which means that a higher frequency was used for the modulation of the voice signal. However, analogue signals degrade over time and space, leading to call quality issues.

The second generation (2G) introduced global system for mobile (GSM) technology in the early 1990s. It enabled data and digital voice communication, and also improved security using signaling and data confidentiality (SDC) and mobile

TABLE 1.1: Brief overview of the different generations of mobile communication [3].

Generations	1G	2G	3G	4G	5G
Deployment Year	1981	1992	2001	2010	2020
Data Rate	2 Kbps	64 Kbps	2 Mbps	100 Mbps	10 Gbps
Frequency Bands	900 MHz	900/1800 MHz	800/900 MHz $1700-1900$ MHz 2100 MHz	800/900 MHz 1800 MHz 2100/2600 MHz	2.5/3.5/5.8 GHz 28/38 GHz 60 GHz

station authentication (MSA). As a result, many important services, such as short message service (SMS), international roaming, conference calls and call waiting, were made possible.

In 2001, third-generation (3G) mobile communications was deployed to improve voice and data capacity, increase data throughput and transfer, and support a wider range of applications [4]. For the first time, 3G communication technology supports fixed wireless and broadband internet access, which enables video calls, online mobile games, mobile TV, navigation maps and digital services. Compared to 2G, 3G technology offers enhanced security features, e.g. application and domain security, and secure network access.

In 2010, the fourth generation (4G) of mobile communications technology was launched, with the aim of providing mobile consumers with increased speed, capacity and quality, as well as improved security, voice and data services at lower cost and internet over IP [5]. 4G communication technology has also introduced the long term evolution (LTE) standard, which supports IP networking and packet switching. However, LTE was not able to fulfill all specifications, but its advanced version did [6]. LTE-Advanced 4G networks used 40 different frequency bands [4, 6] and achieved a maximum data rate of 1 Gb/s through the use of carrier aggregation and MIMO technologies [7].

Mobile data traffic is expected to grow rapidly around the world over the next decade. On the other hand, there were fears that the 4G mobile network would be unsuitable in the long term. Therefore, research organizations and industries have developed fifth-generation (5G) cellular system. The main concern of which is to

provide improved capacity, latency and mobility [8]. In addition to the current microwave bands, millimeter wave (mm-wave) bands have been identified as a potential candidate for the frequency band of 5G cellular networks [9]. To better understand 5G technology, a brief discussion is provided in the next sections.

Numerous organizations, research institutions, and industry leaders worldwide are actively working on defining and proposing future 6G standards. However, it is in conceptual and early research stages. Some anticipated key features and technologies that might be part of 6G standards could include extremely high data rate, ultra-low latency, enhanced spectrum utilization, AI driven networks, advanced antenna technologies, sustainability and energy efficiency.

1.2 Evolution in Mobile Communication

In mobile communication systems, antennas are used to transmit and receive signals between mobile devices and a network of base stations. The design of these antennas is critical to the performance of the overall system. Antennas used in mobile communication systems generally fall into two categories: base station antennas and mobile device antennas. Base station antennas are generally larger and more powerful than mobile device antennas and are used to cover a large area with a strong signal. These antennas are often mounted on towers or buildings and can be omnidirectional or directional, whereas directional antennas can only concentrate the signal in one direction, omnidirectional antennas may disperse the signal in all directions.. Mobile device antennas are generally smaller and less powerful than base station antennas, and are designed to be portable and efficient. These antennas are usually built into the device and can be internal or external.

One of the main limitations of 1G networks was their limited capacity and lack of security. Because the networks were analog, they could only support a limited number of simultaneous callers, and because the calls were unencrypted, they were vulnerable to eavesdropping. Additionally, these systems were also prone to poor sound quality, poor call clarity, and poor security. Although 1G networks

were quickly replaced by 2G digital networks, they laid the foundation for the development of later mobile communication technologies.

2G networks can be divided into two main types: GSM and code division multiple access (CDMA). While GSM is a widely used standard for mobile networks and is used in over 80% of mobile networks worldwide. It uses a time division multiplexing (TDM) technique to provide multiple users with access to the same frequency band. CDMA, on the other hand, uses a spread spectrum technique that divides the total available bandwidth into smaller frequency bands and assigns each user a unique code. Therefore, CDMA systems are able to support more concurrent users than GSM systems. 2G networks have introduced many key features, for example, SMS, wireless application protocol (WAP) and circuit-switched data (CSD) which laid the foundation for next-generation mobile networks, while 2G networks continue to be used in many regions of the world, especially in remote areas with limited infrastructure. 2G networks have largely been replaced by 3G network in developed countries.

Compared to 2G networks, these systems represented a significant leap forward in terms of capacity, speeds data transfer and services. The main improvement of 3G networks over 2G networks is the support for higher data transfer rates. The maximum data transfer rate for a 3G network is 2 Mbps, which is significantly faster than the data transfer rates allowed by 2G networks. This allows 3G networks to support new services such as mobile internet, video calls and mobile TV, which were not possible with 2G networks.

Enhanced data rates for the evolution of GSM (EDGE), general packet radio service (GPRS) and high-speed circuit-switched data (HSCSD) are all innovations made possible by 3G networks that have greatly increased the data transmission speeds and capabilities of mobile devices. Overall, 3G networks have represented a significant advancement in mobile communication systems. However, with the increasing use of smartphones and mobile devices, the demand for high-speed mobile internet and data transfer has led to the development of even faster 4G and 5G networks.

In terms of antenna design, 3G networks have introduced several new challenges and requirements compared to 2G networks. One of the main challenges was the need to support higher data transfer rates, which required antennas to be able to transmit and receive signals at higher frequencies and with greater accuracy. To meet these requirements, 3G networks typically use directional antennas, such as sector antennas and panel antennas, at base stations. These antennas are capable of transmitting a signal with high gain in a specific direction, which helps increase network capacity by reducing interference between cells. They are also designed to operate at higher frequencies than 2G antennas, typically in the $2 - 3$ GHz frequency band.

Additionally, 3G mobile devices needed an antenna design that was both more efficient and more compact so that it could fit into the limited space available in mobile devices. The number of people using smartphones and other mobile devices was growing rapidly, and people were using these devices for a wider variety of activities, such as streaming videos and music, participating in social media, and playing mobile games. These activities put a strain on 3G networks, which were not intended to support such high data transfer rates and large amounts of data that they are currently subjected to. Along with the growing demand for mobile data, there was also a proliferation of new technologies that required faster data transfer rates in order to utilize their full potential. The IoT, virtual and augmented reality, and telemedicine are all examples of technologies that fall into this category. In order to meet this requirement 4G technology, has been developed in response to the growing demand for mobile data and the requirement for faster data transfer rates.

The growing desire for mobile data and electronic devices, 4G networks were also designed to meet this demand. The most widely used technologies for 4G networks are LTE and WiMAX (global interoperability for microwave access). These technologies have been developed to provide faster data transfer rates and increased capacity, with data transmission speeds of up to 1 Gbps for mobile and 100 Mbps for stationary devices.

4G networks are built on the same basic concept of cells as previous generations, but they divide the area into smaller cells, use advanced modulation schemes and MIMO technology in an effort to increase network capacity. This allows more users to access the network and have a better experience with faster data transfer rates, fewer dropped calls, and better signal quality. In terms of antenna design, 4G networks require antennas that can support high data transfer rates, support MIMO, and operate at higher frequencies than previous generations. In 4G networks, a large number of antennas are used for beamforming and spatial multiplexing. Antennas like these can be found in base station and mobile devices. This contributes to the overall improvement in network performance. 4G networks also use a technique called adaptive networking, which adjusts the phase of each antenna in real time to improve signal quality and increase capacity.

1.3   5G Technology

The current 4G is going to be superseded by 5G very soon to meet the demands of high-speed traffic consumption worldwide and open another advanced chapter of the telecom industry. 5G communication technology is measured beyond 2020 mobile communication technologies. Since the first generation standard introduced in 1982; every 10 years new standards have been introduced to serve mobile users. But, with the rapid increase in mobile traffic, the percentage of users is expected to continue to increase over the next few decades, and the current 4G cellular systems will be unmanageable in the long term. The primary concern with 5G systems is to provide improved capacity at lower cost compared to 4G systems, as capacity is directly proportional to user demands for higher and faster data rates. Research organizations have agreed that next-generation 5G mobile networks will be capable of delivering speeds of over 100 Mbps in densely populated areas and up to 10 Gbps for fixed users and 1 Gbps for mobile users [3].

5G communication technology will bring unique new features to consumers. It will provide access to users everywhere and select the best performance among

other technologies such as wireless fidelity (Wi-Fi), wireless local area network (WLAN), 4G, etc. The selection of the best performance will not only be based on throughput but also on the most appropriate metrics depending on the nature of the service. Additionally, 5G systems will facilitate other services like the internet of things (IoT) by connecting a wide variety of devices. In addition to this, 5G systems will also cover services, such as, vehicle-to-vehicle (V2V) communication, remote health services, etc.

1.4   5G Frequency Bands

The mobile communications industry faces challenges regarding particular choices and at this stage the entire frequency range up to 100 GHz is under consideration for 5G services.

Various organizations had done extensive research globally on the feasibility of sub-6 GHz spectrum for wide area coverage and outdoor-to-indoor communications. Lower frequency bands were preferred from the viewpoint of propagation properties. So, possible frequency bands for 5G communication are $470 - 694$ MHz, $1427 - 1518$ MHz, $3300 - 3400$ MHz, $4800 - 4990$ MHz.

Large bandwidth is also required for 5G technology to ensure high data throughput; this can be done using higher frequency ranges as shown in [10]. So, to achieve high data rate and bandwidth in 5G communication, mm-wave frequency bands are the best option. In the mm-wave range, the ITU defines the frequency bands $24.25 - 27.5$ GHz, $37 - 40.5$ GHz, $42.5 - 43.5$ GHz and 60 GHz [11]. This type of integration will increase system capacity and expand transmission bandwidth for high data rates in dense deployments [12, 13].

1.5 Patch Antenna

The patch antenna was first introduced in the 1960s. A patch antenna is a type of RF antenna that is made by attaching a flat metal patch (typically made of metal such as copper) to a ground plane. This design creates a resonant element that emits electromagnetic energy in a specific direction. Due to the fact that they are compact, lightweight and inexpensive, patch antennas are frequently used in wireless communication systems. Some examples of these systems include cell phones, WiFi networks, and satellite communications. They can also provide relatively high gain, making them useful for long-range communications.

Patch antennas introduced in mobile communication systems in the early 1990s. The patch antenna is an example of a microstrip antenna, and it is characterized by the fact that its conductive elements are suspended on a dielectric substrate. It has become a popular design due to its compact size and low profile, which is convenient in many wireless applications.

1.6 Antennas for 5G Technology

Due to the strict requirements of 5G technology, this requires a complete overhaul of the devices. The architecture of the antenna typically dictates the design of the air interface. As a result, it calls for the development and verification of next-generation antennas with features not seen in earlier generations. Additionally, the antennas must meet the needs defined by 5G transceiver technologies such as massive MIMO. Despite this, radio propagation route loss models of lossy millimeter-wave channels show that a high-performance antenna design is required [14, 15]. Additionally, due to limited space in portable devices, small, inexpensive, low-loss antennas that are simple to combine with mm-wave electronics are required.

Planar antennas have grown in popularity over the past few years for a wide variety of microwave and mm-wave applications. This is mainly due to the fact that

planar antennas are very compact, have low production costs, and are easy to integrate into portable devices. Since mm-waves have a particularly short wavelength, it is easier for antenna designers to design compact antennas that are also highly efficient for use in 5G communication. Furthermore, it is feasible to create antenna designs that are both electrically and physically large enough to offer adequate performance. Furthermore, mm-wave frequencies suffer from higher losses than microwave frequencies, requiring careful substrate selection by design engineers to minimize losses and maximize radiation efficiency [16]. One of the techniques to increase the efficiency of mm-wave antennas is to design arrays. Second, metasurfaces can be used to achieve high efficiency. A brief discussion of the two technologies is presented in the following sections.

1.7 High Gain Antennas for 5G Communication

High-gain antennas play a crucial role in 5G communications as they enable efficient and long-range wireless connections. These antennas help to enhance signal strength, extend coverage, and improve overall network performance. Few types of high-gain antennas commonly used in 5G communications are Directional Antennas, Yagi-Uda Antennas, Parabolic Dish Antennas, Phased Array Antennas and MIMO antennas. The choice of antenna depends on various factors, including the specific application, coverage requirements, environment, and available infrastructure. Antenna design and deployment are crucial to ensure optimal performance and efficient utilization of the 5G network.

High-gain antennas are indispensable in 5G communication systems to extend coverage, overcome signal loss, improve signal quality, increase capacity, and enable advanced techniques like beamforming and MIMO. They are vital components for delivering reliable, high-performance wireless connectivity in 5G networks.

1.8   Antenna Arrays

An antenna array is defined as a radiating element formed by placing different individual antennas according to an electrical and geometric (phase and distance) scheme. The term 'antenna element' refers to each individual antenna that constitutes a multi-element array. Any type of antenna, including apertures, dipoles, microstrips, loops, reflectors, and horns, can be used as array elements. Large single antennas (arrays) may have high gain and directivity characteristics even though the radiation pattern from a single element is generally wide and each has low gain (directivity). Increasing the number of individual antenna components in a multi-element array produces highly directional characteristics. If the current through each element is the same and mutual coupling is ignored, the vector sum of the fields that each element radiates defines the overall field pattern. Therefore, constructive interference provides strong directivity in the desired direction, while the destructive interference cancels out in all other directions. By adjusting the geometric structure of the array, the excitation amplitude, phase, spacing between elements, and the relative shape of each element are the primary means by which the radiation characteristics of an antenna array can be modified [17].

1.8.1   Types of Antenna Arrays

According to the geometric layout, the arrays are fundamentally classified as follows:

(a) Linear array

(b) Planar array

(c) Circular array

1.8.1.1 Linear Array

It's one of the easiest array configurations to use a linear array. It is clear from Fig. 1.1, the antenna components of a linear array are arranged in a linear fashion. The primary array lobes are generated and subsequently focussed into a single beam by the linear phase tapering of the signal that is supplied to the array elements. The field strength produced by a single antenna element at the array's center can be multiplied by an array factor (AF) to get the total field strength produced by the array. Eq. (1.1) describes the typical far-field distribution of an N-element linear array.

$$f\left(\theta, \phi\right) = E_n\left(\theta, \phi\right) \times \mathrm{AF}_n\left(\theta, \phi\right) \tag{1.1}$$

where

$$\mathrm{AF} = \sum_{n=1}^{N} e^{-j(n-1)\psi} \tag{1.2}$$

where, $\psi = kd\cos\left(\theta\right) + \beta$, β is a relative phase between elements, and d denotes the distance between the array elements [17]. It implies from Eq. (1.2) that the relative phase between elements can be used to control AFs of uniform linear arrays. A uniform array is a one that contains elements of the same nature, amplitude and progressive phase.

There are two configurations of linear arrays with respect to the direction of the radiated field.

(a) Broadside array

(b) End-fire array

A broadside array is an arrangement of antenna elements where the elements are positioned parallel to each other and orthogonal to the axis. The main lobe direction of this type of array arrangement is perpendicular to the array axis. The elements are evenly distributed and powered with similar amplitude and phase
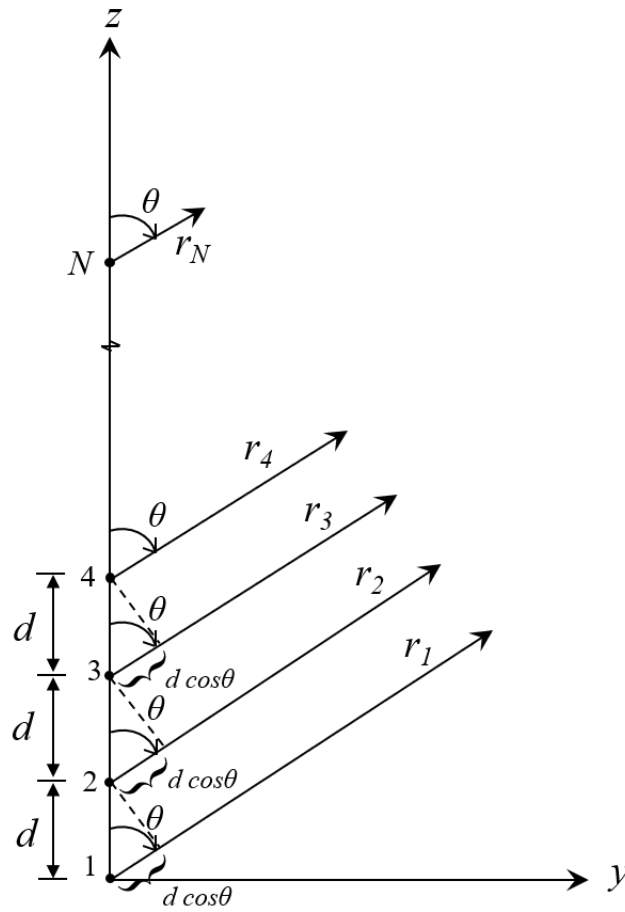
FIGURE 1.1: Linear array with N-elements that have uniform excitation amplitude and spacing [17].

current [17]. Depending on the desired beamwidth, a number of equal sized dipoles are used. Identical phase pulses are sent to all the dipoles. A broadside array can improve gain and directivity when combined with a reflector, and it also becomes unidirectional. The same array can be used behind it at a distance of $\lambda/4$ supplied with a current having a phase shift of 90° [17].

However, there are many similarities between the broadside array and the end-fire array. The direction of the radiation's primary beam determines the difference. In particular, it extends perpendicular to the antenna array's center in an end-fire array. In an end-fire configuration, every antenna points in the same direction. Additionally, while each antenna element receives the same current, the phases of the currents alter as the array progresses, resulting in a unidirectional setup
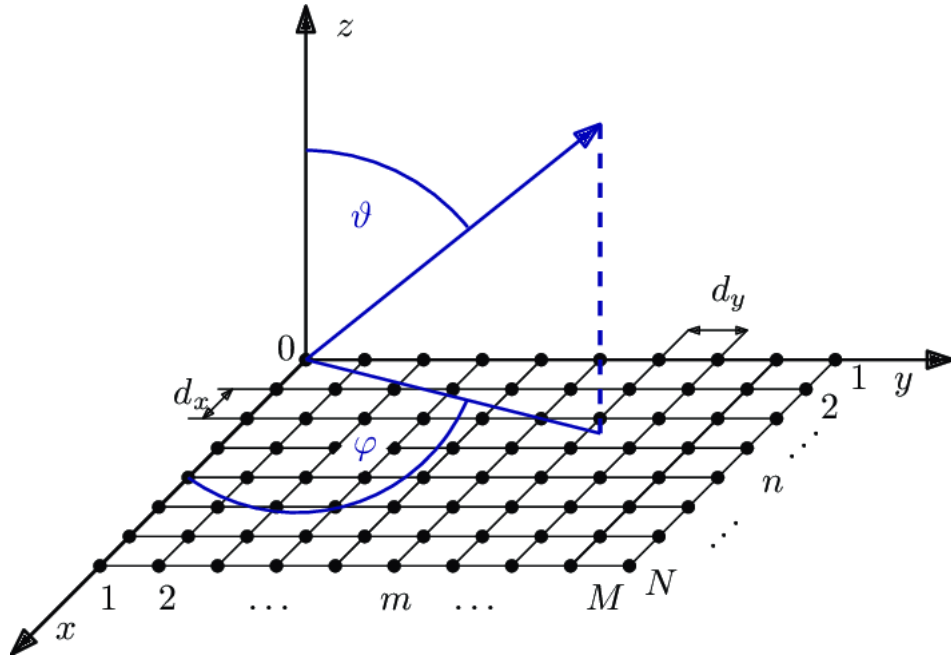
FIGURE 1.2: N×M planar array structure distributed in xy plane [18].

overall. The main lobe field orientation is parallel to the array axis [17].

1.8.1.2 Planar Array

Planar arrays are formed when the elements of an array are arranged in a plane rather than along a single axis, as shown in Fig. 1.2. Compared to the low directivity of each individual element, planar arrays offer directional beams, symmetrical patterns with minimal sidelobes and high directivity (narrow beamwidth). The beam can be pointed in any direction as shown in Fig. 1.2 [18]. The y axis has M evenly spaced arrays, and the x axis has N arrays. If the current distribution along each axis is assumed to be the same, then the normalized AF can be written as [18]:

$$\text{AF}(\theta, \phi) = \left[\frac{1}{M} \cdot \frac{\sin\left(M.\frac{\psi_x}{2}\right)}{\sin\left(\frac{\psi_x}{2}\right)} \right] \times \left[\frac{1}{N} \cdot \frac{\sin\left(N.\frac{\psi_y}{2}\right)}{\sin\left(\frac{\psi_y}{2}\right)} \right] \tag{1.3}$$

where

$$\psi_x = d_x \cos\theta \sin\phi + \beta_x \tag{1.4}$$

and

$$\psi_y = d_y \cos\theta \sin\phi + \beta_y \tag{1.5}$$

Element spacing, phase shift, frequency, and elevation angle all determine linear phase functions. The main lobe is directed by the phase shift (β_x and β_y) of the inter-elements, while the beamwidth and level of the side lobes (SLL) are determined by the amplitude distribution and the inter-element spacing. Larger side lobes and smaller main lobe width result from increasing the spacing value between elements. Despite the fact that an increase in directivity is observed with increasing number of antenna elements, [19].

1.8.1.3 Circular Array

Circular array is a type of planar configuration in which the radiating elements are distributed in a circular pattern, as shown in Fig. 1.3. There are no edge elements in circular array. The beam pattern of a circular array can be electronically rotated without any edge limitations. The AF of the circular array is given by the following equation [17]:

$$\text{AF} = \sum_{n=1}^{N} I_n e^{-jka(\cos\psi_n - \cos\psi_{0n})} \tag{1.6}$$

where

$$\psi_n = \cos^{-1}\left[\sin\theta \cos\left(\phi - \phi_n\right)\right] \tag{1.7}$$

and

$$\psi_{0n} = \cos^{-1}\left[\sin\theta_0 \cos\left(\phi_0 - \phi_n\right)\right] \tag{1.8}$$
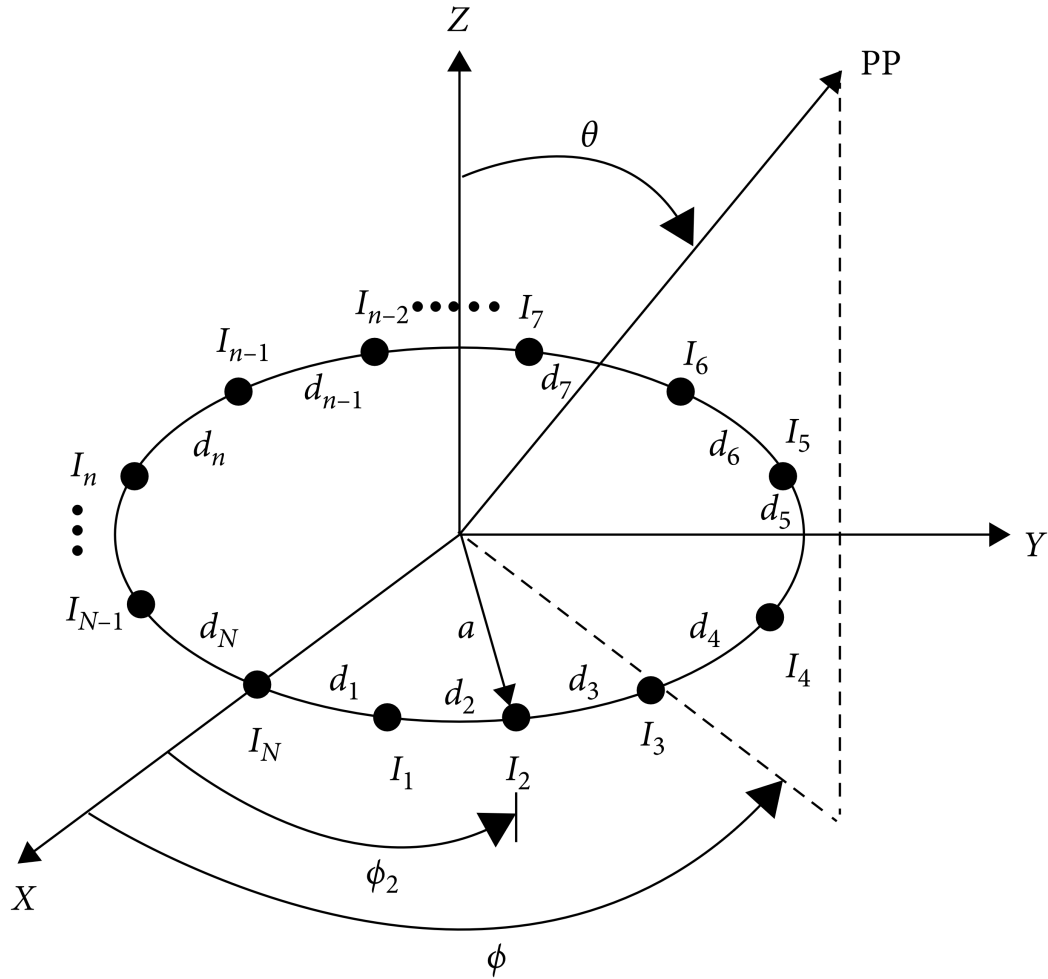
FIGURE 1.3: Circular array structure [17].

1.9 Metasurfaces

Metasurfaces are planar metamaterials with length of the unit cell below the wavelength, as shown in Fig. 1.4. They are the potential 2D analogue of massive metamaterials [20–22]. Metasurfaces are not characterized by the constitutive features used to describe their bulk analogues in metamaterials, but rather by the sheet impedance and boundary conditions of the metasurfaces. Moreover, the usefulness of the latter is limited by the difficulty of producing it at the micro− and nanoscale due to its complicated three-dimensional (3D) shape. However, when periodic designs are modeled on flat substrates, it becomes easier to create metasurfaces. A single-layered or multi-layered metasurface structure is allowed, but the total thickness of the metasurface must be less than the working wavelength [23–27]. They provide less loss in the propagation path than bulk metamaterials

because their thickness is on the order of a single sub-wavelength. Even though metasurfaces have planar geometries, their association with electromagnetic (EM) waves is powerful enough to provide practical functionality.
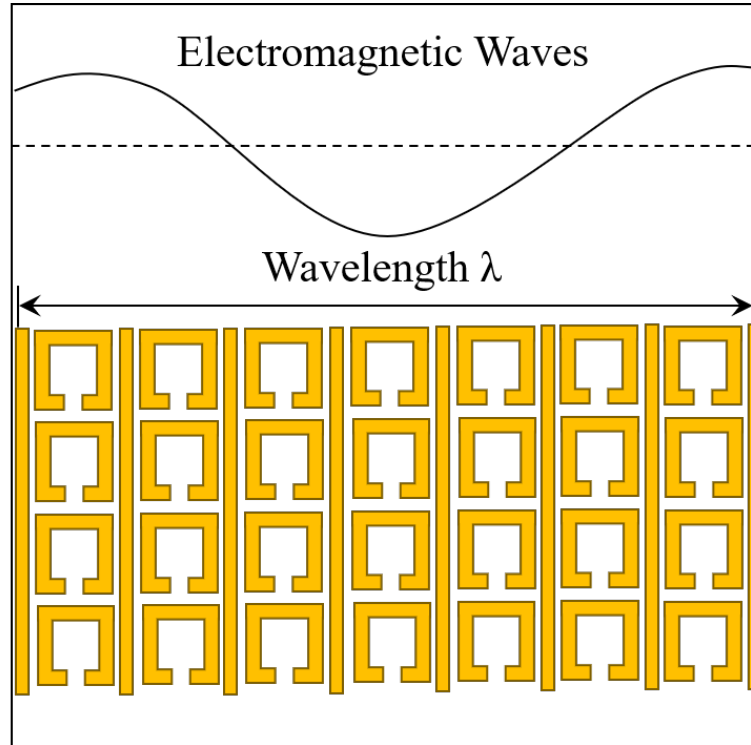
FIGURE 1.4: Metasurface configuration [28].

The theoretical framework for studying and creating metasurfaces has undergone considerable development and improvement in recent years. The authors in [29] give a summary of analytical and numerical techniques for studying two-dimensional (2-D) and 3-D metamaterials. The study of electrically thin metamaterials or metasurfaces has shown that the physical significance of the parameters obtained using the usual effective medium approximation approaches is not high. An efficient electrical and magnetic susceptibility sensor can be used to represent a metasurface. According to the authors of [30], a metasurface is a periodic configuration of metallic/dielectric sub-wavelength unit cells that behave as artificial atoms, or meta-atoms, that are capable of being either electrically polarized or magnetized. The average surface impedance of a metasurface can be directly related to the input electric field due to the passage of magnetic and electric polarization over its surface [31]. By describing the metasurface as a series of resistance, capacitance, and inductance, the comparable circuit method makes metasurface

analysis and design more physiologically accessible [32, 33]. The values of these components are dictated by the geometric configuration of the metasurface.

Careful construction of the unit cell below the surface of a metasurface is necessary to regulate the amplitude, phase, and polarization of reflected and transmitted waves. The spatial inhomogeneity of the optical scatterers inside the unit cell can be designed to redirect the wavefront of the interfering wave after reflection or transmission. Reflective grating metasurfaces have been shown to exhibit anomalous reflection of incident waves while completely eliminating transmission and specular reflections [34]. Generalized Snell's law can be used to determine the direction of anomalous reflection [35]. Furthermore, these metasurfaces allow total phase control for scattered electromagnetic waves by optimizing sub-wavelength inhomogeneous optical scatterers.

It is possible to create a metasurface in such a way that it obtains an abnormal refraction as well as an abnormal reflection of the light during its transmission. In order for these metasurfaces to be reflection-free, their input impedances must be equalized to that of air. According to [36], there is an anomalous refractive metasurface that achieves 86% transmission efficiency in the microwave frequency range. Another metasurface that works on the principle of an optical nano-circuit is described in detail in [37]. This metasurface allows complete phase control of the light that is transferred through it. According to [38, 39], some metasurfaces have been discovered that display flawless anomalous refraction at terahertz, infrared, and visible light frequencies.

1.10 Key Requirements for 5G Communication

For 5G communication, the allocated frequency is in GHz regime starting from sub-6 GHz to 60 GHz. Number of bands have been allocated in this range for 5G communication by the ITU. One of the key requirements of 5G communication is that it should support average data rate of 100 Mbps. Whereas, the maximum perceived speed of data is up to 10 Gbps. In these days mobile devices commonly

use patch antenna of various topologies. These patch antennas are naturally to be accommodated within the device thus, there is always a restriction on the space which put constraints on the design of the antenna.

In this dissertation, various design topologies have been explored to comply with 5G communication requirements for different regime of allocated frequencies. Although, these designs are scattered in nature, yet they are linked because all of these designs are studied in compliance to 5G communication so that at the end of the day any design which suited the most can be adopted for a given application. Couple of designs are investigated through simulation tools which are highly reliable in the industry and then based on the simulation data their suitability for 5G communication is assessed. On the other hand, those designs which offered exciting results, are fabricated and tested to ensure their performance as per the predicted data. Thus, the designs discussed in Chapter 5 and Chapter 6 are the one which are thoroughly investigated, i.e. simulated, fabricated and tested.

1.11 Research Motivation and Objective

It has been described in Section 1 that the deployment of 5G technology is considered necessary for various reasons, e.g. faster data transfer speed, reliable connectivity and to enable new technologies that will shape the future of communication and commerce.

(a) 5G technology requires the use of mm-wave spectrum as it offers several advantages over lower frequency bands. First, mm-wave frequencies offer much higher bandwidth than lower frequency bands. Second, mm-wave frequencies have much shorter wavelengths than lower frequency bands. Third, the use of mm-wave frequencies allows for much higher capacity networks, which means more devices can be connected to the network at once without affecting performance.

(b) In densely populated areas, it is more difficult to create an antenna for mm-wave frequencies, because the antenna must have high directivity, high gain and wide bandwidth. Additionally, due to portability constraints, low cost, low loss antennas that are simple to combine with mm-wave circuitry are in high demand. Therefore, there is a need to create small high gain antennas for use in this type of transmission.

(c) The objective of this research is to design planar antennas and arrays. Planar antennas are used because they are lightweight, easy to manufacture, and can easily integrate into portable devices compared to multilayer antenna designs [40]. To reduce the size of the antenna, different types of techniques, for example slot loading and fractal geometry, have been used. On the other hand, planar array configurations with metasurfaces can be designed to achieve high gain and improved efficiency.

1.12   Dissertation Organization

This chapter introduces the details of 5G communication technology. The chapter begins with the historical background of the different communication systems. After that, a discussion is provided on why 5G technology is a promising option for the development of future communication systems. A detailed discussion of 5G frequency bands and antenna requirements is also provided in this chapter. The motivation behind the proposed work is presented and based on this, the research objectives are identified. The remaining formation of the dissertation is given below:

Chapter 2 presents a detailed overview of the antennas and antenna arrays presented earlier for 5G mm-wave applications. The chapter begins with the discussion of previously reported antenna designs intended for mm-wave applications. The second section of the chapter describes antenna array designs, while the last section discusses metasurface-based antenna designs for 5G applications.

Chapter 3 presents the design of an equilateral triangle loaded rectangular patch antenna for mm-wave wide-band communication systems. The designed antenna provides high impedance bandwidth, high efficiency and high gain using a simple structure.

Chapter 4 discusses two different designs of 1×2 patch arrays for 5G mm-wave communication systems. The antenna arrays described are well suited for 5G networks due to their high gain and wide bandwidth.

Chapter 5 presents the design of a 1×4 planar fractal antenna array for 5G mm-wave applications. A fractal geometry is used to achieve compactness, while the high gain is achieved by designing a planar array. According to the presented results, the antenna array works well and offers high gain for 28 GHz frequency band.

Chapter 6 presents the design of a wide-band planar antenna based on a meta-surface reflector, which can be used in 5G communication systems. To achieve high impedance bandwidth, a simple antenna structure with partial ground plane and parasitic elements is developed. Additionally, a metasurface reflector placed behind the antenna to improve antenna gain. The results show that using a meta-surface reflector tends to achieve directional radiation characteristics within the operating bandwidth.

Chapter 7 discusses the conclusion drawn from this research and its extension as future work.

Chapter 2

Literature Review

The process of designing an antenna involves determining the type and size of antenna that is best suited for a particular application and then building it according to the chosen design. Many factors must be considered when designing an antenna, including the frequency of the signal it will transmit or receive, the type of transmission (eg, radio waves, microwaves, infrared, etc.); the distance the signal must travel, the space available for the antenna and any potential interference. There are many types of antennas, for example; dipoles, Yagis and helical antennas, each with its own characteristics and suitability for different applications. The literature review is divided into the following parts.

1. Single patch antenna

2. Patch array antenna

3. Size reduction techniques

4. Gain enhancement techniques

5. 5G antenna arrays

2.1 Single Patch Antenna

A metallic patch covered in a dielectric substrate is the basic building block of a patch antenna. Because of its small size, ease of production, and capacity to be customized for certain frequency ranges and performance needs, single patch antennas are adaptable, affordable, and frequently utilized in a variety of wireless communication applications. Few patch designs are discussed below.

A square microstrip patch antenna with a quarter wavelength impedance matching line was designed for 32 GHz in [41]. On the patch, rhombus-shaped slots were introduced to reduce the return loss level to 11.241 dB and boost the system bandwidth to 52 MHz. In [42], the design performance of a 28 GHz microstrip patch antenna (MSPA) was examined. FR-4 substrate material with a thickness of 0.244 mm and a ϵ_r of 4.4 was used in the antenna's design. By introducing combined optimization of parameters, inset-feed and quarter-wavelength impedance matching, the beam-gain of 7.587 dBi, directivity of 7.509 dBi, radiation efficiency of 98.214 %, and bandwidth of 1.046 GHz were achieved. A 28 GHz rectangular microstrip patch antenna with a return loss of -13.48 dB, bandwidth of 847 MHz, gain of 6.63 dB, and efficiency of 70.18% was created by the authors in 2019 [43]. The patch measured $6.285 \times 7.235 \times 0.5$ mm^3 in size. To match the radiating patch, an inset feed transmission line approach was employed. For fifth generation (5G) wireless applications, a patch antenna in the shape of a rectangle with a slot was created and studied [44]. The purpose of adding the slot was to enhance antenna performance. The substrate employed was a Roger RT duroid 5880 type, with a height of 0.5 mm, a loss tangent of 0.0009, and a relative permittivity of 2.2. With a bandwidth of 1.06 GHz and a reflection coefficient (S_{11}) of -20.95 dB. Table 2.1 presents a summary of single patch antennas discussed in section 2.1.

TABLE 2.1: Summary of single patch antennas.

Authors	Year	Developments	Ref.
Darboe *et al.*	2019	An inset-fed microstrip patch antenna for 28GHz.	[43]

Authors	Year	Developments	Ref.
Prabhu *et al.*	2019	Design of a square microstrip patch antenna for 32 GHz with a quarter wavelength impedance matching line.	[41]
Rahman *et al.*	2022	An inset-fed microstrip patch antenna for 28GHz using FR-4 substrate material.	[42]
Didi *et al.*	2022	A rectangular-shaped patch antenna with a slot for fifth generation (5G) wireless applications.	[44]

2.2 Patch Array Designs

Designing a patch array involves creating an array of individual patches that together form a larger antenna system. Basic steps to design the patch array antennas are defining the operating frequency range, antenna type (circular, rectangular, microstrip, etc.), designing of individual patchs, array configuration, feed network design, simulation and analysis, fabrication and testing, iterative optimization, integration and deployment. During the design process, substrate material selection, manufacturing tolerances, environmental effects, and other practical factors are considered that may affect the performance of the patch array. The following sub sections discusses different array designs.

2.2.1 Series-Fed Arrays

Microstrip elements are low profile, so they can be used to fabricate planar antennas on a single substrate. A simple eight-dipole array antenna with a planar structure was designed in [45]. A total of eight dipoles were used, which served as both reflectors and directors. To create a serial link between the dipoles on the left side of the substrate, a microstrip feed line was positioned above the substrate.

The microstrip input line that was fastened to the substrate's bottom was utilized to connect the dipoles on the right side of the substrate. To receive substrate feed from a quarter-wave transformer, one stripline was positioned on top of the substrate, while the other was positioned at the bottom to act as a ground connection. The purpose of these two striplines was to be fixed to the substrate. In the frequency band of 23.5 to 51.9 GHz, the results revealed a gain of 10.8 dBi.

The authors in [46] describes the construction of an antenna that has a high gain and a structure similar to a ladder. A microstrip line with a 50 Ω impedance supplies power to a rectangular patch. A ladder-like structure was created by replicating several patches (see Fig. 2.1). To increase the reflection coefficient, the sides of extreme four corner patches were cut. To the left of the microstrip line in [47] a horn-shaped stub was used to design a low-profile series-fed antenna array. The magnetic current in the microstrip line of the traveling wave was periodic and had symmetrical surrounding fields at the guided wavelength, denoted by λ_g. A microstrip line was put out to the strip line's left, and four trapezoidal stubs were incorporated into this antenna's design. Central to a microstrip line was a hub where power was fed in via coaxial wire. An illustration of how the cancellation of anti-phase magnetic current is achieved was given by the current distribution simulation. According to the data, there are two resonant modes located at a frequency of 25.3 GHz and another at frequency of 28.5 GHz. As shown in the Fig. 2.2, the 1×4 architecture was used to construct a 4×4 structure that is comprised of four sub arrays that are linked together by a microstrip line. According to the specifications, the array had a strength of 17.5 dBi and a frequency of $23.39 - 28.2$ GHz. Both frequency ranges exhibit a broadside radiation pattern.

In [48], a multi-layer, circularly polarized, broad band antenna was suggested. This antenna was based on a ground plane with slots for power coupling in the bottom layer, and it used four 45°right-angled rectangular patches. These slots, which are beneath the radiating patch, are shaped like an inverted V. A 50 Ω impedance microstrip input line with a small stub at the end was located on the bottom of the second substrate. The third substrate was placed at the structure's base, while a conductive layer acting as a reflector at the structure's top improved
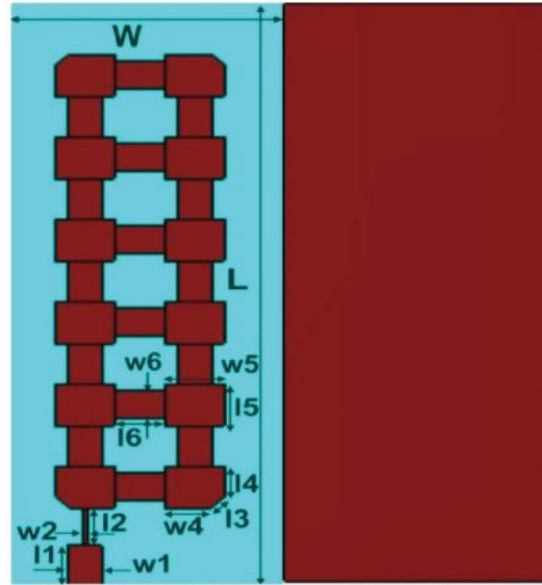
FIGURE 2.1: Millimeter wave high-gain antenna array [46].
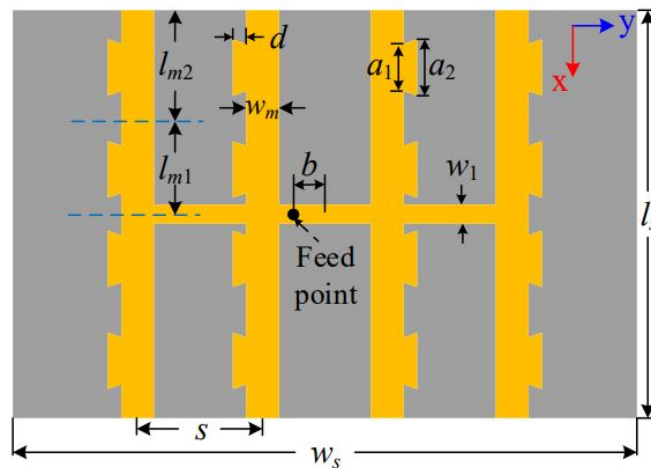
FIGURE 2.2: Configuration of series-fed, single-layer, and wideband millimeter wave microstrip arrays [47].

its directivity and gain. The patches have been etched with a slit in the center to increase bandwidth. This has led to the production of degenerate modes at the fundamental frequency, consequently leading to a rise in the amount of active routes.

In [49], a non-uniform array was designed to control radiated power and ensure that all elements of a series-fed structure are tuned to the same frequency in a travelling-wave mode. To achieve non-uniform aperture field, the suggested structure incorporated elements with non-uniform shapes and spacing along the

microstrip line. Radiating power can be calculated by adding the input power, the output power, and the ohmic losses for a given component. It is recommended that the array have one type 1 element, two type 2 elements, and three type 3 elements of varying forms to achieve the necessary radiated-to-available power ratio (RAPR). Type 1 had an input/output port-equipped with a rectangle patch. In the type 2 rectangular patch, both the input and output ports were inset. Type 3 was a rectangular patch with a slit-coupled output and an inset feed input ports. By changing the gap of a slit-coupled port, type 3's RAPR is managed. By radiating the remaining power, an inset rectangular patch was used to end the microstrip line and prevent reflections.

The authors in [50] designed a three-layered series-fed rectangular tapering antenna. The antenna's top substrate included a set of five right-angled, tapered rectangular patches and a second set of left-angled, tapered rectangular patches separated by a phase shifter. A 50 Ω microstrip line supplies these two sets in parallel. Patches and a feed line were encircled by grounded co-planar waveguide (CPW) on the top of the upper substrate. A rectangular slit was present on the second and third layers to couple the power. To increase bandwidth while decreasing surface wave losses, a hollow structure of metallic vias was used to enclose the patches and feed line. Antenna gain was calculated to be 9.5 dBi.

Slotted substrate-integrated waveguide with the air-filled, brass-plated array was designed in [51]. The designed array had a 9.5 dBi gain at a resonance frequency of 27.2 GHz. For use in 5G communication devices a 1×4 series-fed elliptical slot-loaded circular patch array was designed in [52]. Dual-frequency response at 28 GHz and 38 GHz was achieved by cutting an elliptical slot inside the circular patch. In addition, it was found that the gain values for both frequencies were 7.6 dBi and 7.21 dBi, respectively. L_a and W_a are the length and width of substrate, W_{f1}, W_{f2} and W_f are widths of feed line, and D is the distance between elements (see Fig. 2.3).

In [53], an improved series-fed array antenna of 2×2 and 3×3 is presented, with the ability to steer the antenna's radiation pattern in a specific direction. Initially,
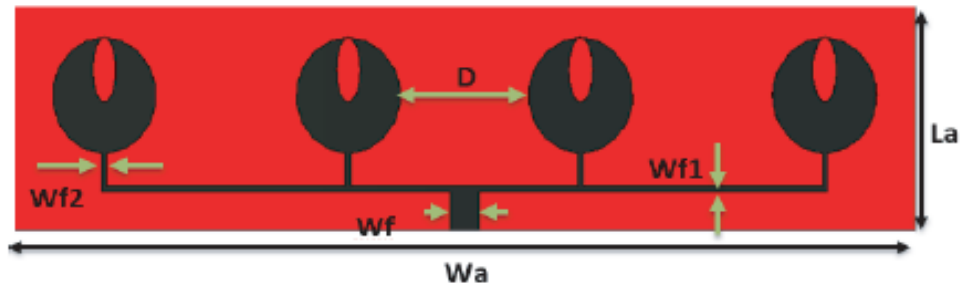
FIGURE 2.3: Front view of the array with design dimension variables presented in [52].

the idea called for the design of a single rectangular patch that would be coupled to a quarter-wavelength transformer, this patch would be supplied by two 50 Ω transmission lines that would be situated on adjacent sides. The stimulation of two ports resulted in the production of surface currents that ran in directions that were both perpendicular and parallel to the feedline. A 2×2 series-fed array design had two ports in the x and y directions was modified to four ports. Gain of 13.2 dBi was attained with broadside radiations when all terminals were activated at zero phases. An antenna for a planar, series-fed, 13-beam array was designed in [54] using a butler matrix (BM) and a branch line coupler (BLC). Based on simulations, the array antenna produced 7 beams from the BM and 6 beams from each of the BLCs. The original design consisted of 1×10 rectangular tapered patches that are tapered from center to end. Table 2.2 presents a summary of series-fed array antennas discussed in section 2.2.1.

TABLE 2.2: Summary of series-fed arrays.

Authors	Year	Developments	Ref.
Khalily *et al.*	2015	Design of phased arrays comprised of series-fed patch antennas with a reduced number of controllers.	[53]
Chao *et al.*	2019	Miniaturized 77 GHz radar instrument using a series-fed cavity-back patch array antenna.	[50]
Khattak *et al.*	2019	Dual-band performance in a circular patch antenna array with elliptical slots.	[52]

Authors	Year	Developments	Ref.
Wang *et al.*	2020	An angled printed dipole array antenna with high gain and broad bandwidth due to series feeding.	[45]
Guo *et al.*	2020	Wideband, single-layer, series-fed microstrip array design for millimetre waves.	[47]
Kang *et al.*	2020	A low-sidelobe microstrip array designed for use with a travelling-wave technique.	[49]
Malviya *et al.*	2021	Antenna array with high gain for millimetre waves in wireless applications.	[46]
Ullah *et al.*	2021	A series inclined slot-fed circularly polarized antenna for 5G 28 GHz applications.	[48]
Linfeng *et al.*	2021	An effective and inexpensive slot array of microstrip-fed air-substrate-Integrated waveguides.	[51]
Najaf *et al.*	2022	Antenna arrays for millimetre waves with multiple beams at a low cost for 5G mobile use.	[54]

2.2.2   Parallel or Corporate Fed Arrays

In [55], a 1×4 planar antenna array with a dual-hexagonal shaped was illustrated for a frequency band of 28 GHz. A broadband feeding network was used to feed the array's elements. To ensure isolation, conducting vias were placed around the array components. The findings show that the array had a 10 GHz impedance bandwidth between $25 - 35$ GHz. In [56, 57], comparable setups were shown. A wide impedance bandwidth in the frequency range of $23.76 - 42.15$ GHz and a gain of 11.5 dBi were achieved in [56] by a spiral-shaped radiator with three parasitic components in the form of a hexagon placed at the bottom of the radiators. Parasitic components were added behind the radiators to achieve this outcome. In [57], a rhombus-shaped patch radiator with square parasitic components was used
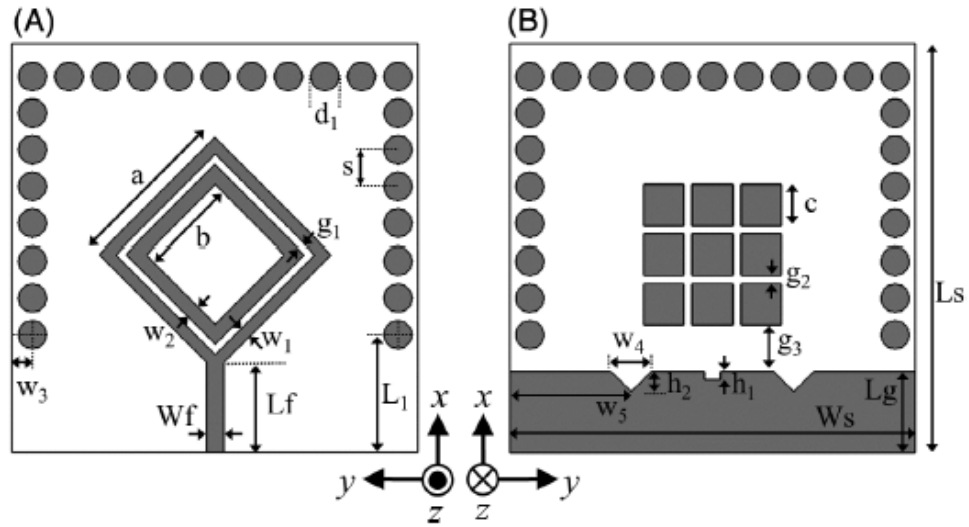
FIGURE 2.4: Single element antenna structure: A, front side; B, back side. The shaded areas show copper coverage on the substrate [57].

to achieve the bandwidth of $26 - 30.63$ GHz (see Fig. 2.4). Furthermore, in [58], a array was designed to be used as a dipole antenna array for 5G communications and had a frequency of $23.41 - 33.92$ GHz. An array of snowflake-shaped fractal antennas operating in the 28 GHz band with a gain of 10.12 dBi was also designed in [59].

For the purpose of 5G technology, a hook-like and doughnut-shaped planar antenna arrays were designed in [60, 61]. A T-shaped planar array with a square frame was presented for use in 5G communication networks in [62]. The ground plane configuration was exactly the same as it was described in [60, 61] (see Fig. 2.4). Although the designs that were illustrated took less space and had a narrower impedance bandwidth. In [45], a dipole array with eight non-uniform elements was designed for mm-wave wide-band applications. With an impedance bandwidth spanning from $23.3 - 51$ GHz, the presented dipole array was unfortunately ineffective due to its low gain.

Broadband planar arrays were designed for use in 5G broadcasting applications in [63]. The array element consisted of a power splitter based on a substrate integrated cavity (SIC), in addition to two dipole radiators. On either side of the
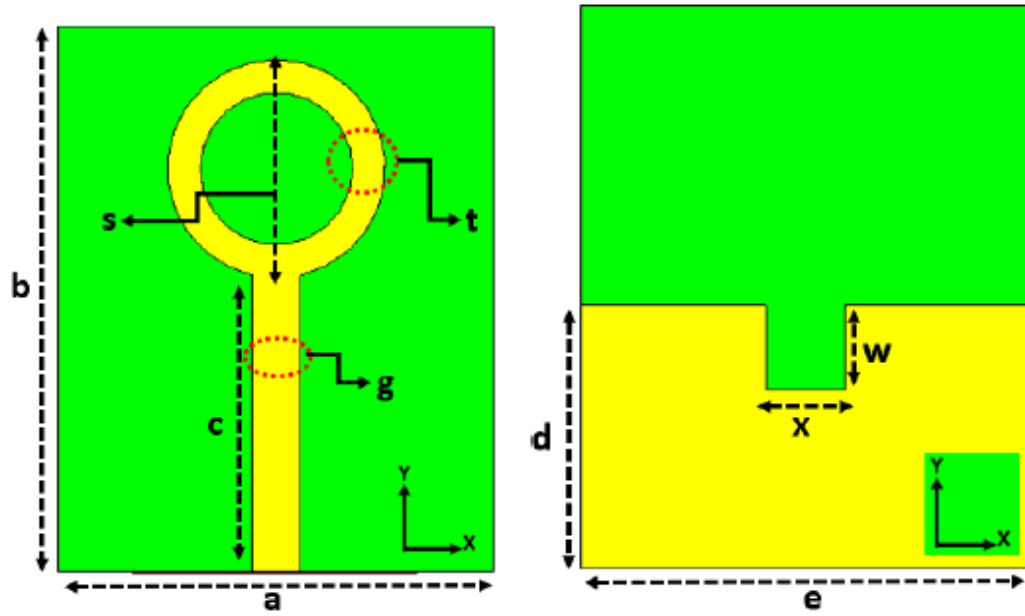
FIGURE 2.5: Proposed Antenna Design. (a) Front View. (b) Back View [60].

SIC-based power splitter, the dipole components were laid out next to one another in parallel configuration. The proposed configuration had a wide impedance bandwidth (24 GHz to 29.5 GHz) and a gain of 10 dBi, but it was extremely complicated and thus unlikely to be used in 5G communication devices. In [64], 1×4 multi-circular ring wide-band antenna array that is both compact and rectangular was presented. There were actually three separate circular rings that made up the single element, with the third ring overlapping the other two and the first two being joined together. The resonance of the antenna was between 28.8 and 38.4 GHz, which were two distinct frequency bands. The resonant frequency moves marginally upward as the ground slit length rises, while the reverse is true for the ring spacing. A 4-element array was designed by merging together a single-element and full-corporate feeds. The antenna array had an impedance bandwidth from 26.2 − 36.7 GHz.

Using a circular patch in resonance with a quasi-TM$_{21}$ mode was another method for obtaining high bandwidth [65]. The design consisted of two substrates and four layers. On top of the substrate two horizontal and one vertical slits were designed, a circular patch array of 4×4 elements was created. Metallic vias connected rectangular strips on the bottom of substrate 1 to circular patches. Substrate 2 featured

a parallel feed structure at the bottom and a ground plane on the top with a slot for power coupling to the radiator. Linear polarization (LP) was generated by an asymmetrical configuration of the four 2×2 feed structures, while orthogonal configurations generate circular polarization (CP). Compared to the CP's 14.69 dBi gain, the 4×4 LP achieved a significant gain of 19.74 dBi. Because of their consistent impedance across a wide range of substrate thicknesses, co-planar strips (CPS) and CPW lines were incorporated in [66], Because the electric-field lines were in the same plane as the ground line and the signal line, isolation was also enhanced. The layout relied on a total of eight radiating elements, all of them were linked by a differential CPS line. The CPW line was developed by splicing together two CPS. In order to set up the array, a connection had to be built to link CPS to CPW, and vice versa. The array has a frequency range of $51 - 53.5$ GHz and $57 - 65$ GHz, respectively. Gain in the favored frequencies was between 12 and 14.5 dBi.

The monopole antenna array with a defective ground was presented by the authors of [67] to increase the bandwidth. The bandwidth of a rectangular patch was increased by rounding off its corners along its length and giving its slot a reversed T-shape structure. The optimized patch had resulted in a higher working frequency. Resonance was shifted to lower frequency bands by altering the ground plane with rings, circular slots, and rectangle slots. The patch was given power via a quarter-wave transformer that relied on a defective CPW ground. This configuration allowed for a maximum bandwidth of 11.6 dBi between 57.2 and 63.8 GHz. Chinese characters in the form of a Jin were arranged into a four-element array in [68]. Signal was fed to four elements using the SIW feed method. Metallic vias connected to the ground plane supplied power to four SIW arms. To create isolation, metallic vias are inserted in the gaps between the slots. Gain of 12 dBi was obtained across a bandwidth of 24.5–27.5 GHz at -10 dB impedance.

An H-shaped slot array antenna was presented in [69] with high gain. Initially, an 8 dBi gain was accomplished with a single-element antenna that was coaxially fed and had a half-wavelength square patch. Then, to achieve better resonances at higher frequencies, a rectangle slot was added, along with two rectangular slits

on either side of the patch. Multilayer implementations of the planar architecture were also introduced. This concept was further developed into a four-element array using a 1×4 power divider and a single coaxial input. Covering the design's borders and connecting them to ground with metallic vias created a magnetic wall that was visible in the current distribution and helped to reduce leakage losses and phase distortion.

In [70], an eight-element array antenna with a cavity-backed SIW was created. Three layers and two substrates made up the design. The coaxial feeding network was connected to an I-shaped SIW cavity that was present in the bottom substrate of top layer. Power was distributed uniformly to the 2×2 subarrays in the second layer, which consisted of four SIW cavity sections with rectangular slots in the top of the upper substrate.. The uppermost stratum consists of four subarrays, each of which was 2×2. The obtained bandwidth fall between $35.25 - 37.1$ GHz.

For 5G networks, an Antipodal Vivaldi Antenna (AVA) array of 1×8 was presented in [71]. The authors described that the AVA array operated between $24.55 - 28.5$ GHz and had a maximum gain of 11.32 dBi. Similar AVA setup was used in [72]. The two radiation components, one on top and one on bottom, were designed with two distinct tapered slot arrangements. The top radiator had a smooth exponential curve, while the bottom radiator, which was linked to the ground plane, had a more complex elliptical curve with a tapered end. Moreover, DGS was used to enhance isolation between array elements. The bandwidth was extended by the AVA with decoupling notch structure from $23.5 - 30.2$ GHz to $22.8 - 31.3$ GHz. The decoupling notch also reduced coupling between the antenna components, leading to a 12.5 dBi gain from the presented configuration.

In [73], an AVA array antenna design was developed that resonates at dual bands. The AVA antenna was comb-corrugated, which enhanced isolation and radiation performance. The patch was etched with a tapering shape made of an exponential curve and a circular arc. The corrugated structure was tuned to get the desired frequency response. A 1×4 array structure, supplied via a corporate feed network,

was created using a single AVA corrugated structure. A ground plane with a rectangular slot cut into it improved the frequency response. The radiation efficiency was found to be higher after corrugation was incorporated into the construction.

In [58], an Antipodal Vivaldi for multiband characteristics with 18 leaf-shaped structure elements was proposed. Three stages went into the development of the single-element antenna. Initially, a curved swell strip line radiator was etched and supplied by a quarter-wave transformer. The radiator's mirror image was attached to the bottom substrate using an extended stub that was partially grounded. Resonance was produced in three bands, starting with 19.81 and going up to 38.17. The radiating area was made larger with greater swell to attain resonance at lower frequencies. In order to integrate tri-band features into the final design, the radiating area was split into two swell- or leaf-shaped structures. Table 2.3 presents a summary of parallel and corporate feed array antennas discussed in section 2.2.2.

TABLE 2.3: Summary of parallel or corporate feed arrays.

Authors	Year	Developments	Ref.
Liu *et al.*	2008	A patch array antenna for 60 GHz package applications.	[66]
Mao *et al.*	2018	Antenna array with improved gain and decreased sidelobes for use at sub-millimeter wavelengths.	[63]
Zhu *et al.*	2018	A compact gain-enhanced vivaldi antenna array for 5G mm-wave application.	[71]
Ullah *et al.*	2019	A 28 GHz band broadband wire hexagon antenna array for 5G mobile networks.	[55]
Ullah *et al.*	2019	Broadband planar antenna array for future 5G communication standards.	[56]
Ullah *et al.*	2020	An array of rhombus monopole antennas optimized for millimetre waves.	[57]

Authors	Year	Developments	Ref.
Ullah *et al.*	2020	For 5G millimetre-wave use, a narrow-beam antenna with high gain.	[74]
Ullah *et al.*	2020	A novel snowflake fractal antenna for dual-beam applications in 28 GHz band.	[59]
Xu *et al.*	2020	Slotted circular patch array with a low profile for use at the Ka frequency range.	[65]
Mneesay *et al.*	2020	Unique monopole array antenna with good gain for 60 GHz mm-wave communications.	[67]
Kim *et al.*	2020	High-gain, H-shaped, planar, shorted-ring antenna array for mm-wave.	[69]
Kamal *et al.*	2021	An innovative 28 GHz hook-shaped antenna for 5G mm-wave applications.	[60]
Kamal *et al.*	2021	Donut-shaped mm-wave printed antenna array for 5G technology.	[61]
Kiani *et al.*	2021	5G antenna array with a square frame and a T-shape at 28 GHz.	[62]
Jiang *et al.*	2021	Chinese-characters Jin-shaped patch antenna array.	[68]
Hammu *et al.*	2021	Antenna array for mm-wave transmission using SIW cavities.	[70]
Ramanujam *et al.*	2021	A compact wide-bandwidth antipodal Vivaldi antenna array.	[72]
Dixit *et al.*	2021	A highly compact AVA array for 5G millimeter wave applications.	[73]
Ullah *et al.*	2021	Wideband, high-gain Vivaldi antenna designed for 5G mobile networks.	[58]
Munir *et al.*	2022	A new mm-wave antenna array with wideband characteristics.	[64]

2.2.3 Hybrid-Fed Arrays

The series feed structure is superior to the parallel feed structure because it is more compact, requires less space, and has low losses. The corporate feed, in contrast, divides the power evenly among the elements and allows for flexible inter-element spacing due to the equal arm lengths for all of the elements. As a result, a 16-element linear array was designed in [75] by taking advantage of series and corporate feed.

A microstrip line of quarter-wavelength connected an eight-element. Two of these series were fed by the Y-junction power divider. It was found that the design's simulated bandwidth ranged from 26.4 to 28.9 GHz and had an average gain of 16.4 dBi. To compensate low bandwidth, parasitic patches were added to an 8×6 array antenna [76]. The design was composed of two-layers, with rectangular tapered patches of eight sub arrays, each with six elements, engraved on the top and bottom substrates. The corporate feed was used to feed these sub arrays. The upper substrate's top side had parasitic patches resembling the radiating element, which helps to increase bandwidth.

Using 4×4 components, a hexagonal CPW series feed array antenna was designed in [77]. The patch and feed line have the CPW ground surrounding them. By expanding the array to 14 elements fed by a corporate feed, the surface wave coupling was decreased. By employing a series feed to quadruple the number of radiating elements from four to sixteen, gain and bandwidth were increased. A sequence of three extra radiating hexagonal patches was provided for each 1×4 radiating element. By using a 4×4 array, authors were able to accomplish dual-band resonance with a gain of 8.98 dBi between $21 - 23.1$ GHz and $26.86 - 28.8$ GHz.

The authors in [78], utilized a multilayer structure consisting of a SIW bandpass filter, power divider, and patch antenna radiator to create an anti-phase filtering power divider. Bandpass filtering was accomplished by three SIW made by a lower substrate surrounded by metallic vias operating in TE_{110} mode. It had a input

port for power coupling and a slot in middle for power coupling to higher layer. A coupling slot and two parallel lines of metallic vias functioning in the TE_{20} mode were present on the middle substrate. The power divider was made out of the common ground shared by the bottom and middle substrates. Four microstrip line ports were located on the middle substrate's top layer. The current at terminals 2, 4, and 5 generated a differential signal with a phase difference because their symmetries were either even (in-phase current) or odd (180° out-of-phase current). On the top substrate, a 1×4 patch array was made using a 1×2 series-fed sub array stimulated in TE_{10} mode. Each patch's top substrate had two coupling slots at its bottom. Results show an increase of 10 dBi between 27.2 and 28.5 GHz, suggesting the presence of a dual-resonance at those frequencies. Table 2.4 presents a hybrid fed array antennas discussed in section 2.2.3.

TABLE 2.4: Summary of hybrid-fed arrays.

Authors	Year	Developments	Ref.
Mohamed *et al.*	2019	A 28 GHz rectangular patch antenna array with 16 elements in the corporate series feed.	[75]
Jin *et al.*	2019	Millimeter-wave filtration patch antenna array with integrated design.	[78]
Wang *et al.*	2020	A microwave/millimeter wave dual-band shared aperture patch antenna array.	[77]
Harini *et al.*	2022	Hexagonal millimetre-wave CPW series fed antenna with 16 elements.	[76]

Patch antennas have several limitations in the context of 5G communication, despite their many advantages. Some of the notable limitations include: limited bandwidth, size and form factor, limited gain, radiation pattern and beamwidth. To address these limitations, as discussed above 5G networks use a combination of various antenna types, such as series-fed array antennas, coporate fed arrays and hybrid fed arrays. These antenna systems can provide the necessary gain, beam-forming capabilities, and coverage required for 5G communication, especially in

challenging deployment scenarios like urban environments and mm-wave frequency bands. The techniques that are discussed in above sections have been utilized for designing the antenna arrays presented in chapter 4 and 5.

2.3 Size Reduction Techniques

In antenna design, achieving smaller sizes while maintaining or improving performance is essential for applications where space constraints are critical. Several techniques are employed to reduce the size of antennas.

2.3.1 Size Reduction Using Fractal Geometries

The multiband response, compact size, and low profile are trademarks of fractal geometry methods. Radiation efficiency and electrical length of the antenna are improved by filling in fractal spaces. Mandelbrot first demonstrated the term fractal geometry to characterize a class of complex forms with a self-similar geometric structure. Natural features like mountains, coastlines, and clouds serve as inspiration for these geometries [79]. These kinds of geometries can be applied to design antennas to achieve goals such as multiband characteristics, and size reduction, etc [80]. This objective had previously been achieve through the use of numerous fractal shapes, including the Koch fractal [81], the Hilbert curve [82], the Sierpinski gasket [83], etc.

By combining two dual Koch fractals, a dual-reverse-arrow fractal (DRAF) antenna was designed in [84]. It was constructed on a patch in the shape of an equilateral triangle, and its dimensions were more compact when compared to those of the rectangular structure. These structures can be used in a variety of ways to design compact antenna arrays. Moreover, [85] created a miniature circularly polarized antenna based on Koch fractal geometry for usage in UHF RFID applications. By positioning two Koch asymmetric fractal structures in the x and y planes, the antenna's size was decreased. In addition, the diagonal axis of the

radiator was carved with four arrow-shaped slots. It was believed that the size of an antenna might be decreased by increasing the arrow-shaped slots and Koch fractal geometry's indentation angles. Table 2.5 presents size reduction techniques using fractal geometries discussed in section 2.3.1.

TABLE 2.5: Summary of size reduction techniques using fractal geometries.

Authors	Year	Developments	Ref.
Puente *et al.*	1998	Multiband fractal antennas and their sierpinski behaviour.	[83]
Gianvittorio *et al.*	2002	Applications of fractal antennas, a new method for miniaturizing antennas.	[79]
Lizzi *et al.*	2009	A DVBH/GSM/UMTS planar antenna for multimode wireless devices.	[80]
Krishna *et al.*	2009	Compact wideband Koch fractal printed slot antenna.	[81]
Azaro *et al.*	2009	A monopolar quad-band antenna based on a hilbert self-affine prefractal geometry.	[82]
Orazi *et al.*	2014	Miniaturisation of the triangular patch antenna by the novel dual-reverse-arrow fractal.	[84]
Farswan *et al.*	2015	The development of a Koch fractal circularly polarized antenna for use in portable UHF RFID readers.	[85]

2.3.2 Size Reduction Using Metamaterials

Meta-materials are artificially created materials that can support, simultaneously, negative permittivity (ε_r) and permeability (μ_r) [86, 87]. One of the most attractive branches of meta-material is the Left-handed meta-materials (LHMs). By utilizing LHMs, antennas with compact size can be designed and realized because it introduces unique features in the design that does not depend on the wavelength.
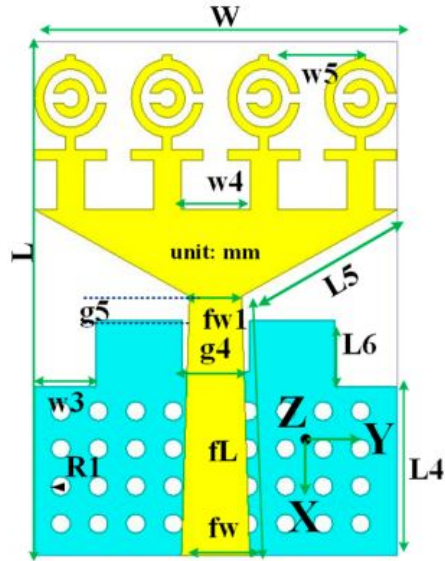
FIGURE 2.6: Metamaterial (MTM) antenna layout [91].

rather it depends on the capacitance and inductance values, which are responsible to generate negative permittivity and permeability.

Composite meta-materials were used earlier to design a compact antenna for dual-band characteristics [88]. The designed antenna showed a significant size reduction compared to similar reported antenna designs. In [89], complementary split ring resonator (CSRR) based uni-planar antenna design was presented for multiple cellular applications. The CSRR meta-material was etched from the radiating element to achieve compactness for low frequency bands. In [90, 91], a compact negative-index meta-material loaded UWB antennas were designed for breast phantom imaging. There were four individual meta-material cells in the presented antennas (see Fig. 2.6). The authors minimized the size while achieving a wide impedance bandwidth of 2.97 GHz to 15 GHz and 3.07 GHz to 19.91 GHz, because of their compact size and high gain these antenna configurations can be used in the development of mm-wave application antennas. Table 2.6 presents size reduction techniques using metamaterials discussed in section 2.3.2.

TABLE 2.6: Summary of size reduction techniques using metamaterials.

Authors	Year	Developments	Ref.

Authors	Year	Developments	Ref.
Caloz *et al.*	2005	Electromagnetic metamaterials: transmission line theory and microwave applications.	[86]
Marquees *et al.*	2011	The theory, design, and microwave uses of negative-parameter metamaterials.	[87]
Si *et al.*	2013	A dual-band antenna influenced by metamaterials that is compact, planar, and CPW-fed.	[88]
Wahba *et al.*	2014	A uni-planar microstrip CSRR metamaterial antenna.	[89]
Islam *et al.*	2015	Compact metamaterial antenna for UWB applications.	[90]
Islam *et al.*	2018	Metamaterial-inspired nine-antenna sensor array for breast phantom imaging experiments.	[91]

Size reduction techniques as discussed above are essential in 5G communication systems to design compact and efficient antennas. These techniques are crucial, especially as 5G networks require a wide range of frequency bands and advanced technologies. It's important to note that size reduction often comes with trade-offs in terms of performance, such as reduced gain or bandwidth. In this dissertation the size constraints with performance requirements while implementing the techniques in chapter 5 and 6 have been carefully looked out.

2.4 Gain Enhancement Techniques

Printed antennas have many benefits, including small size, simple fabrication, and seamless integration, and are therefore seen as ideal for many microwave and mm-wave uses. However one of their main limitations is low gain and less efficiency, which can be improved by utilizing several gain enhancement techniques.

One of the possible techniques is to use DGS, which can be developed by constructing a "defect" in the ground plane for improved antenna's performance [92]. The defects can take on any form, and they are the cause of induced perturbations, which disrupt the regularity of the ground plane and the continuity of surface currents. In addition to this, the defects have the potential to change the current distribution in the ground plane, which not only makes surface wave propagation through the substrate easier, but also makes controlled wave excitation easier. Therefore, changes the inductive and capacitive response of the feed line (transmission line) [93].

The second technique is to use frequency selective surfaces (FSSs) as the superstrate. Applications involving RF and antennas have sparked an interest in FSSs. They are typically employed as band-pass and band-stop filters, and their periodic patterns comprise either a 1D or 2D lattice [94]. To enhance the efficiency and gain of planar antennas, currently, they are being utilized as substrates or superstrates.

In [95], the authors designed a square-loop element FSS as superstrate and used it with an aperture-coupled microstrip patch antenna (ACMA). They observed that the proposed configuration offer wide impedance bandwidth with high gain. Hosseini *et al.*[96] also presented FSS superstrate design to enhance the gain of planar antenna for 60 GHz wireless applications. Some other FSS superstrate designs are also presented in the literature, which can be utilized for performance enhancement of planar antennas. Table 2.7 presents gain enhancement techniques discussed in section 2.4.

TABLE 2.7: Summary of gain enhancement techniques

Authors	Year	Developments	Ref.
Munk *et al.*	2005	Frequency selective surfaces: theory and design.	[94]
Breed *et al.*	2008	An overview of microstrip circuits with defective ground elements.	[92]
Weng *et al.*	2008	An overview on defected ground structure	[93]

Authors	Year	Developments	Ref.
Pirhadi *et al.*	2012	Microstrip antenna with a FSS substrate layer for wide-band, high-directivity aperture coupling.	[95]
Hosseini *et al.*	2014	Gain enhancement of a V-band antenna using a Fabry-Pérot cavity with a self-sustained all-metal cap with FSS.	[96]

In 5G communication systems, achieving high gain in antennas is crucial for improving signal strength, extending coverage, and supporting high data transfer. Various techniques used to enhance gain in 5G communication systems are discussed above. These techniques are utilized in chapter 5 and 6 to design high gain antenna array for 5G communication.

2.5   5G Antenna Arrays

It is established that the 5G technology provides low latency and high data rate. To accomplish the demand of high data rate, large bandwidth is required to accomplish, and higher frequency bands can be used to do this. The easiest way to accomplish high bandwidth and a high data rate for this purpose is to use mm-wave frequency ranges. ITU assigned a few potential frequency bands in the mm-wave spectrum because they allow the operators to accomplish speed, dependability, latency, and capacity. However, due to the oxygen molecules being absorbed at these frequencies, the losses are significant. Additionally, the mm-wave require small antenna and this feature can be accomplished by using printed antennas, for 5G communication systems. In order to overcome this issue, high gain antennas will need to be utilized, and one of the strategies that can be utilized to increase gain is the designing of antenna arrays. Numerous researchers have

introduced various array designs for use in 5G applications; some of these designs are discussed below:

In [97], an antenna grid array for 28 GHz 5G mobile communications was demonstrated. The proposed array had broadside radiation properties, a peak gain of 12.66 dBi, and a bandwidth of 7.16 GHz (23.86–31.02 GHz). Although the designed antenna was compact but it provides high back lobe radiations especially in H-plane. In [98], a patch antenna array was designed on LCP substrate for 60 GHz frequency band. The authors designed two arrays, each with a distinct gain of 16.7 and 17.1 dBi. Due to high mutual coupling between antenna elements, the designed arrays offer low radiation efficiency.

For use in high-speed mm-wave communication devices, a dielectric resonator (DR) filled 1×4 SIW antenna array was designed in [99]. The top metal layer was etched to form an H-shaped longitudinal slot, and then two DR layers were adhered on top of that. On the opposite side of the substrate, a transition layer from 50 Ω microstrip to SIW was placed. In [100], a 16-element mesh grid patch array was designed for 5G cellular applications operating at 28 GHz. Metallic vias spaced closely together on a 10-layer FR-4 substrate formed the radiating structure. The 5th PCB layer was used for the microstrip line's design. During the experimental testing, a significant conductor loss was detected, which meant that the antenna that had been designed could not function well in the band of interest.

In [101], a dense dielectric (DD) patch antenna array was demonstrated for 28 GHz 5G communication systems. The power for the patch array's four components, which were arranged in a circular pattern, came from a 1×4 Wilkinson power divider. Gain was improved by using an electromagnetic gap (EBG) structure ground plane and topping the array with a superstrate. Both of these modifications were made in order to improve radiation properties. A steerable antenna array was first introduced in [102] in order to support communication in the 28 GHz range. The BLC provided power for the array, which produced a wide-band response from 23.1 to 35 GHz. In addition, the array that was exhibited had a gain of 14 dBi. A radial line slot array (RLSA) for mm-wave communication networks

was presented by the authors in [103]. The bandwidth was increased by creating an air gap between the main reflector and the ground plane. For mm-wave broadband applications, a 2×2 antenna array was designed in [104]. They designed a novel U-shaped radiator supplied by a via network. The array arrangement that was shown had a gain of 10 dBi on average and a response of 24 GHz to 34 GHz. However, the size of the conceived arrangements limits their implementation in handheld gadgets.

A four-element slot array was designed in [105] for dual-band 5G communications. An elliptical slot etched from the ground plane held a sector-disk shaped radiating patch, which was fed by a proximity feed line, in each antenna element. An extra link was created between the feed line and a rectangular patch in order to enhance the antenna's transmission capabilities. In order to feed the single elements of the array, a Wilkinson power divider with a factor of 1×4 was utilized. The designed antenna had a single element that provided a wideband response that spanned from 20 GHz to 46 GHz, but the array was unable to function for wide bandwidth. A patch antenna array for 5G networks that operates at 28 GHz was presented in [106]. This array had 8×8 elements. Two patch antennas that were to be installed on opposing sides of the substrate had their feed lines connected by a via. The configuration that was offered to the authors enabled them to achieve a gain of 20 dBi while preserving a distance of −20 dB between adjacent antenna elements..

In [107], a 28 GHz series-fed MIMO phased array was presented for 5G applications. The arrays that were designed had a compact size while still having desirable characteristics. A 2D array was designed for use in multiband mm-wave applications in [108]. The idea behind the array came from the Franklin linear array. The antenna array on display has a triple-band response, with gains at 28 GHz, 33 GHz, and 38 GHz, respectively, of 13.5 dBi, 8.33 dBi, and 9.58 dBi. An inset-fed microstrip patch array was introduced in [109] for 5G applications. To boost the bandwidth, the authors applied a parasitic patch on top of each inset-fed patch. Maximum isolation between the array items could be attained by
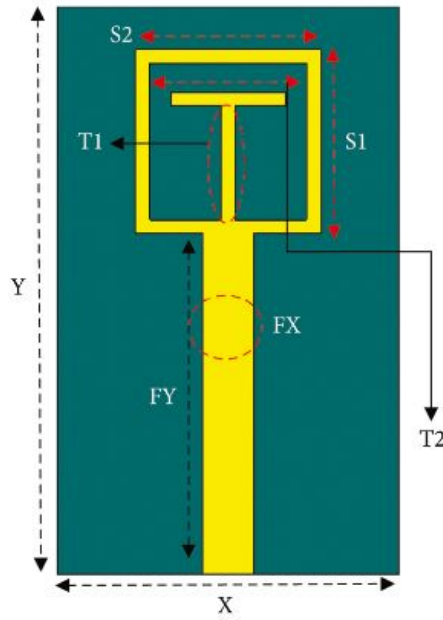
FIGURE 2.7: Square-Framed T Shape mm-wave Antenna Array [62].

not aligning them. Furthermore, the authors discovered that the suggested setup yielded a gain of about 20 dBi.

In [56], a 1×4 array of antenna elements and its associated feed network are presented for use in future 5G communication. It was proposed to use a four-way planar feeding network with its own T-junction and 90° turns for each individual section. In addition, over 83% radiation efficiency was attained across the full operating range, with a peak gain of 11.5 dBi. A planar mm-wave antenna with a high gain of 10.7 dBi and a broad bandwidth of 10.51 GHz was presented in [74]. This antenna was able to function at frequencies ranging from 23.41 to 33.92 GHz. Each antenna element in the linear array was excited by using a low transmission loss four-way feed network. The antenna array's dependability and outstanding performance despite its small and compact dimensions make it a prime candidate for use in the forthcoming 5G communication in the mm-wave spectrum.

A 10.12 dBi gain antenna array at 28 GHz was reported in [59] for mm-wave communication. In the mm-wave band, the antenna demonstrated several beneficial features that were quite helpful when used for high-speed transmission. Using the 28 GHz band for millimeter wave applications, a new hook-shaped antenna

displayed broadband properties [60]. An impressive 3.65 dBi gain was achieved over a typical single-element antenna. The gain was enhanced to as much as 10.3 dBi by integrating the suggested antenna into a four-element array for millimeter wave systems. Additionally, the radiation and overall efficiency were both higher than 85%. With each element measuring just 10×8 mm^2 and the entire array measuring 26×19.5 mm^2, the suggested antenna had a modest footprint. The proposed antenna's useful features and high efficiency made it a viable candidate for inclusion in future high-speed mm-wave transmission systems.

A unique T-shaped planar antenna structure has been presented in [62] for mm-wave applications operating at a frequency of 28 GHz (see Fig. 2.7). With just one element, the efficiency of the proposed antenna is over 97%, and its gain is 4.25 dBi. The suggested T-shaped antenna can be transformed into a four-element linear array to provide it radiation properties of two narrow beams at 180° and 0°, and high gain of up to 11.5 dBi. These attributes are achievable with the suggested antenna. The antenna array measures 18.5×24 mm^2 in total surface area.

Table 2.8 presents 5G antenna arrays discussed in Section 2.5.

TABLE 2.8: Summary of antenna arrays for 5G applications.

Authors	Year	Developments	Ref.
Chen *et al.*	2013	Antenna array grid for 5G mobile communication at 28 GHz.	[97]
Cabrol *et al.*	2014	Patch antenna array on LCP substrate.	[98]
Ashraf *et al.*	2014	DR loaded SIW antenna array for high speed mm-wave communication systems.	[99]
Hong *et al.*	2014	28 GHz 5G cellular applications using a 16-element mesh grid patch array.	[100]
Haraz *et al.*	2014	5G wireless networks using a DD patch antenna array at 28 GHz.	[101]
Orakwue *et al.*	2015	Steerable antenna array for 28 GHz frequency band.	[102]

Authors	Year	Developments	Ref.
Maina *et al.*	2015	Radial line slot array for 5G communication systems.	[103]
Zhai *et al.*	2015	Broadband 2×2 antenna array for mm-wave applications.	[104]
Haraz *et al.*	2015	Four elements slot antenna array for dual-band 5G communication networks.	[105]
Haraz *et al.*	2015	8×8 elements based patch antenna array for 28 GHz 5G applications.	[106]
Khalily *et al.*	2016	Series-fed MIMO phased arrays for 28 GHz 5G applications.	[107]
Jilani *et al.*	2017	2-D array design for multiband mm-wave applications.	[108]
Khalily *et al.*	2018	16-elements based linear antenna array for 5G applications.	[109]
Ullah *et al.*	2019	Broadband planar antenna array for future 5G communication standards.	[56]
Ullah *et al.*	2020	A high gain and wideband narrow-beam antenna for 5G millimeter-wave applications.	[74]
Ullah *et al.*	2020	A novel snowflake fractal antenna for dual-beam applications in 28 GHz band.	[59]
Kamal *et al.*	2021	A novel hook-shaped antenna operating at 28 GHz for future 5G mm-wave applications.	[60]
Kiani *et al.*	2021	Antenna array for potential 5G devices in the form of a squared-off T operating at 28 GHz	[62]

While 5G antenna arrays offer numerous advantages, they also come with certain limitations and challenges such as complexity and cost, size, power consumption, deployment challenges, propagation at mm-wave frequencies, limited coverage area and latency. To address these limitations, 5G network operators and equipment

manufacturers are continually researching and developing solutions, including advanced signal processing algorithms, efficient power management, interference mitigation techniques, and regulatory compliance strategies. Some design techniques are proposed in chapter 4, 5 and 6 to mitigate the issues related to 5G antenna arrays.

2.6   Research Gaps and Problem Formulation

From the discussion presented above, it can be noted that the antennas and arrays presented earlier provide good performance parameters, but for a simple structure, the majority of them have a narrow bandwidth. To mitigate this problem, the researchers used complex feed structures or antenna geometries, which tend to increase the complexity of the system. On the other hand, high gain is also achieved but at the cost of large sizes. To overcome these limitations, research gaps, as appended below, have been identified, which could possibly be addressed in this dissertation.

(a) The major problem of techniques for reducing the size of antenna arrays is to maintain their electrical performance. Currently, there are a limited number of reported designs where size reduction has been done without sacrificing performance. Additionally, for such designs, there is a need for improved methods to reduce transmission line mismatch between elements. Other new technologies are also in demand where one can have better control over the radiation pattern of an antenna array.

(b) The main problem with series-fed antenna arrays is that they require the transmission line to be matched at both ends. This is difficult to achieve and requires careful tuning and adjustment of the antenna system. Alignment of antenna elements is also important, as this ensures that they will receive the same signal. Otherwise, the array will not work properly. Additionally, series-fed antenna arrays are not as efficient as other types of antenna arrays

and may be more prone to interference. Another related research gap is the efficient optimization of serial-fed antenna arrays. Although there has been progress in this area, much remains to be done. Finally, further study of the design of series-fed array antennas for particular uses is also a potential area of investigation.

(c) Hybrid array antennas are generally more expensive than other types of antenna arrays, but offer greater flexibility and efficiency. A research gap in hybrid array antenna systems is in the area of optimized design. Currently, most designs are limited to narrow-band applications. There is also a need for improved techniques for managing the antenna array radiation pattern and minimizing transmission line mismatch between components.

(d) For 5G applications, it is necessary to have high-performance broadband planar antennas that are compatible with current technological needs. Apart from its compatibility, the proposed design should also be compact to ensure efficient use of space. In addition to these constraints, the designed antenna must offer relatively better or compatible bandwidth to verify its usefulness in mobile devices. Besides the usual design techniques, size reduction as well as acceptable electrical performance can be realized by engaging metasurfaces. It is therefore envisaged that a combination of metasurfaces with an innovative design structure can be investigated to meet these requirements.

2.7   Research Methodologies

The development of antennas for 5G technology involves various research methodologies to create efficient and high-performance antenna systems that meet the demanding requirements of 5G networks. Some of the key research methodologies used in this dissertation for designing antennas includes: simulation and modeling, mm-wave frequency band, metasurfaces, fabrication and testing. The simulation and modeling of all the designed antennas and arrays are done using Computer Simulation Technology (CST) Microwave Studio 2021. The designed antenna and

arrays operates in mm-wave frequency spectrum. To measure far field performances an anechoic chamber room is utilized for chapter 5 and 6. Precision network Analyzer (PNA) E8363C by Agilent technologies is used to measure the fabricated prototype to validate simulations results of chapter 5. Furthermore, metasurfaces are also utilized in chapter 6 to enhance the gain of antenna. While Precision network Analyzer (PNA) from keysight is used to measure the fabricated prototype to validate the results of chapter 6.

2.8   dissertation Contribution

In this dissertation, an effort would be made to design antennas and arrays using simple structures for 5G communication. The proposed structures must be compact and easy to manufacture. In order to reduce manufacturing costs, the proposed designs must be compatible with a low cost chemical etching technique. The end product should provide high gain and wide impedance bandwidth for its potential use in 5G communication technology.

2.9   Summary

In this chapter, an in-depth literature review on antennas and mobile communication, their evolution from 1$^{\text{st}}$ to 5$^{\text{th}}$ generations was presented. It has been established that in the growth of mobile technology, the antenna has played a central role, especially the patch antenna. 5G mobile technology now requires strict conditions to be met by the antenna in order to meet user needs in totality. In this respect, on the one hand, the technology requires a high efficiency antenna; while, on the other hand, the downsizing of various mobile gadgets requires the antennas to be as small as possible for economical use of space.

The patch antenna has been shown to play an important role in the future growth of mobile technologies, especially in the mm-wave regime. An increased use of

patch antennas and arrays in mobile applications has been seen due to their light weight and ease of fabrication. It has been noticed that series, parallel, corporate and hybrid fed arrays play a phenomenal role in determining the characteristics of a patch antenna. Thus, should be given a due consideration in an antenna design.

It is discussed that a continuous effort has been made by industry/researchers to reduce the size of the antenna, involving various techniques. The chapter discusses the size reduction of an antenna using fractal geometries and meta-materials. It has been shown that either of these two technologies can be used to reduce the size of patch antennas without compromising their electrical performance. In addition, gain enhancement techniques are also described in detail for mm-wave applications.

The chapter further presents details regarding 5G antenna arrays, normally used to improve gain and add beam steering capabilities. It was also mentioned that with the massive growth of mobile technology, 5G MIMO antenna arrays are also being rolled out. Based on the survey presented in this chapter, research gaps in patch antenna technology have been identified. It has been established that for 5G mm-wave communication, there is still a strong demand for efficient patch antennas of relatively small sizes.

Chapter 3

Equilateral Triangular Slot-based Planar Rectangular Antenna for Millimeter-wave Applications

3.1   Introduction

As discussed in Chapter 2 different design topologies have been explored by the researchers that can be utilized for future 5G communication. In this chapter, a novel design topology has been investigated in compliance to 5G communication requirements. The chapter presents the planning and execution of a small rectangular patch antenna for wide-band mm-wave communication devices, featuring a slot in the shape of an equilateral triangle. The proposed antenna design has a high impedance bandwidth of 16.86 GHz from 22.28 to 39.14 GHz, an antenna efficiency of >85%, and a peak gain of 6.86 dBi. The antenna structure that has been proposed is simple and easy to fabricate.

5G mm wave spectrum has become a popular option because it provides high bandwidth, low latency, and increased data throughput compared to its counterparts [110]. A large bandwidth is required to provide a high data rate, which can be done by using higher frequency bands [111]. Potential prospects for future 5G

standards in the mm wave spectrum include the 28/38 GHz band, the $57-64$ GHz (O_2 band),and $164-200$ GHz (H_2O) band. The frequency range of 57–64 GHz, also known as the 60 GHz band, plays a specific role in 5G communication. The 60 GHz band is particularly interesting for 5G due to its large bandwidth availability. However, it's important to note that the 60 GHz band has some unique characteristics. Signals at this frequency have shorter wavelengths and are subject to higher atmospheric absorption and attenuation compared to lower frequency bands. This means that the signals have a shorter range and are more susceptible to being absorbed by atmospheric gases and obstacles like buildings and foliage. Consequently, deploying 5G in the 60 GHz band requires careful planning and deployment strategies to overcome these challenges and ensure reliable coverage. The frequency range of 164–200 GHz (H_2O) band is part of the extremely high-frequency (EHF) spectrum. This frequency range is often referred to as the "THz band" since it falls within the terahertz frequency range. Water vapor absorption plays a significant role in this frequency range because it exhibits strong absorption characteristics within the 164–200 GHz range. As a result, the propagation distance of signals in the THz band is relatively short, typically limited to a few meters or less. Due to the high absorption and limited propagation characteristics, the practical applications of the 164–200 GHz frequency range in 5G communication are limited. However, this frequency band can be used for short-range, high-speed communication links, such as point-to-point wireless links or localized indoor applications where the signal does not have to propagate through the atmosphere over long distances.

The frequency bands at 26 GHz (24.25-27.5 GHz) and 28 GHz (26.25-29.5 GHz) are the most crucial in terms of speed, dependability, latency, and capacity. The development of low-profile, high-bandwidth, and high-gain antennas is necessary for seamless integration into mm-wave transmission devices [15]. Researchers have proposed a wide range of antenna designs for use in 5G networks. SIW antennas [70, 112], empty substrate integrated waveguide (ESIW) antennas [113], and planar antennas [60, 61, 114] are some examples. The most practical of these structures

are planar antenna configurations because they are easy to fabricate, affordable, and adaptable for use in small communication devices.

3.2   Targeted Specifications

3.2.1   Bandwidth

A bandwidth antenna is the range of frequencies where its performance meets predefined requirements for specific characteristics. The spectrum is the range of frequencies that are on either side of a center frequency (usually the dipole resonance frequency) where the antenna characteristics (i.e., radiation efficiency, gain, side lobe level, beam direction, input impedance, pattern, beam-width, polarization, and side lobe level) fall within a reasonable range of those situated at the center frequency. A broadband antenna's bandwidth is commonly obtained by dividing its upper and lower operational frequencies by their ratio.

3.2.2   Efficiency

Radiation efficiency, another name for an antenna's efficiency, is defined as the ratio of the power that the antenna receives to the power that it emits and it can be written as:

$$\eta = \frac{P_{rad}}{P_i}$$

where η is the efficiency of an antenna, P_{rad} and P_i are radiated and input power, respectively.

3.2.3   Directivity

The percentage of the antenna's radiation strength in a given direction relative to the total average radiation intensity across all directions. Average radiation

intensity is calculated by dividing the total power radiated by 4π. In the absence of a direction statement, the direction of maximum radiation intensity is presumed.

$$D = \frac{4\pi U}{P_{rad}}$$

where radiation intensity is denoted by U (W/unit solid angle).

3.2.4 Gain

An antenna's gain is defined as the ratio of its intensity in a given direction to the radiation intensity that would arise from the antenna accepting power radiated isotropically (in that direction) and can be written as:

$$G = \eta D$$

where D is the directivity. The targeted specifications of the proposed antenna are discussed in Table 3.1.

TABLE 3.1: Specification Table.

Variable	Target
Bandwidth	15 GHz
Efficiency	>75%
Peak gain	6 dBi
Size	6×8 mm²

3.3 Millimeter-wave Antenna Design

The design of the proposed planar wide-band antenna is depicted in Table 3.2, and its design is expressed in Fig. 3.1. The fundamental expressions governing the designs are appended below:

$$f_r = \frac{c}{2\sqrt{\varepsilon_{\text{eff}}\, \varepsilon_0}}\sqrt{\frac{\varepsilon_{\text{eff}}}{L-W}} \tag{3.1}$$

The speed of light in a vacuum is represented by c, which is approximately $3{\times}10^8$ meters per second. The length and width of the antenna are L and W, the resonant frequency of the patch antenna is f_r (in Hertz), the effective relative permittivity of the substrate material, on which the patch antenna is built, is ε_{eff}, and the permittivity of free space is ε_0, which is approximately 8.854×10^{-12} farads per meter.

$$W = \frac{1}{2f_r\sqrt{\mu_0\varepsilon_0}}\sqrt{\frac{2}{\varepsilon_r+1}} = \frac{v_0}{2f_r}\sqrt{\frac{2}{\varepsilon_r+1}} \tag{3.2}$$

where the relative permittivity of the substrate is ε_r, the permeability of free space is μ_0, and the speed of light in free space is v_0.

$$L = \frac{1}{2f_r\sqrt{\varepsilon_{reff}}\sqrt{\mu_0\varepsilon_0}} - 2\Delta L \tag{3.3}$$

A broad impedance bandwidth is achieved by constructing the back side of the antenna element as a partial ground plane. The antenna element's front side has an equilateral rectangular patch filled with triangles, which receives electricity from a 50Ω microstrip feeding line. Designing antennas makes use of the Rogers RT/Duroid 5880 low-loss dielectric substrate. The chosen values for the substrate's thickness and dielectric constant are 0.51 mm and 2.2, respectively. Calculations show that the total dimensions of the antenna are $W_S \times L_S = 6.5{\times}8.5$ mm^2.

Three distinct stages make up the design process for the suggested antenna. A partial ground plan is built for a rectangular patch antenna, as shown in Fig. 3.2(a). The rectangular patch does not resonance, as the result is displayed in Fig. 3.4. Fig. 3.2(b) shows that an equilateral triangular groove is carved into the rectangular patch to trigger higher-order modes. The desired band's wide impedance bandwidth was achieved by adding a slot to the patch (see Fig. 3.4).

TABLE 3.2: Design parameters used for planar wide-band antenna design (all dimensions in mm).

Parameter	Value	Parameter	Value
W_P	5	L_P	6
W_F	1.4	L_F	2
W_1	4	L_1	5
W_2	1	L_G	1.8

The bandwidth can be further increased and optimal impedance matching can be achieved by moving the feeding line from $x = 0$ to $x = 0.3$ mm, as shown in Fig. 3.2(c). This change shifts the lower frequency response to 22.28 GHz and the upper frequency response to 39.14 GHz. As shown in Fig. 3.3, the designed antenna was also investigated with full ground plane and it is observed that the antenna does not resonate in the band of interest.

To gain greater insight into the performance of the antenna, a parametric research is carried out. For this reason, by changing the values of W_1 and W_2, the impact on the antenna's reflection coefficient (S_{11}) is evident. Fig. 3.5(a) illustrates how the value of W_1 affects the antenna's performance when it is changed in steps of 0.5 mm, from 2 to 4 mm. It is evident that at lower values of W_1 (between 2 and 3 mm), the antenna's impedance bandwidth is rather narrow and its impedance matching is not good. Fig. 3.5(a) illustrates the antenna's wide impedance bandwidth when the value of W_1 is increased. Conversely, when W_2 fluctuated between 1 and 5 mm, the antenna exhibited different behavior. As W_2 is increased, there is a noticeable decrease in the impedance bandwidth, as Fig. 3.5(b) illustrates. It is possible to conclude from the results that W_2 is a key factor in delivering favorable qualities.
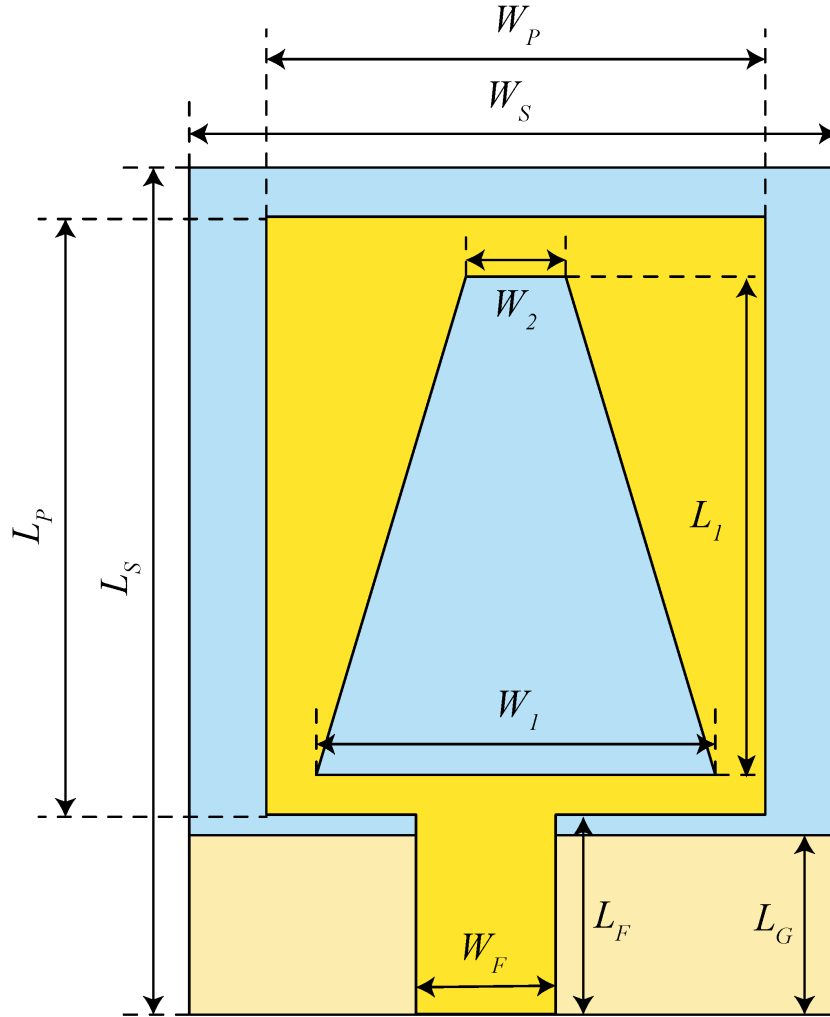
FIGURE 3.1: Schematic of the proposed mm-wave antenna (blue: substrate, light orange: ground plane, orange: radiating structure).

3.4 Simulation Results and Discussion

Using Computer Simulation Technology (CST) Microwave Studio 2021, the proposed wide-band antenna was designed and simulated. The simulated S_{11} response of the proposed antenna is depicted in Fig. 3.6. The antenna performs in the frequency range of 22.28–39.14 GHz when measured according to the criteria of -10 dB impedance bandwidth, and it has a resonant frequency range of 24.18–37 GHz when measured according to the criteria of -15 dB impedance bandwidth. This can be seen in Fig. 3.6. The observed impedance bandwidths for both ranges are 16.86 and 12.82 GHz, respectively, while the fractional bandwidths are noted to be 50.94% and 41.9%, respectively. Based on these findings, one can conclude
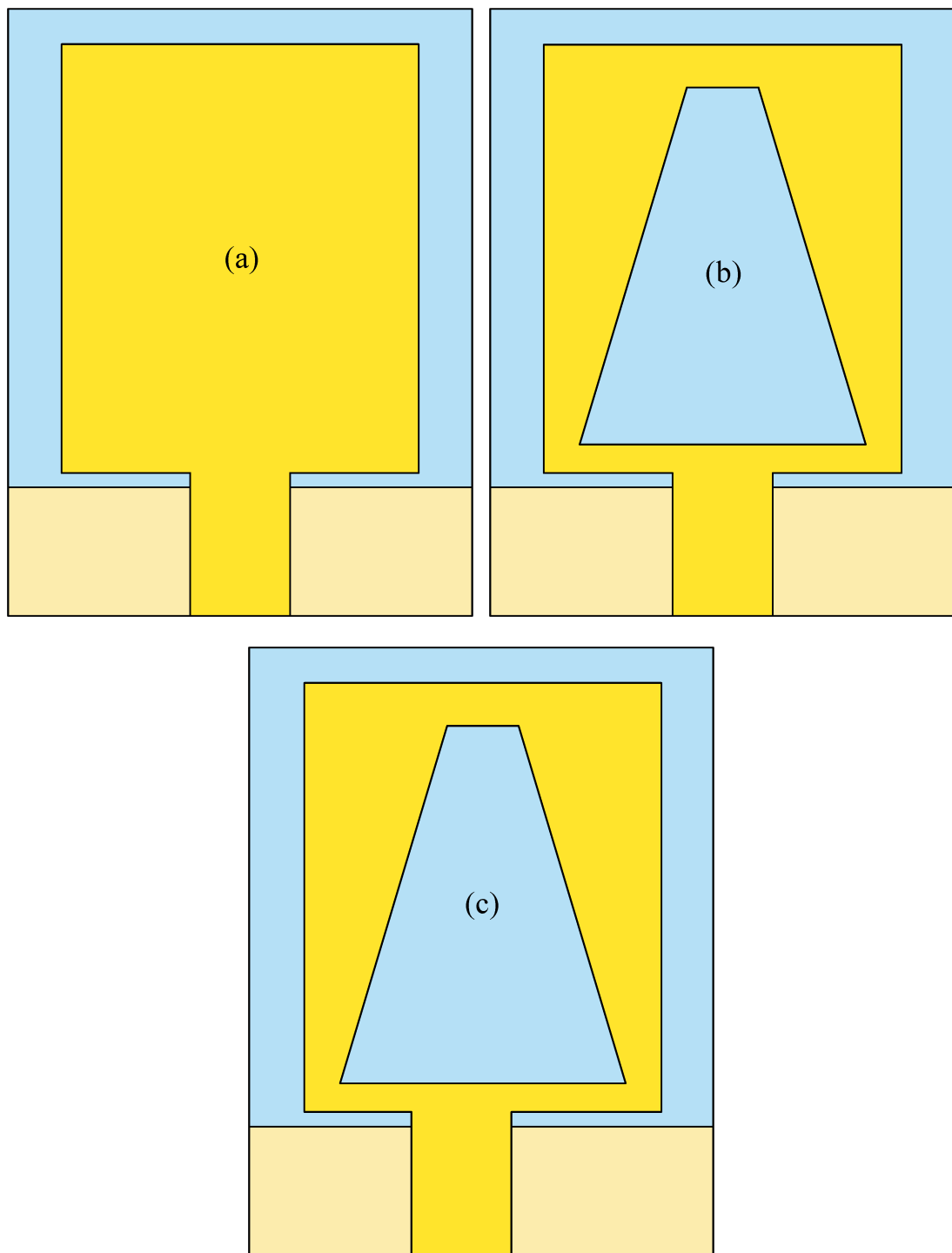
FIGURE 3.2: Design iterations of the proposed mm-wave antenna (a) Step-1, (b) Step-2, and (c) Step-3 (Proposed).
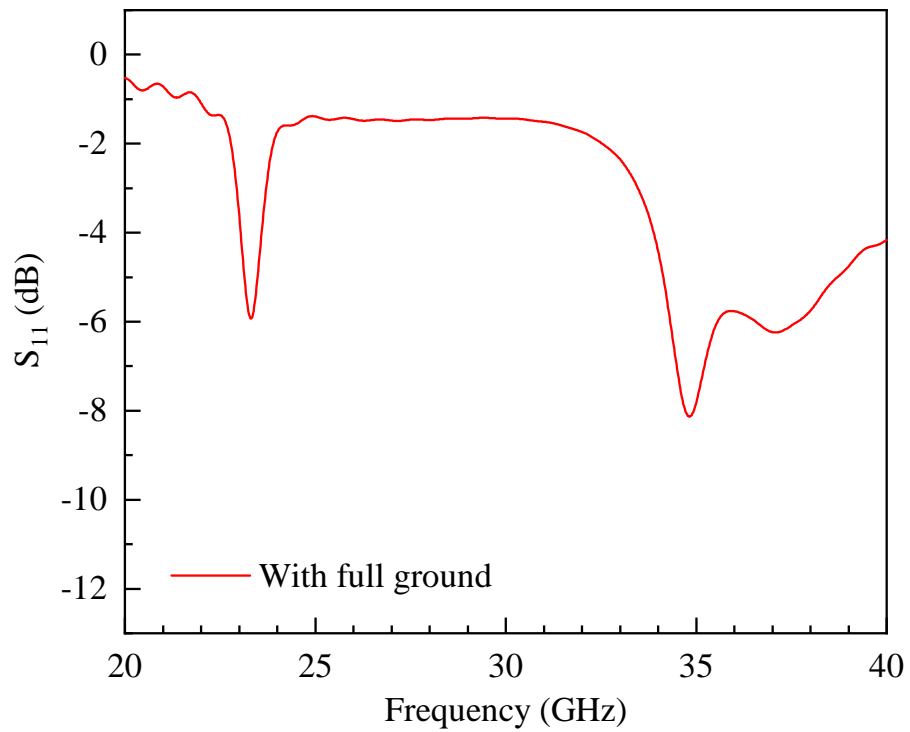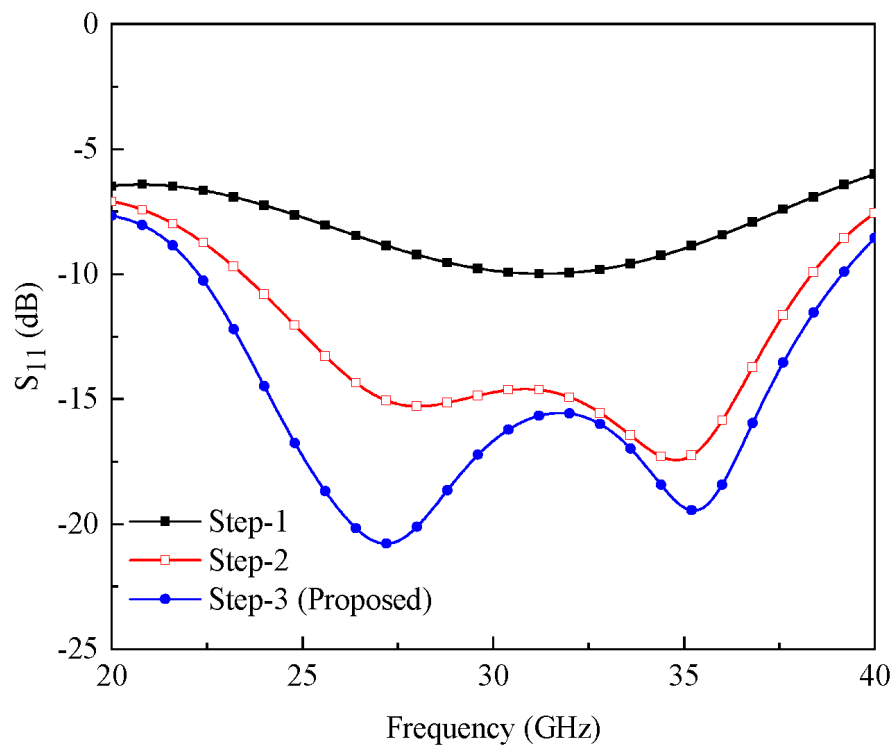
FIGURE 3.3: Simulated S-parameters with full ground.

FIGURE 3.4: Simulated reflection coefficients (S_{11}) for different design stages.
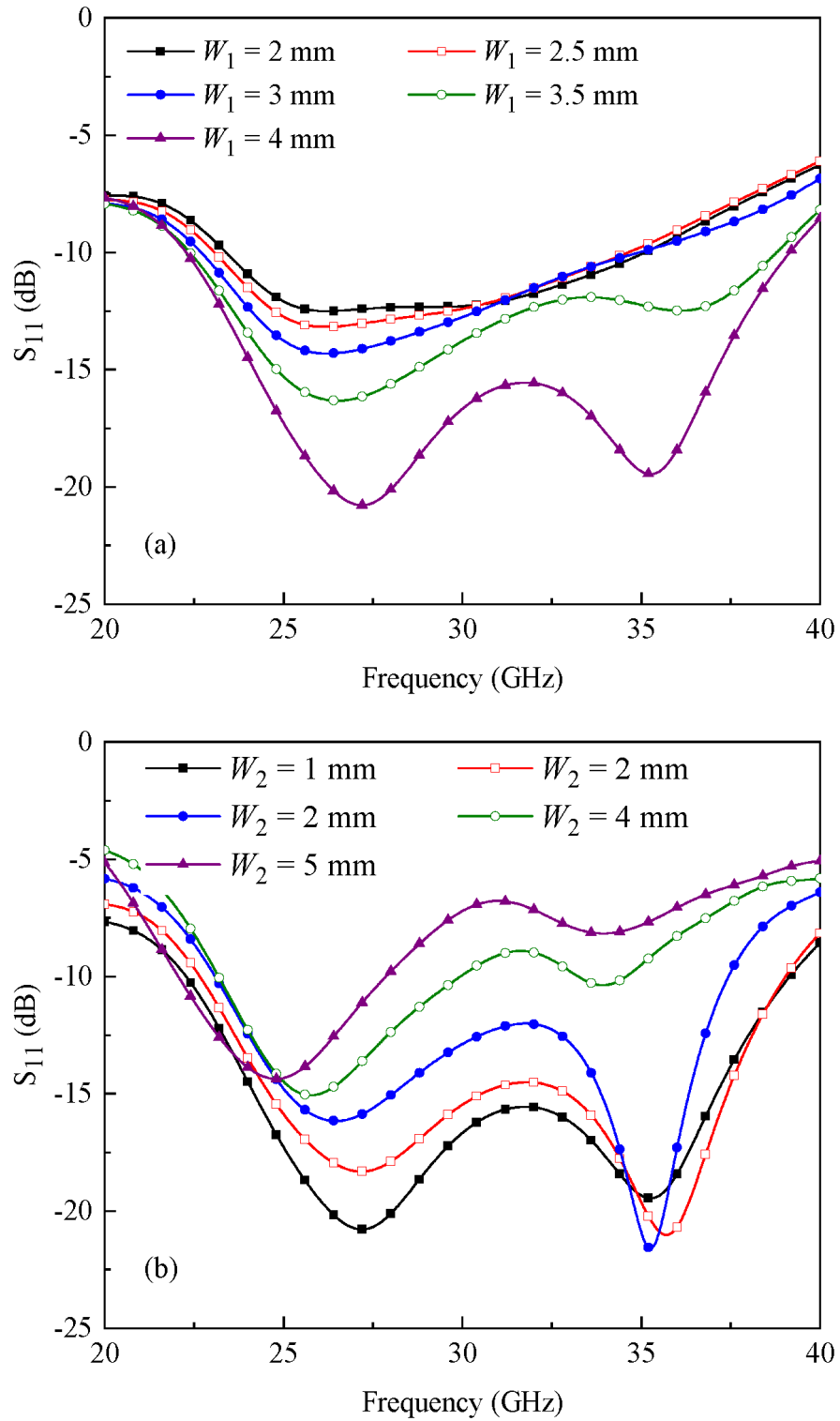
FIGURE 3.5: Impact of (a) W_1 and (b) W_2 on antenna's performance.

that the developed antenna, with its wide coverage of the frequency bands, is a suitable option for mm-wave 5G applications.

The simulated surface current distribution of the proposed planar antenna at 27 and 35 GHz is shown in Fig. 3.7. It can be observed from the figure that the current is distributed uniformly on the ground plane and on the radiating zone. Additionally, dense current distributions are observed around the lower parts of the triangular slots for both frequencies, i.e., 27 GHz and 35 GHz, indicating minimal reflection on these frequencies, and hence the contribution of the slots to obtain maximum transmission in the bands of interest. Fig.3.8 depicts that the current seems to flow without congestion anywhere along the antenna. Fig. 3.9 illustrates how a uniform current distribution resulted in a large gain.

The total efficiency and realized antenna gain are depicted in Fig. 3.9. The proposed antenna has an efficiency of more than 85% over the desired bandwidth, with a peak efficiency of 90.3% at 34.5 GHz. Moreover, the gain of the suggested antenna rises linearly with frequency. The antenna has an average gain of 5.47 dBi over the whole operating frequency range, according to observations. A gain of 3.89 dBi is obtained at 22 GHz, and a gain of 6.86 dBi is observed at 36 GHz (Fig. 3.9).

The simulated radiation characterisitics for the H and the E planes in terms of co-polarization (co-pol) and cross-polarization (X-pol) are depicted in Figs. 3.10 and 3.11. Four different frequencies, including 26 GHz, 28 GHz, 32 GHz, and 36 GHz, are used to plot the radiation patterns. The extensive radiation coverage of the suggested antenna is demonstrated by the co-pol pattern. As can be seen in Fig. 3.10, the radiation pattern of the H plane antenna is directional for 26 and 28 GHz, with the primary beam pointing in the direction of 90°. For 32 and 36 GHz, on the other hand, it resembles a monopole. As seen in Fig. 3.11, the antenna provides dual-beam in the case of the E plane, with patterns titled towards ±30°. In addition, the cross-polarization (X-pol) components for both planes are noted to be ≤ -10 dB, as shown in Figs. 3.10 and 3.11. The 3-D radiation pattern of the designed antenna is shown in the Fig. 3.12, it is observed that the designed
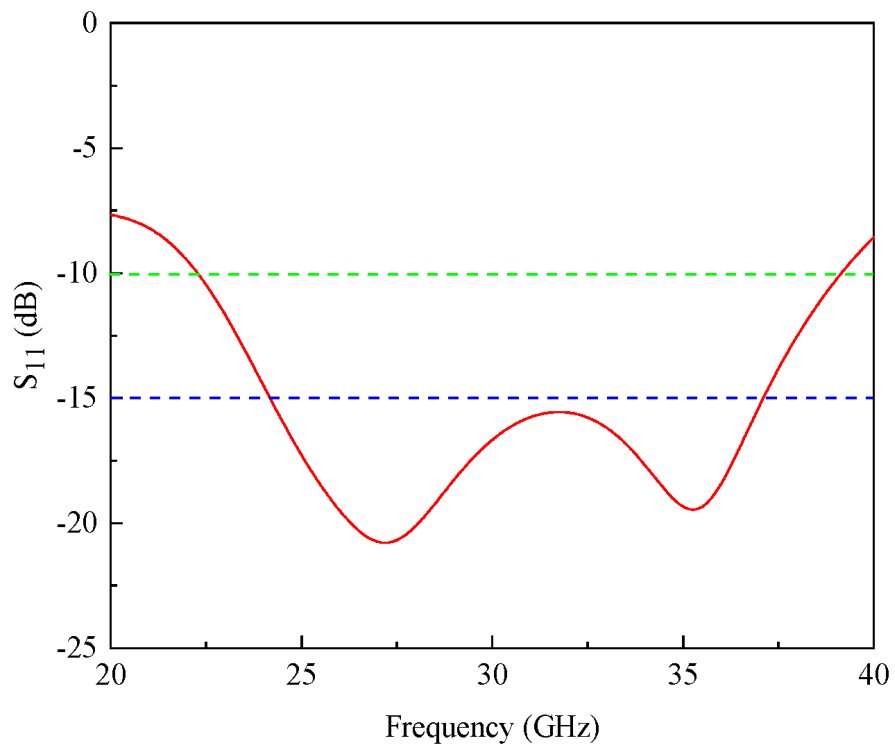
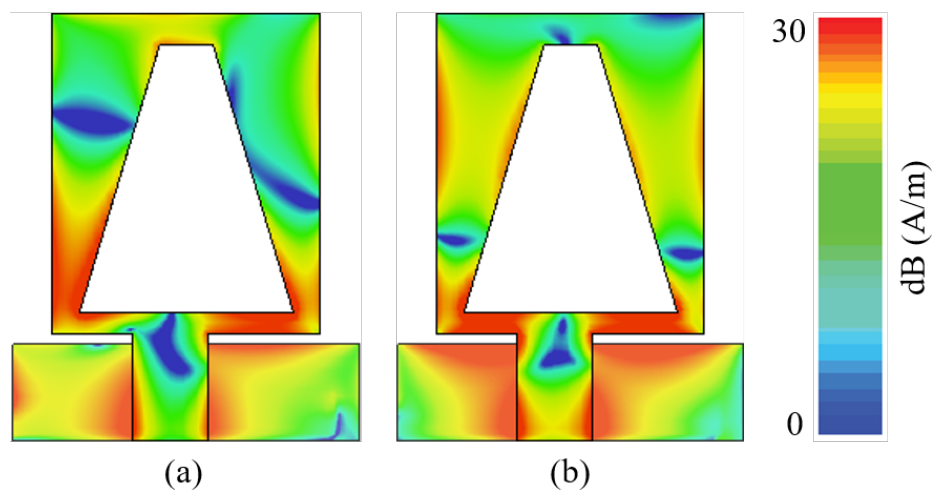FIGURE 3.6: Simulated reflection coefficient of the proposed mm-wave antenna.

FIGURE 3.7: Simulated surface current distribution of the proposed mm-wave antenna at (a) 27 GHz and (b) 35 GHz.
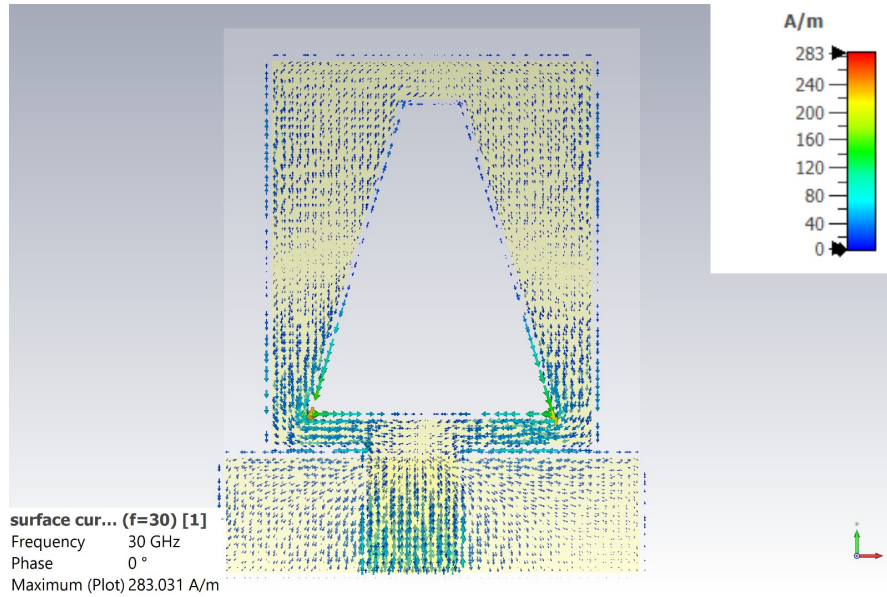
FIGURE 3.8: Simulated current plot of the proposed mm-wave antenna.
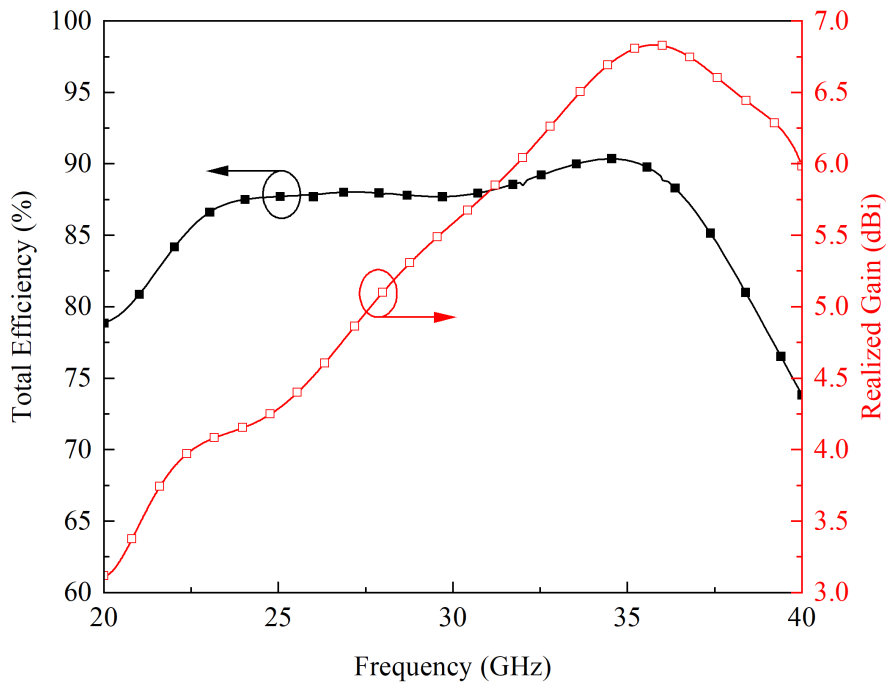

FIGURE 3.9: Simulated total efficiency and realized gain of the proposed mm-wave antenna.

antenna exhibits linear polarization. Table 3.3, provides a comparative analysis of previously planned and exhibited antennas. The table shows that the designed antenna is significantly smaller in size with relatively high efficiency and gain than the designs presented in the literature.
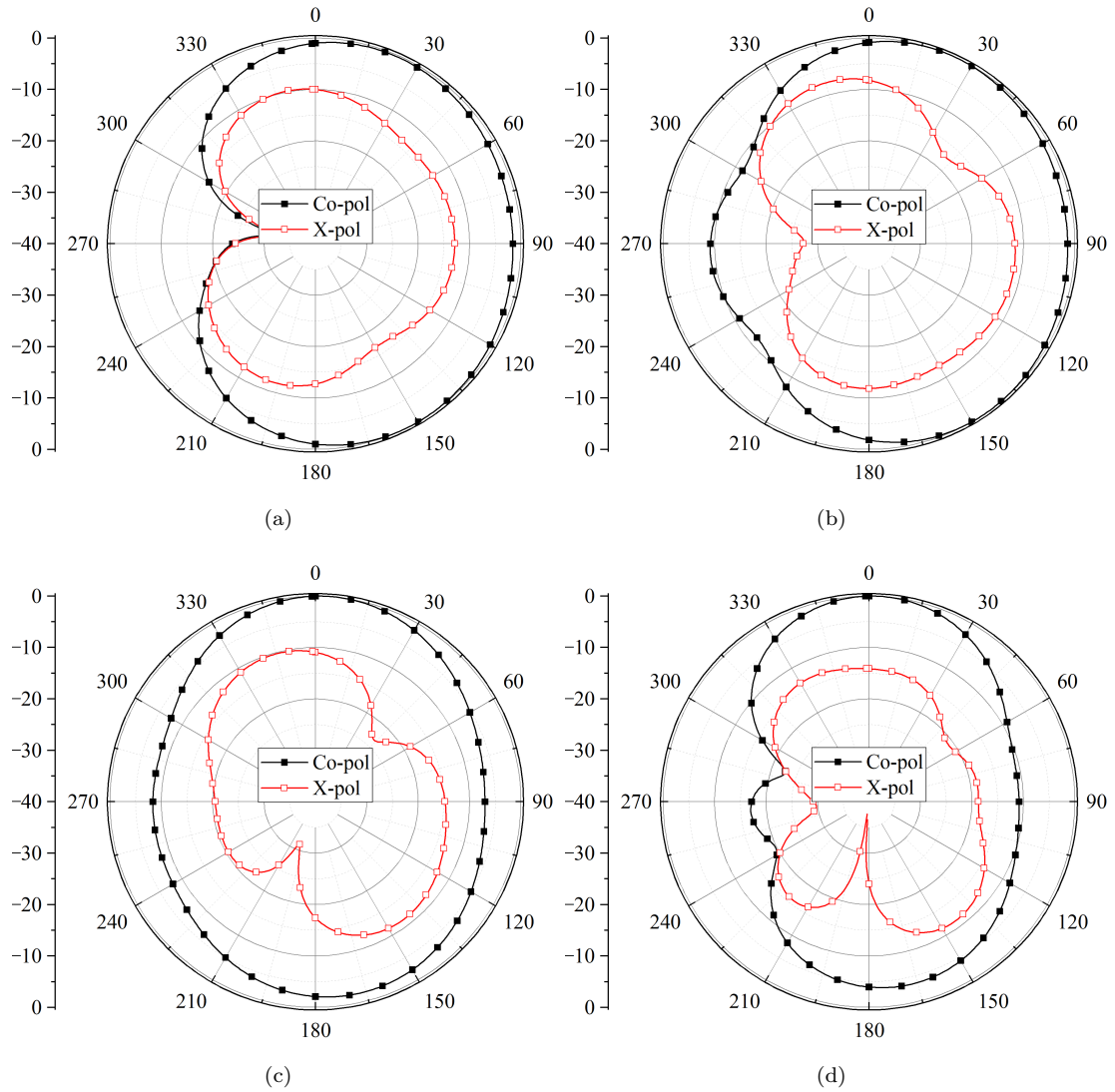
FIGURE 3.10: Radiation characteristics of the proposed mm-wave antenna for H plane at (a) 26 GHz (b) 28 GHz (c) 32 GHz (d) 36 GHz.

TABLE 3.3: Comparison between proposed antennas and previously published literature.

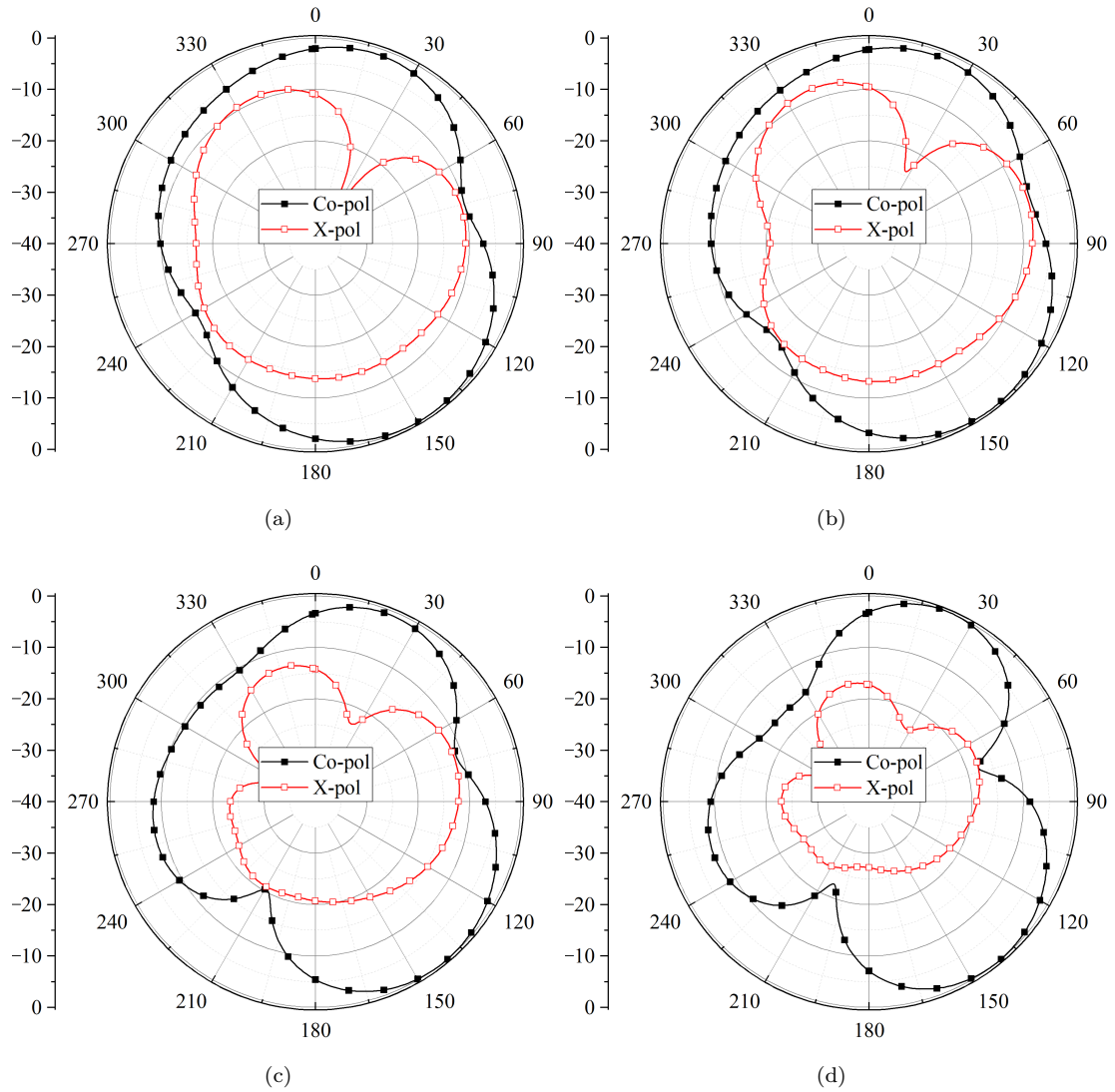| Ref.	Dimensions		Frequency	Efficiency	Gain
	(mm^2)	(λ^2)	(GHz)	(%)	(dBi)
[115]	12×12	1.12×1.12	28	94	4.54
[116]	55×110	5.1×10.2	28	89.74	7.88
[117]	5×5.26	0.467×0.491	28	-	5.2
This work	6.5×8.5	0.606×0.794	28	> 85	6.86

FIGURE 3.11: Radiation characteristics of the proposed mm-wave antenna for E plane at (a) 26 GHz (b) 28 GHz (c) 32 GHz (d) 36 GHz.

3.5   Summary

This chapter presents a wide-band antenna designed to be used for millimeter wave applications. The designed antenna is structured as a rectangular equilateral triangular slot resonator supported by a partial ground plane. In addition to the findings, a comprehensive study of the design process and its individual stages is presented. The antenna has a broad impedance bandwidth of 16.86 GHz, spanning from 22.28 to 39.14 GHz, as the simulated data demonstrates. Furthermore, an efficiency of more than 85% and a maximum gain of 6.86 dBi are reported when the antenna is employed within its operational bandwidth. Additionally, the proposed
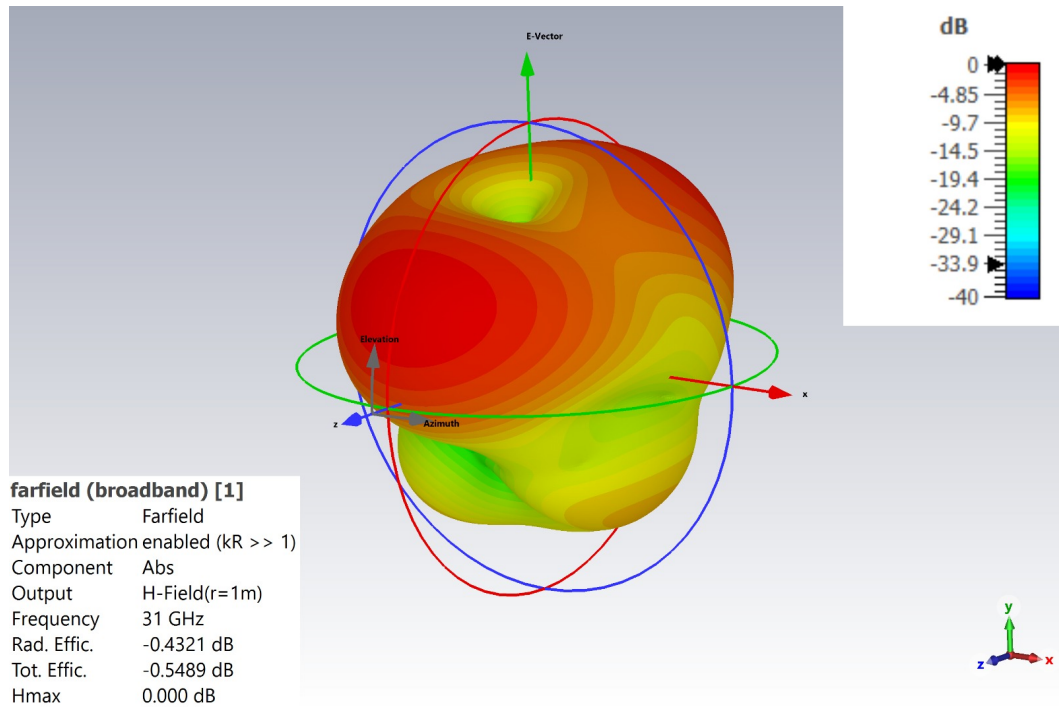
FIGURE 3.12: The 3D Radiation pattern using CST simulation technique.

antenna is compact and can be easily used in devices where the space available for antenna integration is limited. However, the observed gain is not that exciting and its applications in 5G technology might be limited. To overcome this problem, it is planned in the next chapter that another design technique will be studied and simulated as a possible candidate for future 5G communication devices.

Chapter 4

Semi-Ring Patch Array Antennas for High Gain mm-wave Applications

4.1 Introduction

In the previous chapter, a simple patch antenna was designed and studied for 5G communication devices using the millimeter wave band. Continuing the same concept, additional design topologies have been explored in this chapter to overcome the gain problem observed in the previous design. Two different designs of 1×2 patch antenna arrays are presented for 5G mm-wave applications. High gain and wide bandwidth are the two main characteristics of the reported antenna arrays that made them suitable for 5G communications systems. Additionally, the arrays investigated are simple and compact in size, which enable their potential use in 5G smart devices.

In the modern era, the non-stop expansion of wireless devices has noticeably developed the standard of mobile communication [118, 119]. The annual increase in data rates is swiftly rising from 40% to 70%. Furthermore, future wireless communication systems will require 1,000 times the bandwidth of today's systems. To

fulfill the demand, mm-wave 5G communication technology is a promising solution. 5G networks are able to provide a high data rate of up to 20 Gbps [120, 121] and high bandwidth [122]. However, there are some challenges in the mm-wave spectrum, such as free-space propagation losses, atmospheric attenuation, and signal degradation. The development of high-gain antennas is a potential solution to this issue [123].

To achieve the above-mentioned requirement, many high-gain antenna designs have been presented in the literature. For example, in [55], a 1×4 planar array was presented for a 28 GHz application. A hexagonal-shaped patch was selected as a radiating element, and the array was built using a broadband corporate feeding network. For dual-band 5G communications systems, a circular patch array of 1×4 that is fed in a series was presented in [52]. By etching an elliptical slot in a circular patch, a dual-band response was achieved. Moreover, the peak gain values in both frequency bands were observed to be 7.6 dBi and 7.21 dBi, respectively. In [56], a spiral-like patch radiator-based 1×4 planar antenna array was designed. The bandwidth was enhanced by designing three hexagonal parasitic elements behind the antenna elements.

A rhombus patch radiator was used in the design of a four-element planar array in [57]. Using square parasitic elements, a wide impedance bandwidth from 26 to 30.63 GHz was achieved. In [45] a non-uniform series-fed eight-element dipole array for use in wide-band mm-wave applications was presented. The observed bandwidth of the array was 27.7 GHz, ranging between 23.3 and 51 GHz. For 28 GHz applications, the authors in [59] designed a fractal antenna array consisting of four snowflake-like radiating structures. The designed array had a peak gain of ≈ 10 dBi and functioned at frequencies ranging from 25.28 to 29 GHz. In [60, 61], hook-shaped and donut-shaped 1×4 patch antenna arrays were designed for use in 5G mm-wave communication systems. The utilization of a partial ground plane with square notches resulted in an increase in the bandwidth of the arrays. The authors in [62] designed a planar antenna array that functions in the frequency band of 28 GHz and has four elements shaped like a square T. They utilized the same ground plane configuration as presented in [60, 61]. The previously presented

antenna arrays were able to provide wide impedance bandwidth and high gain, but at the cost of a large array size. The targeted specifications of the proposed antenna are discussed in Table 4.1.
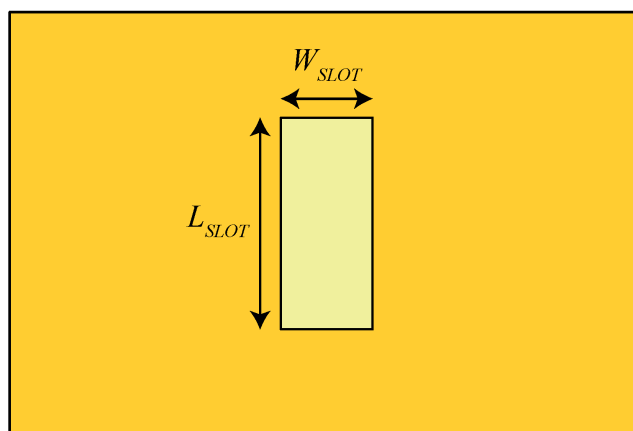
TABLE 4.1: Specification Table.

Variable	Target
Bandwidth	3 GHz
Efficiency	>80%
Peak gain	12 dBi
Array Size	1×2

TABLE 4.2: Design parameters used to build patch arrays (all dimensions in mm).

Parameter	Value	
	Design-1	Design-2
W_{SUB}	18	19
L_{SUB}	12	17
W_f	2.5	3
L_f	3.5	7
L_{T1}	8	8
L_{T2}	3	3
W_T	1	0.5
D_R	4.2	4.2
W_R	0.6	0.5
W_{SLOT}	2.6	–
L_{SLOT}	6	–
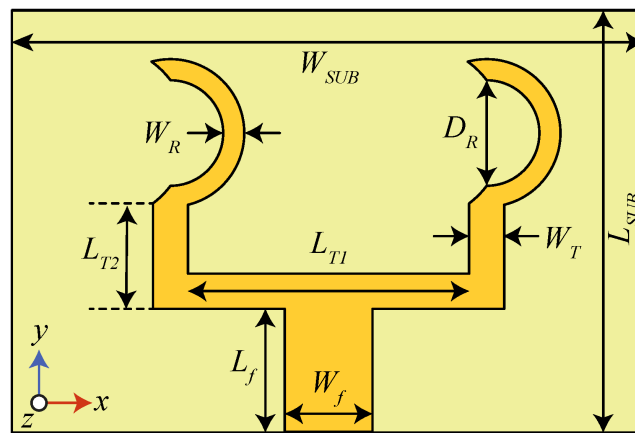
(a)

(b)
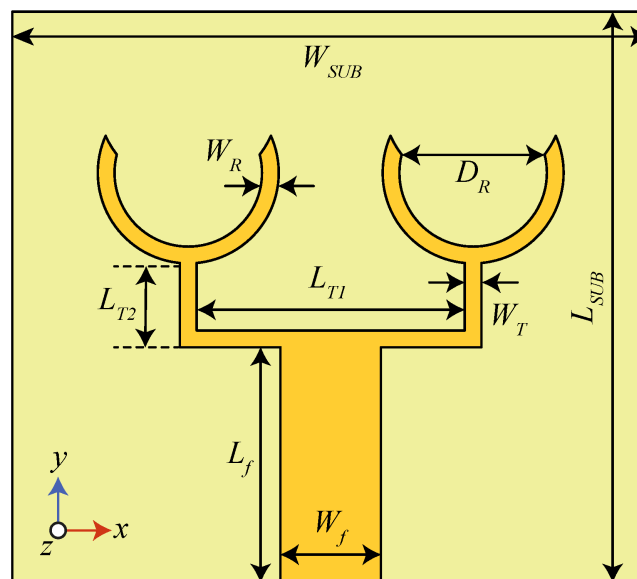
(c)

FIGURE 4.1: Design of a semi-ring-based patch antenna arrays (a) design-1 front side (b) design-1 bottom side (c) Top view of design-2 and it has full ground plane.
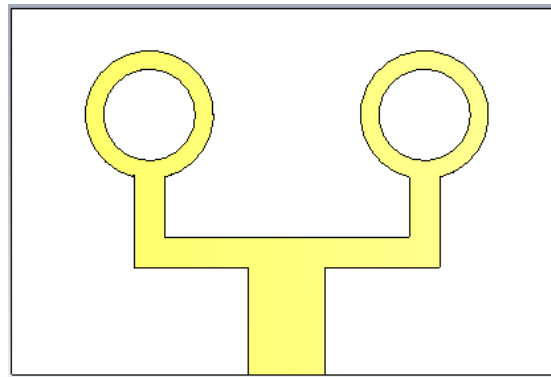
(a)
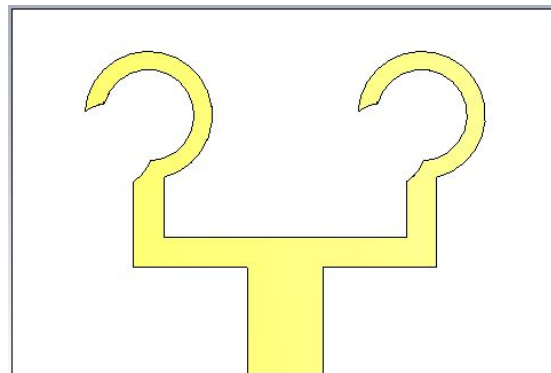
(b)

(c)

FIGURE 4.2: Design evolution (a) step-1 (b) step-2 (c) step-3 (proposed) for design-1

4.2 Patch Array Design

4.2.1 Design Evolution

The complete design parameters of the proposed arrays are listed in Table 4.2, while Figure 4.1 depicts the configuration of the patch antenna arrays. The Rogers

FIGURE 4.3: S_{11} characteristics for design-1 in Fig. 4.2

RT/Duroid 5880 low-loss, high-frequency dielectric substrate is used in the design. This particular substrate is 0.787 mm thick and possesses a dielectric permittivity of 2.2. The arrays that have been des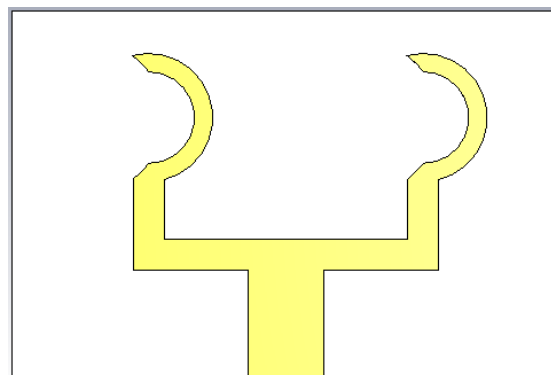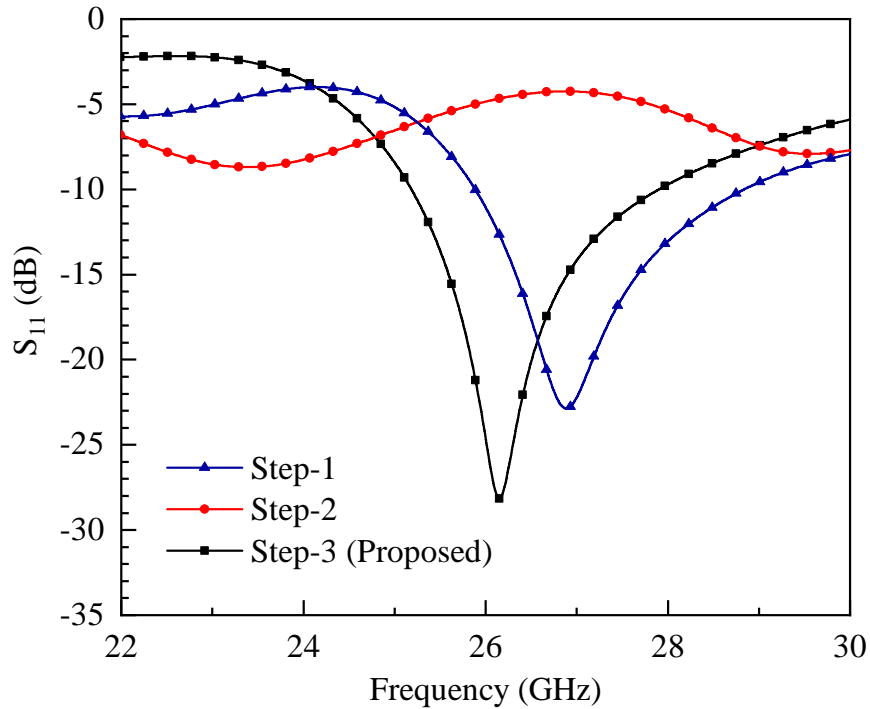igned are comprised of a 1×2 array of semi-ring patch radiators that are excited by a conventional T-junction power divider (see Figs. 4.1a and 4.1c). A conventional T-junction power divider is a passive microwave or RF device used to split an input signal into two equal or unequal output signals. It is called a T-junction because its physical structure resembles the letter 'T'. The T-junction power divider consists of three ports: an input port, a primary output port, and a secondary output port. The input signal is typically applied to the junction of the T, while the output signals are taken from the other two arms of the T. Figure 4.2 depicts the three major steps in the development of 1×2 array. As depicted in Fig. 4.2, the steps feature (a) full ring, (b) hook-shape and (c) semi-ring (proposed design). The bottom side of the design-1 array is comprised of a faulty ground plane with a rectangular slot (see Fig. 4.1b), which is known as a defected ground structure (DGS), while design-2 consists of a full ground plane. The white rectangular slot in Fig. 4.7 shows the faulty ground plane. This faulty ground plane in design 1 helps to tune the network response to
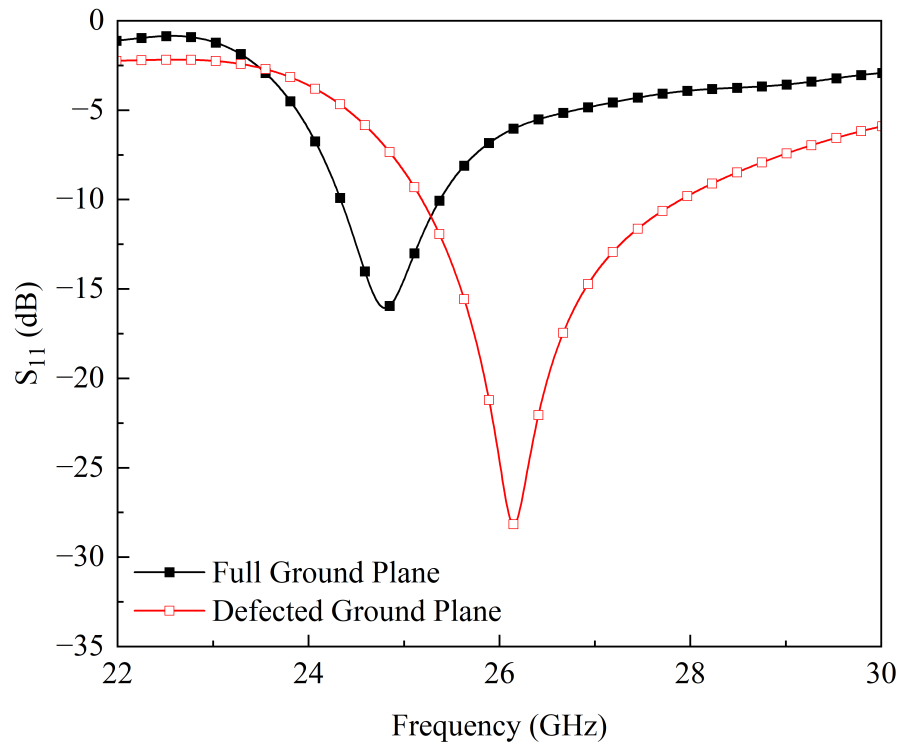
FIGURE 4.4: S_{11} characteristics for design-1 with full and defected ground structure.

the desired frequency band and also improves the impedance matching, as shown in Fig. 4.4. This phenomenon can also be observed from the surface current plot shown in Fig. 4.7. According to Fig. 4.7(a), it can be noted that in design-1, the current is uniformly distributed over the network elements and around the ground slot. This shows that the slot on the ground plane plays its role in achieving maximum impedance matching over the desired frequency band. Fig.4.5 and Fig. 4.6 depicts that the gain and radiation efficiency of design 1 with and without slot.As it can been from the simulated results that defected ground structure has improved the gain and efficiency.

In design-2, the same type of response is observed: the current is uniformly distributed among the network elements, as shown in Fig. 4.7(b). One thing need to be noted that in design-1, the semi-ring is designed by cutting the ring element in the H-plane, while in design-2, the semi-ring is designed based on the E-plane cut.
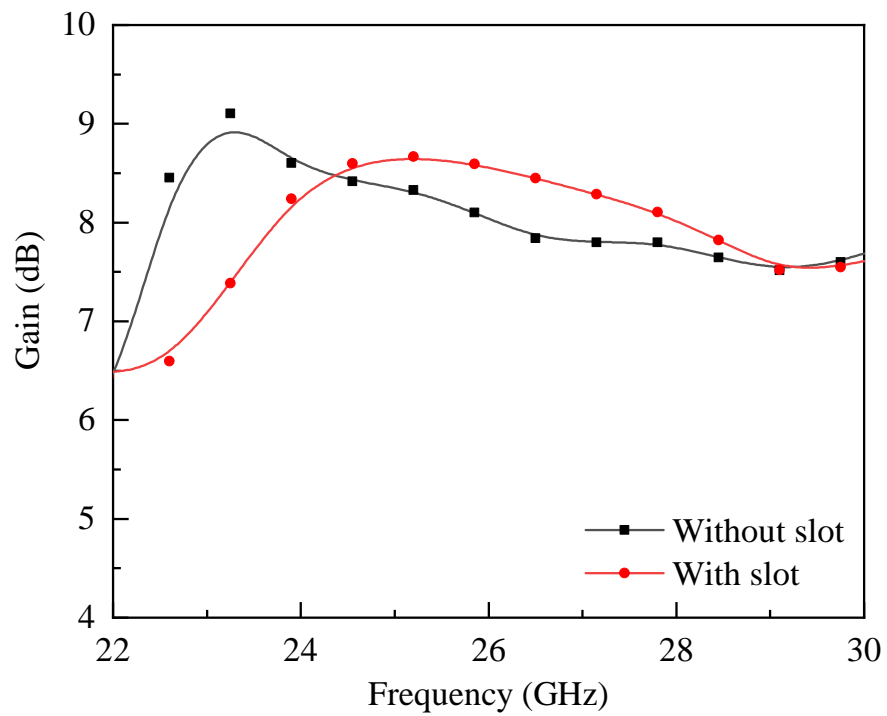
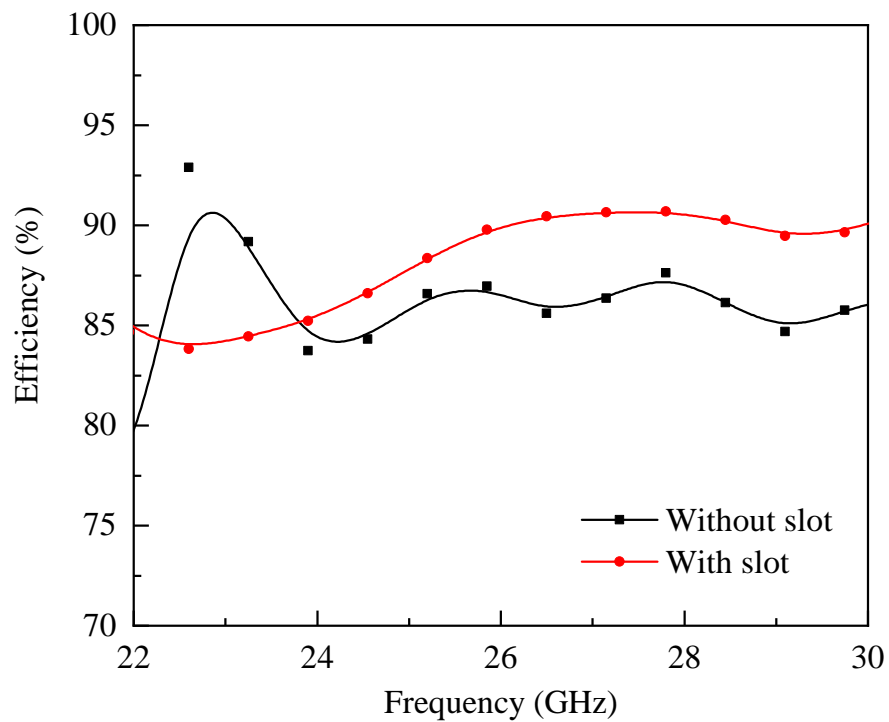FIGURE 4.5: Gain for design-1 with full and defected ground structure.

FIGURE 4.6: Radiation Efficiency for design-1 with full and defected ground structure.
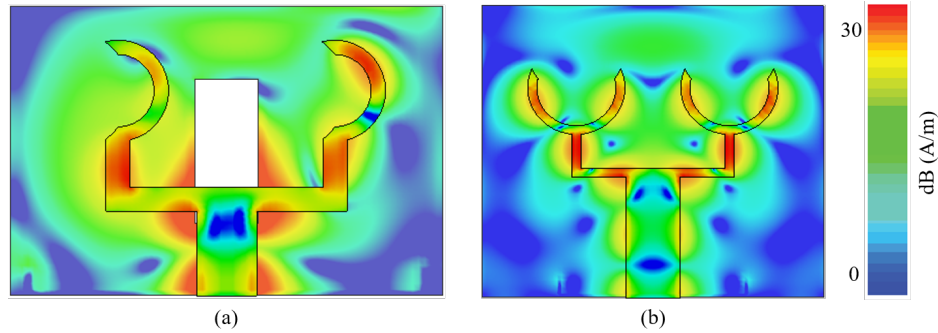
FIGURE 4.7: Surface current distribution for the patch arrays (a) design-1 (b) design-2.

4.3   Results and Discussion

The patch arrays are built and analyzed in the CST Microwave Studio V2021. Figure 4.8 illustrates the reflection coefficients (S_{11}), of the designed patch arrays. As shown by the results, the antenna arrays have a resonant frequency of between 25.35-27.87 GHz and 27.52-29.25 GHz, respectively. The impedance bandwidth of the design-1 array is measured to be 2.52 GHz, and its fractional bandwidth (FBW) is measured to be 9.5%. However, the impedance bandwidth of the design-2 array is 1.75 GHz, and its FBW is 6.16%.

Figure 4.9 depicts the simulated efficiency and realized gain of the antenna arrays. The radiation efficiency for design-1, defined as the ratio of the power radiated by an antenna to the input power, is between 85.7% and 88.6%, as shown in Fig. 4.9(a), while the total efficiency, defined as the power received after losses, is between 80% and 88.4%. However, as can be seen in Fig. 4.9(b), the overall efficiency of design-2 varies between 81.38% to 91.75%, and the radiation efficiency is >90%. Figure 4.9(a) shows that the gain of the first array is between 7.6 and 8.75 dBi across the full operating range, while the gain of the second array is ≥9.5 dBi in the band of interest, as shown in Fig. 4.9(b).

The radiation characteristics of the proposed patch arrays for both E and H planes are depicted in Fig. 4.10. In the case of design-1, for both planes, broadside radiation characteristics are observed at 26 GHz. For E plane, the beam is tilted towards 27°, as shown in Fig. 4.10(a), while for H plane, the main beam is directed
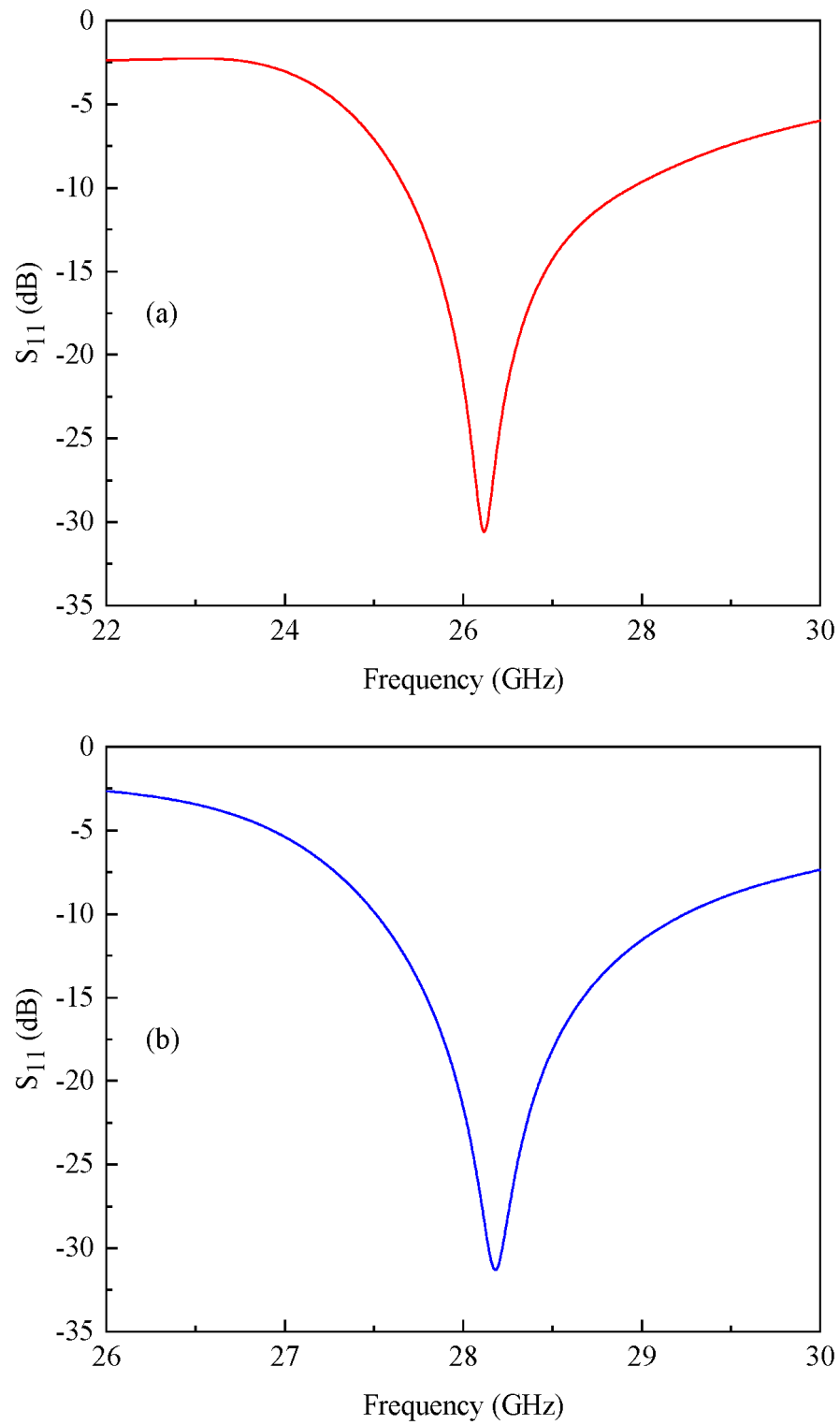
FIGURE 4.8: S_{11} characteristics for the proposed patch arrays (a) design-1 (b) design-2.

FIGURE 4.9: Radiation efficiency, total efficiency, and realized gain of (a) design-1 (b) design-2.
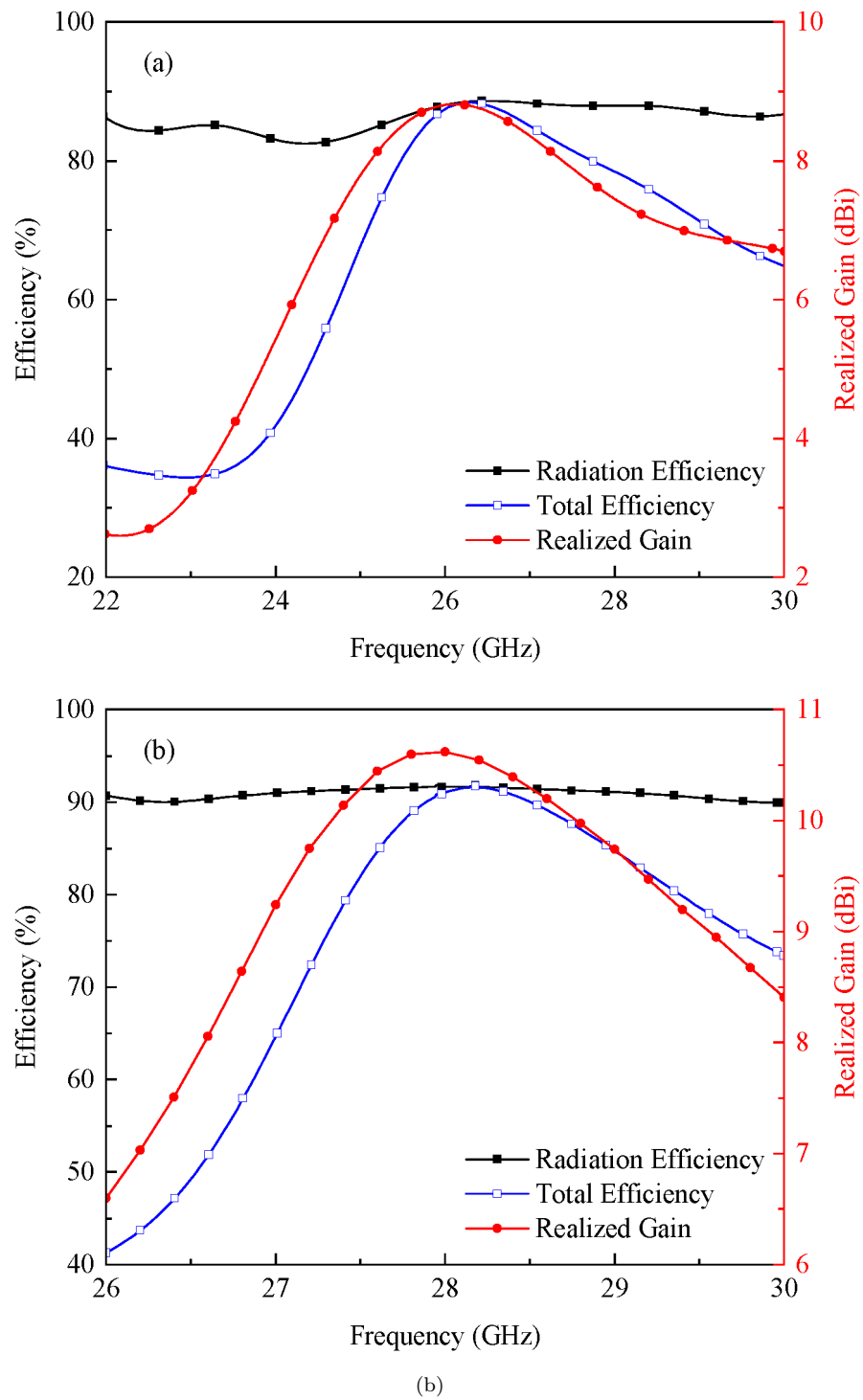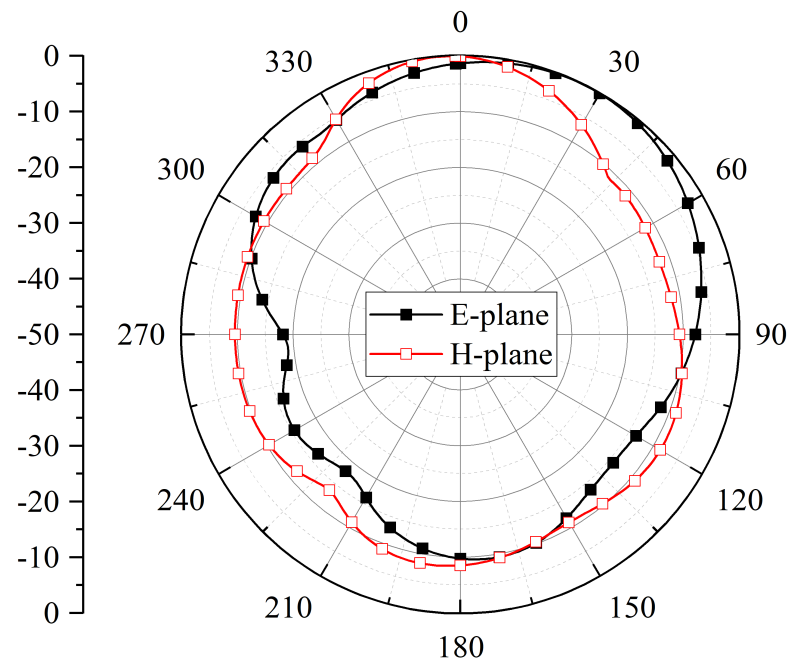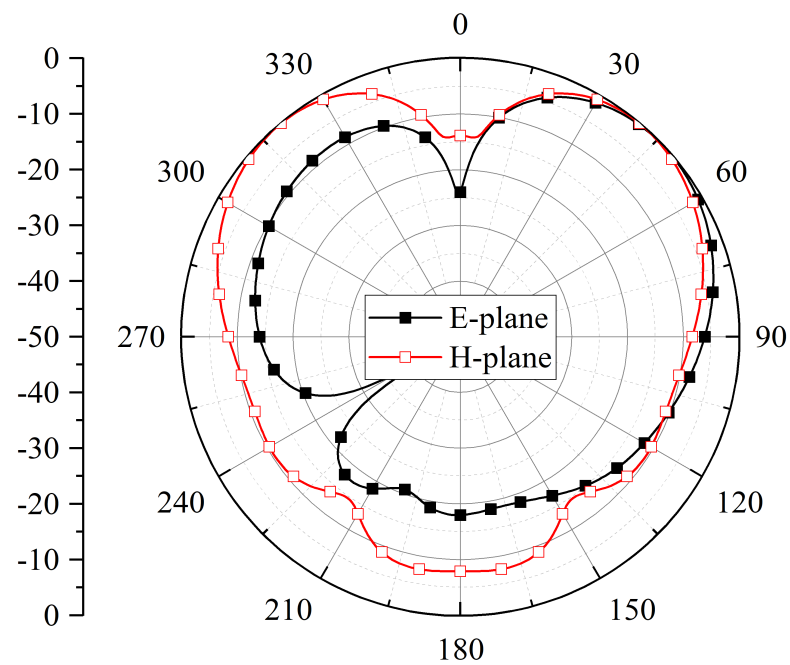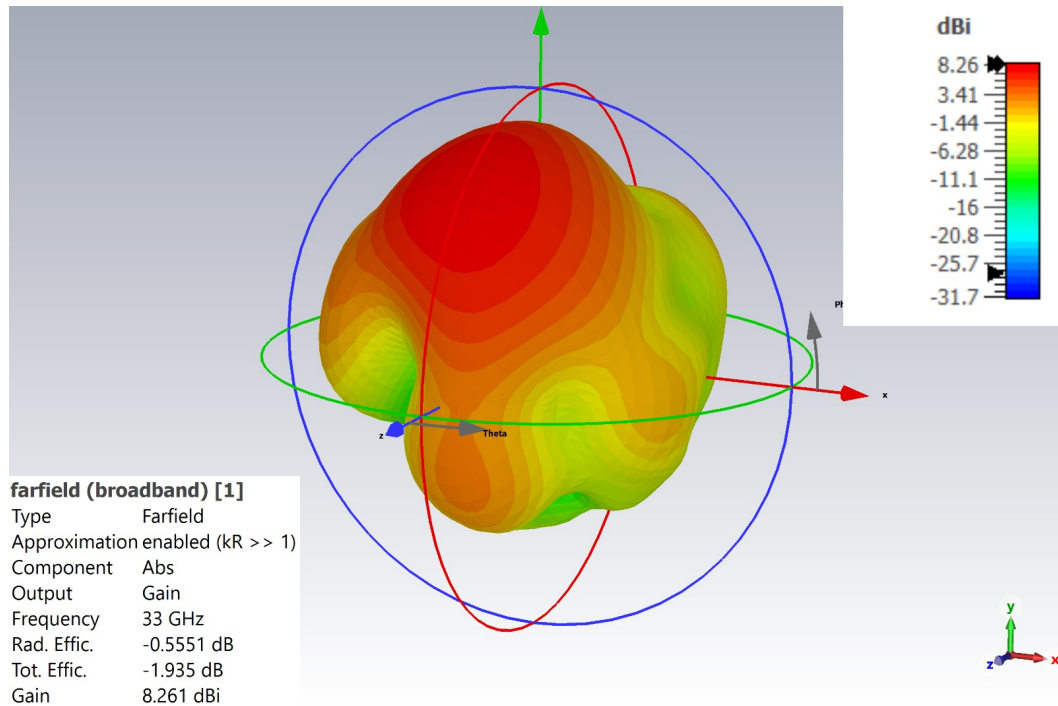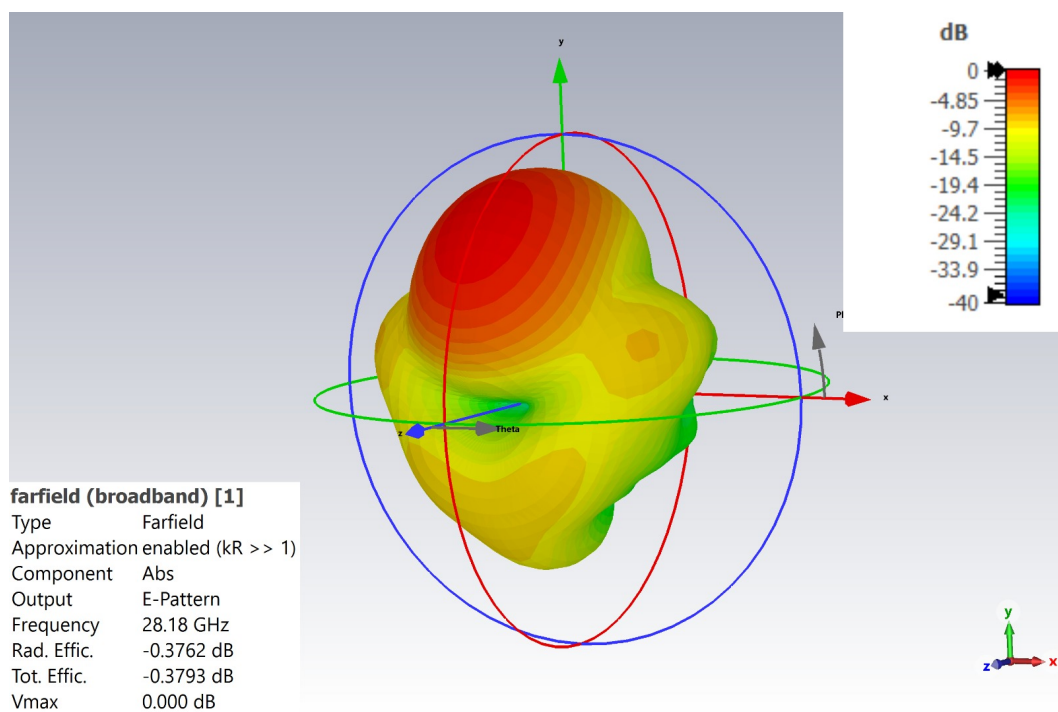
(a)

(b)

FIGURE 4.10: Radiation characteristics of the proposed patch antenna arrays (a) design-1 (26GHz) (b) design-2 (28GHz).

(a)

(b)

FIGURE 4.11: The 3D radiation patterns using CST simulation technique of (a) design-1 and (b) design-2.

TABLE 4.3: Comparison between proposed and previously published antenna arrays.

Ref.	Dimensions		Antenna Elements	Bandwidth	Efficiency	Peak Gain
	(mm^2)	(λ^2)		(GHz)	(%)	(dBi)
[55]	45×20	4.2×1.86	4	10	85	12.15
[56]	40×15	3.73×1.4	4	15.42	83	11.5
[57]	40×19.22	3.73×1.79	4	4.63	85	11.24
[59]	32×12	3×1.12	4	3.76	80	10.12
[60]	26.9×18.5	2.51×1.72	4	2.4	90	10.3
[61]	22×20	2.05×1.86	4	3.7	90	10.2
[62]	24×18.5	2.24×1.72	4	3.7	94	11.5
[124]	9×10.3	0.84×0.96	2	1.43	99.8	9.42
Design-1	18×12	1.68×1.12	2	2.52	85	8.75
Design-2	19×17	1.77×1.58	2	1.75	90	10.6

towards 0° (see Fig. 4.10a). For design-2, the E plane beam is directed towards 47° (see Fig. 4.10b), while the null is located at 0°. For H plane, a dual-beam pattern is observed, where the main beams are directed towards ±47°, as shown in Fig. 4.10(b).The shift in the beam position may be associated with the phase mismatch of the T-junction power divider ports. It is observed that the designed antennas exhibits linear polarization, the 3-D radiation pattern for design-1 and design-2 are shown in the Fig. 4.11.

Table 4.3, provides a comparative analysis of previously planned and exhibited antenna arrays. The table shows that the designed array is significantly smaller in size than the array designs presented in the literature. The reported antenna array has a narrow bandwidth compared to other reported designs [55–57, 59–62], but it provides high gain with a reduced number of array elements. The data in the table also reveals that, despite having less gain than the design-2 array, the design-1 array is more compact and provides a wider impedance bandwidth. In conclusion, both Design 1 and Design 2 have the advantage of being able to be used by 5G mobile technology for efficient data transmission.

4.4   Summary

Two-element patch antenna arrays are designed and presented for mm-wave applications. The arrays consist of patch radiators based on 1×2 semi-rings fed by conventional T-junction power dividers. In the first design, the rear face of the array consists of a faulty ground structure, while the second design has a complete ground plane. From the presented results, it is described that the designed arrays perform well from 25.35 to 27.87 GHz and 27.5 to 29.25 GHz. Comparing the two designs, the first provides a maximum gain of 8.75 dBi and an antenna efficiency of >85%, while the second provides a maximum gain of 10.6 dBi and an antenna efficiency of >90%. From the presented results, it can be concluded that the reported antenna arrays could be potential candidates for 5G mm-wave communication systems.

Chapter 5

Rhombus Inscribed Circular Ring Fractal Array Antenna for mm-wave 5G Applications

5.1 Introduction

In the previous chapter, semi-ring patch array antennas for high gain mm-wave applications were designed and simulated. The geometries of the designed arrays that were discussed in Chapter 4 though comply with the requirements of 5G applications but they offered low impedance bandwidth. To improve impedance bandwidth another design is presented in this chapter. The chapter focuses on 1×4 planar fractal antenna array for use in 5G mm-wave communications. For 5G systems using the 28 GHz band, the proposed array is optimized for maximum gain. The array's single element is a rhombus-inscribed circular ring fractal, and the array's wide impedance bandwidth is accomplished by placing a notch-loaded partial ground plane at the array's bottom. The results show that the antenna array can provide a maximum gain of 10.7 dBi at frequencies between 22.8 and 29.2 GHz. In addition, the designed array is extremely simple, and can be fabricated using low-cost techniques, e.g; chemical etching.

5G communication technology will bring unique features for consumers. It will provide access to users everywhere and will select the best performance among other technologies such as Wi-Fi, WLAN, etc. The selection of the best performance will not only be based on the throughput but also on the most appropriate metrics depending on the nature of the service. Furthermore, 5G systems will support other services like IoT by providing an internet connection to a vast number of objects. In addition to this, 5G systems will also cover services such as V2V, remote health services, etc. The targeted specifications of the proposed antenna array are discussed in Table 5.1.

TABLE 5.1: Specification Table.

Variable	Target
Bandwidth	5 GHz
Efficiency	>85%
Peak gain	12 dBi
Array Size	1×4

The data transfer speeds and latency of 5G networks are unprecedented. It is necessary to have a wide bandwidth in order to achieve high data rate, and this can be achieved through the utilization of higher frequency bands [10]. For this purpose, mm-wave frequency bands can be utilized to achieve high bandwidth in conjunction with high data rate. The ITU designated few frequency bands in the mm-wave spectrum, these bands include 26 GHz, 28 GHz, 38 GHz, and 60 GHz [11]. To achieve speed, reliability, latency, and capacity, the 26 GHz ($24.25 - 27.5$ GHz) and 28 GHz ($26.5 - 29.5$ GHz) frequency bands receive the most importance worldwide. However, due to the fact that oxygen molecules are easily absorbed at these frequencies, losses are high [14, 15].

High-gain antennas are needed to solve this issue, and designing antenna arrays is one way to increase gain. In addition, the mm-wave communication systems require compact antenna designs. This demand can be fulfilled with the use of

planar antennas because they are small in size, have low fabrication costs, and their integration is easy with portable devices. In addition, the short wavelength at mm-wave frequencies allows for the design of highly efficient and space-saving antennas for 5G mobile devices. It's also simple to create miniaturized antennas with a sizable electrical output. Previously, numerous researchers have presented there work on antenna array designs for 5G communication systems. The detailed explanation about previously reported array designs is given in Chapter 2.

5.2   Single Antenna Element

A 50 Ω microstrip feed line supplies power to a rhombus-inscribed circular ring fractal patch on a dielectric substrate, while a square notch loaded partial ground plane is placed on the substrate's backside, as depicted in Fig. 5.1. Rogers RT/-Duroid 5880, a low-loss dielectric base with a dielectric constant of 2.2, is being used in the antenna design. The thickness of the substrate is chosen to be 0.51 mm. The proposed antenna has the following overall design parameters: $W_{SUB} = 7$, $L_{SUB} = 7.5$, $R_1 = 2.6$, $R_2 = 1.5$, $L_1 = 3.6$, $L_2 = 1.6$, $L_F = 2$, $W_F = 1.4$, $L_G = 1.6$, $G = 0.5$, and $S = 0.25$ (all dimensions are in mm).

Fig. 5.2 depicts the four major steps in the development of a single antenna element. As depicted in Fig. 5.2(a) the iteration-1 design features a notch loaded partial ground on the bottom side and a circular ring patch radiator that is powered by a 50Ω microstrip feed line. Design expressions described in [125] are used to determine the ring's circumference and diameter. In iteration-2, a rhombus shape is designed within the circular ring without changing the other dimensions, as shown in Fig. 5.2(b). In iterations-3 and 4, another circular ring and rhombus are designed as depicted in Figs. 5.2(c) and (d).

Figure 5.3 depicts reflection coefficient (S_{11}) characteristics for each iteration presented above. One can notice from the result of Fig. 5.3 that the iteration-1 design offered an impedance bandwidth of 4.44 GHz ($25.98 - 30.42$ GHz). With every step, the bandwidth of the antenna is improving. Although iteration-2 and
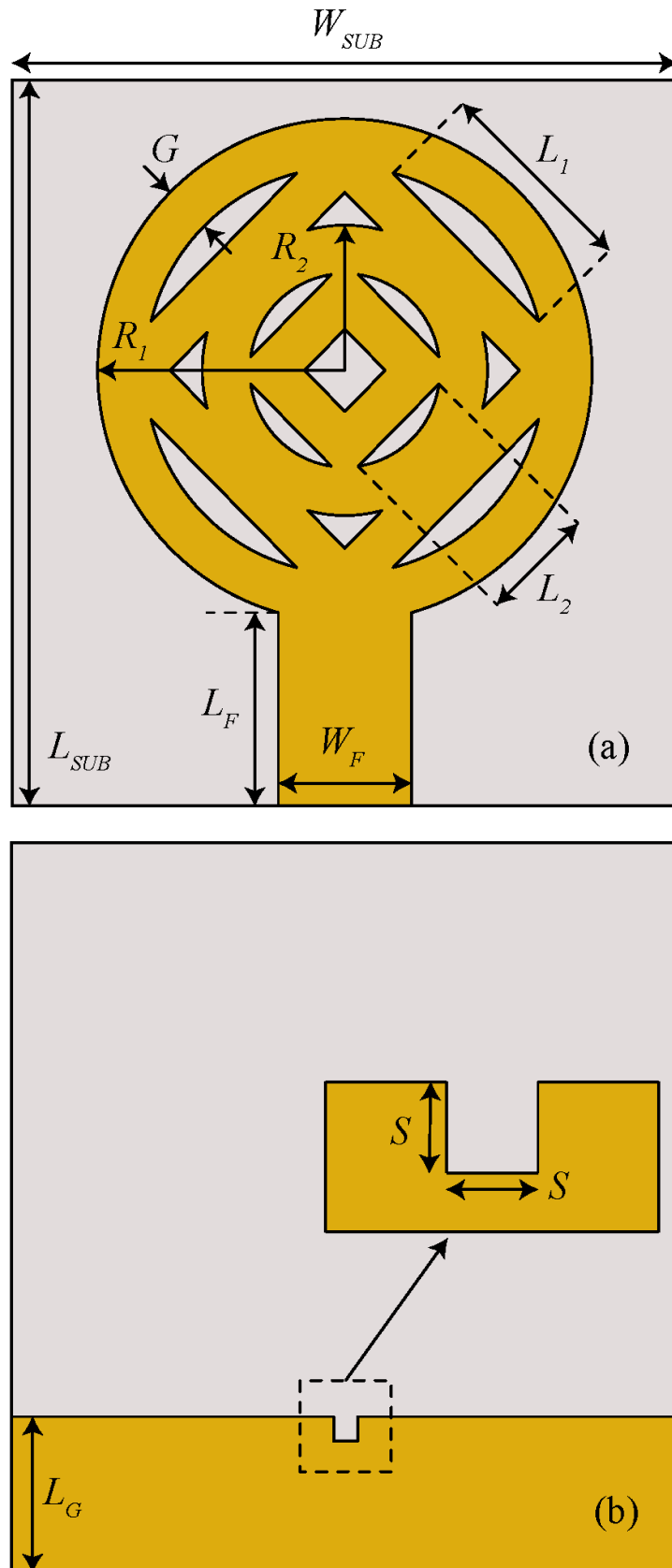
FIGURE 5.1: Schematic of the proposed fractal antenna: (a) front side (b) back side.
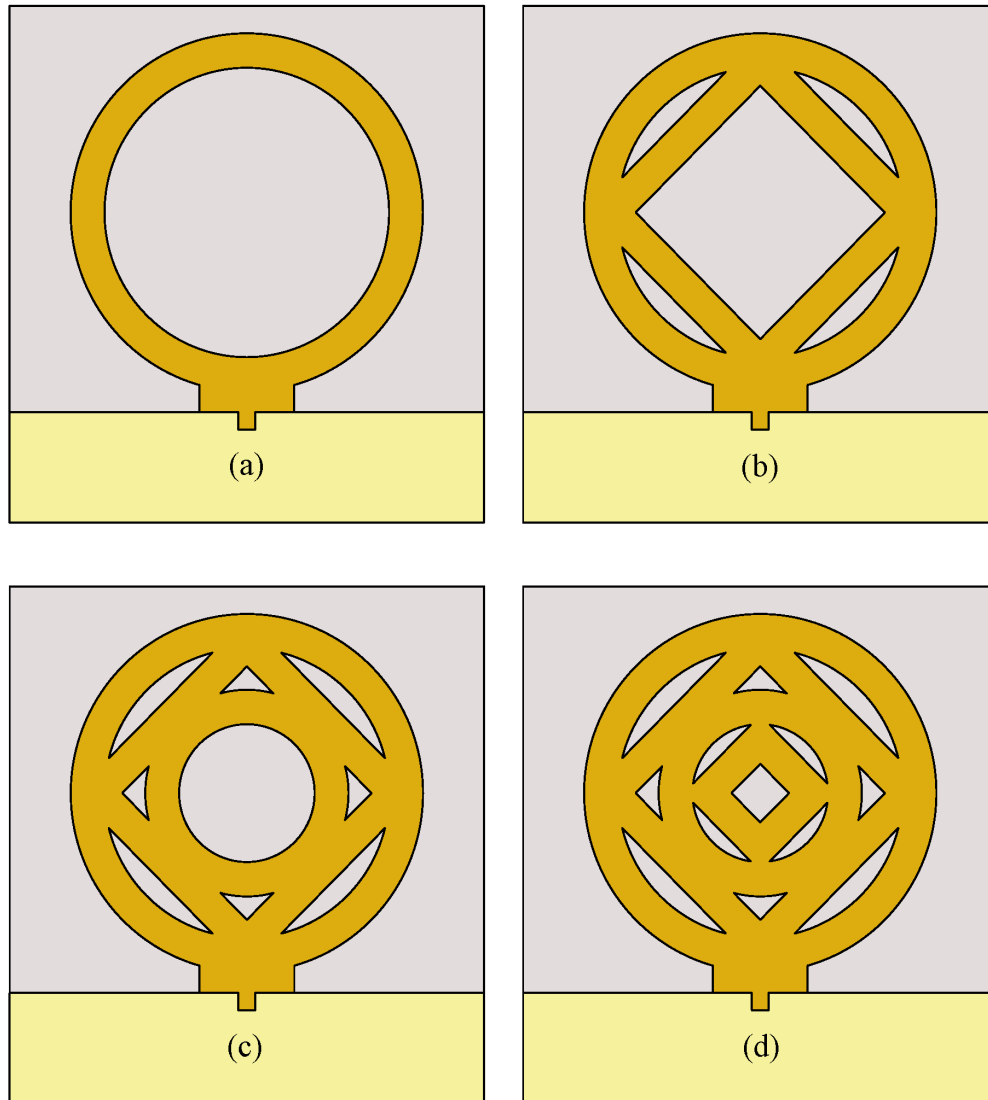
FIGURE 5.2: Design evolution of the proposed fractal antenna: (a) iteration-1 (b) iteration-2 (c) iteration-3 (d) iteration-4 (proposed design).

iteration-3 designs provide better impedance matching, they have less bandwidth compared to iteration-4 design. The observed impedance bandwidth of the design is equal to 10.72 GHz (22.28 − 33 GHz).

Fig. 5.4 depicts the radiation properties of a single antenna element. One can see from the figure that the proposed antenna exhibits a bidirectional radiation pattern in the E plane and a quasi-omnidirectional pattern in the H plane. As shown in Fig. 5.4, the E plane has a main beam directed towards 150° and a null at 68°.

The radiation efficiency, total efficiency, and simulated gain of a single antenna
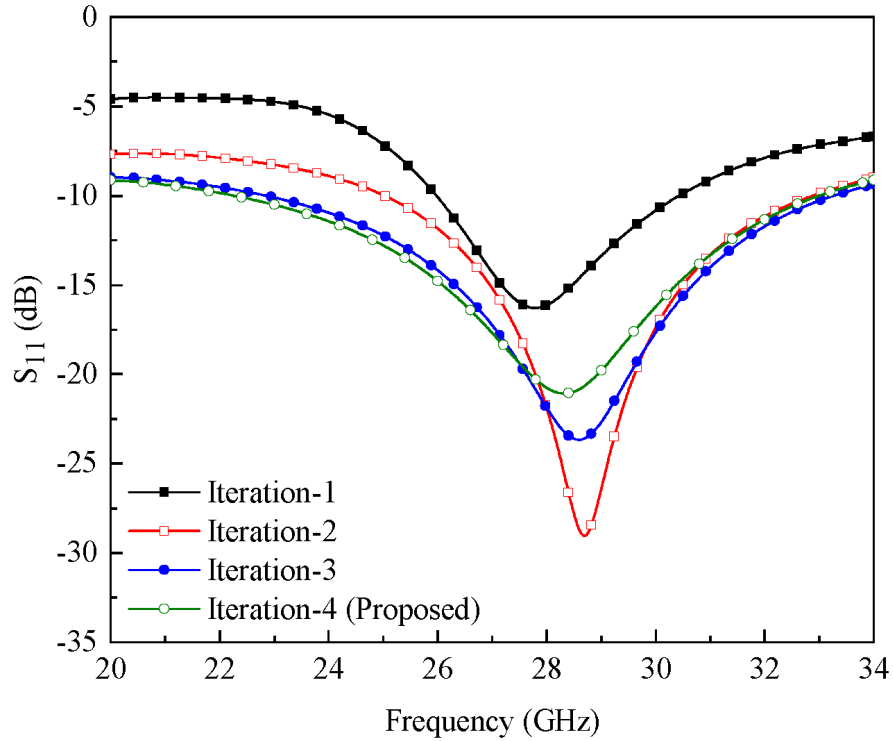
FIGURE 5.3: Simulated S_{11} for each iteration presented in Fig. 5.2.

element are depicted in Fig. 5.5. the observed radiation and total efficiencies are $\geq 90\%$ and $>80\%$, respectively [see Fig. 5.5(a)]. Furthermore, the antenna gain fluctuates in the range of 3.5-4.5 dBi within the operating frequency range, as depicted in Fig. 5.5(b). The 3-D radiation pattern for designed single element is shown in the Fig. 5.6.

5.3 Design of 1×4 Antenna Array

One of the requirements for 5G communication systems is high gain and narrow beamwidth, to meet this requirement a 1×4 linear array is designed, as depicted in Fig. 5.7. A conventional 1:4 corporate feeding network is utilized to feed the array elements as can be seen in Fig. 5.7. The technique for designing the corporate feeding network can be found in [62]. Because of the need for isolation at 28 GHz, the spacing between array elements was set at 7 mm, which is larger than $\lambda_0/2$ (where λ_0 is the wavelength in free space).

FIGURE 5.4: Simulated radiation characteristics of the proposed fractal antenna at 28 GHz.
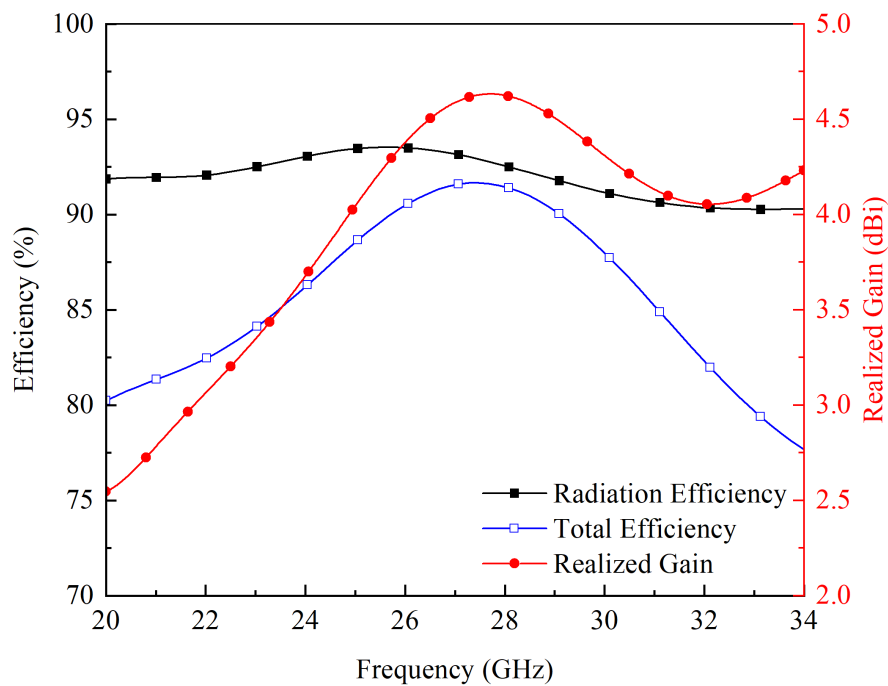
FIGURE 5.5: Simulated radiation efficiency, total efficiency, and realized gain of the proposed fractal antenna.

farfield (f=30) [1]

Type	Farfield
Approximation	enabled (kR >> 1)
Component	Abs
Output	Realized Gain
Frequency	30 GHz
Rad. Effic.	-0.4033 dB
Tot. Effic.	-0.5088 dB
Rlzd. Gain	4.474 dBi
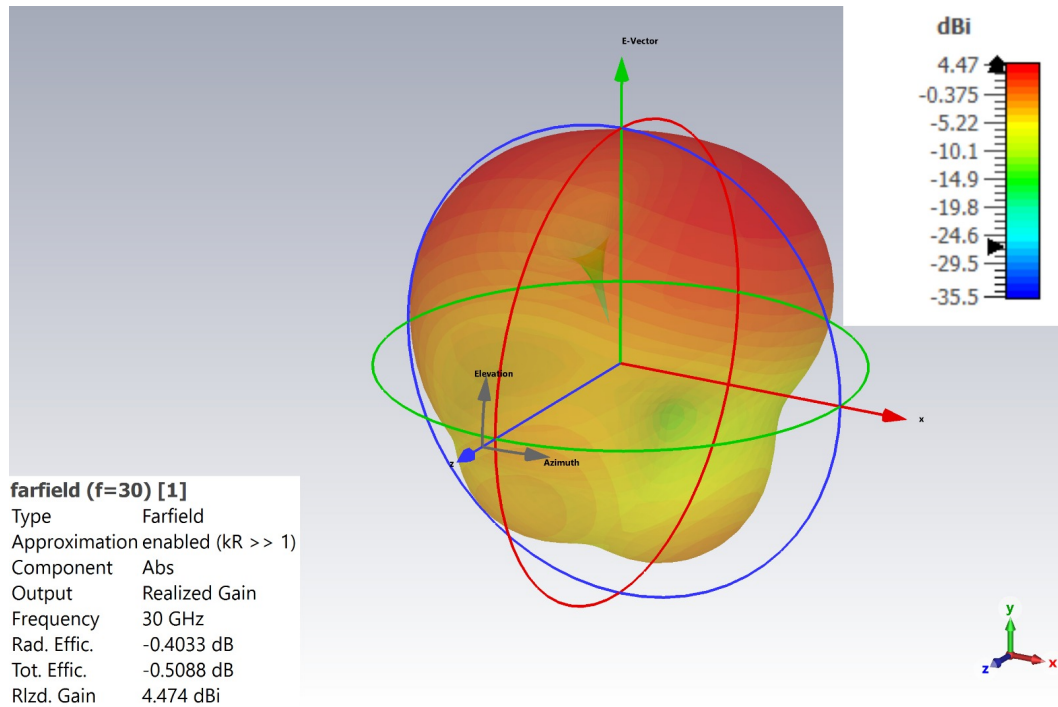
FIGURE 5.6: 3-D Radiation pattern for single element.
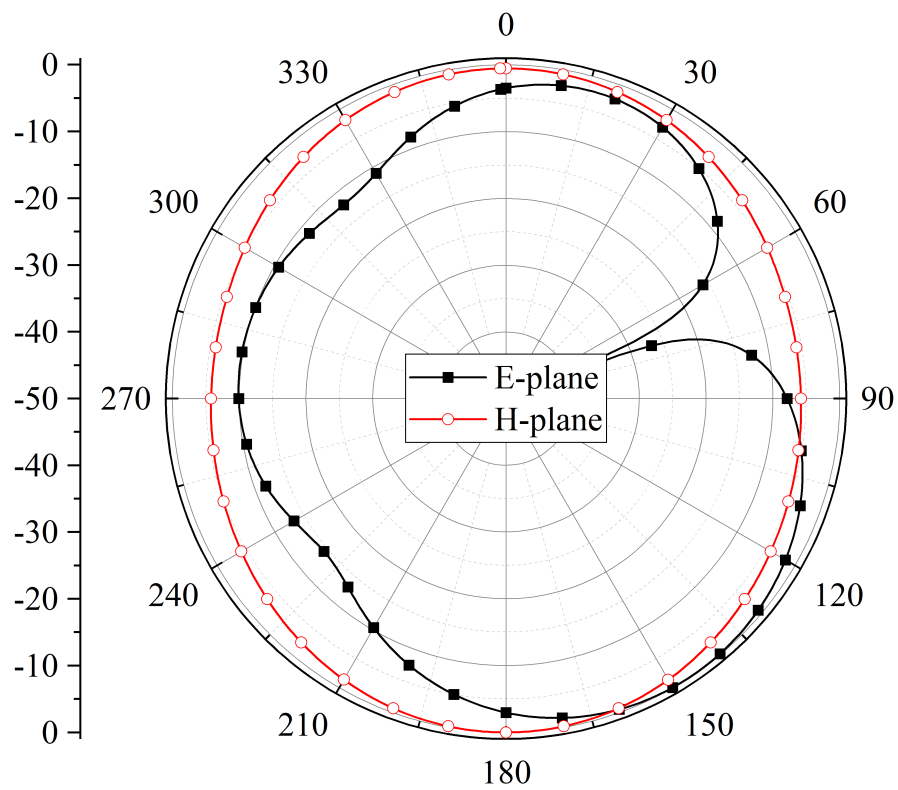
The proposed four-element linear antenna array is manufactured on a Rogers RT/-Duroid 5880 substrate that has 0.51 mm thickness, after being designed and simulated in CST Microwave Studio. Fig. 5.8 depicts the prototype array that was fabricated. As can be seen in Fig. 5.8 an End Launch Screw-on type RF connector from Cinch Connectivity Solutions of 2.92 mm is used for the measurements. Precision Network Analyzer (PNA) E8363C by Agilent Technologies is used to measure the fabricated prototype to validate simulation results.

Figure 5.9 displays the antenna array's simulated and observed S_{11} characteristics. Measurements indicate that the proposed array resonates in bandwidth of $22.8 - 29.2$ GHz, while simulations show that it works from 22.92 to 29 GHz according to -10 dB bandwidth criteria. In addition, the observed S_{11} is satisfactory according with the simulated one.

The measurements of the array's far-field performance are carried out in an anechoic chamber using a conventional technique, during this measurement the transmit and received antenna was configured in such a way that the impact of cross-polarization was zero. The block arrangement of the measurement setup is shown
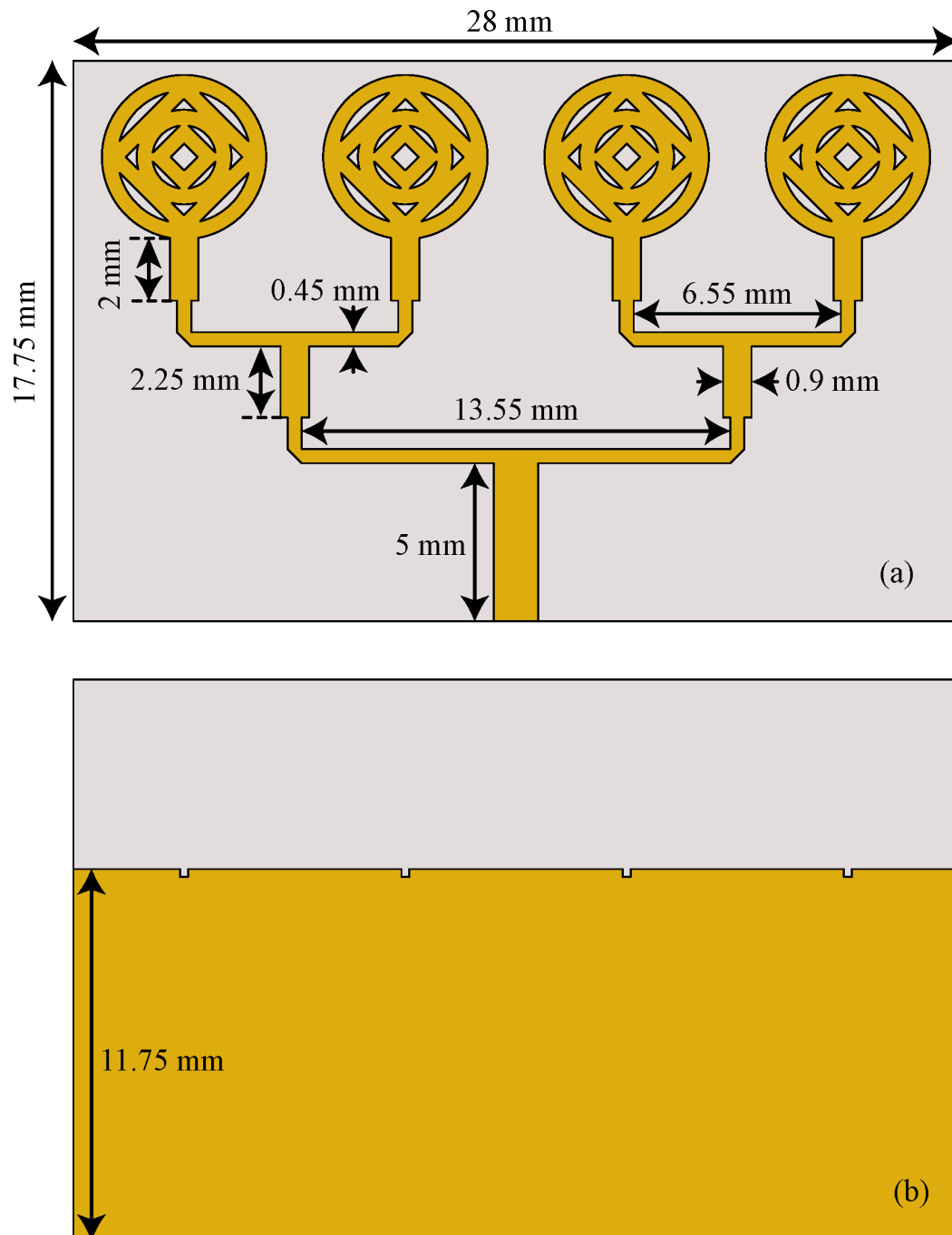
FIGURE 5.7: Design of the proposed 1×4 linear antenna array: (a) front view (b) back view.

in the Fig. 5.10. The array is arranged in a horizontal fashion on a turntable directly opposite a reference antenna (horn antenna) that has an effective bandwidth of 15–40 GHz. As shown in Fig. 5.10 the walls of anechoic chamber are covered with RF absorbers in order to create a reflection-free environment.

Fig. 5.11(a) depicts the gain of the proposed array, and Fig. 5.11(b) depicts
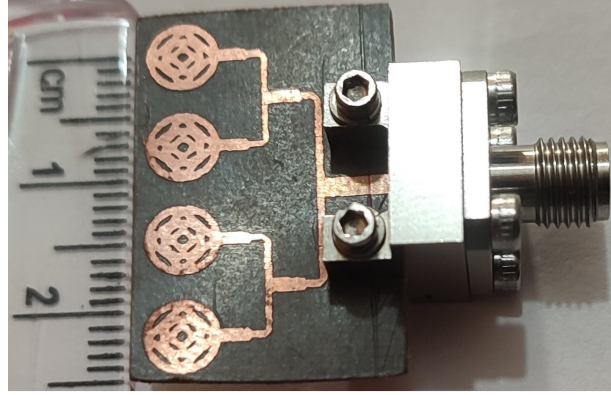
(a)
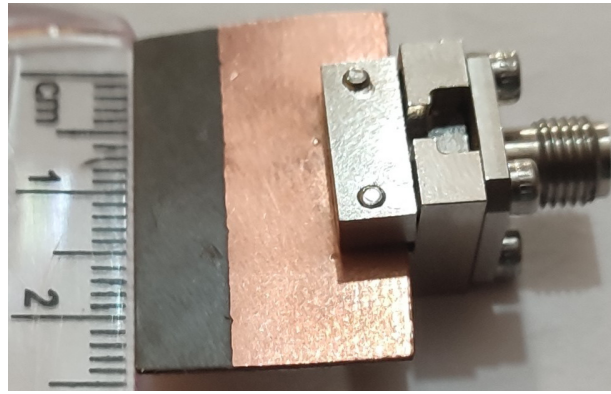
(b)

FIGURE 5.8: Fabricated prototype of the proposed array: (a) front view (b) back view.

the radiation efficiency. As shown in Fig. 5.11(a) the average gain of the designed array is ≈10.3 dBi in simulations, where as the measured average gain is 10 dBi. In addition, Fig. 5.11(b) presents that the radiation efficiency of both measured and simulated results is greater than 95% across the entire frequency spectrum. The figure also shows that the measured and simulated far-field radiation properties are in good agreement. It is pertinent to mention here that the antenna efficiency (η) as a function of frequency was calculated using the far-field radiated power (P_{rad}) and the incident power (P_{in}) using the following expression:

$$\eta = \frac{P_{rad}}{P_{ac}} = \frac{P_{rad}}{P_{in} - |S_{11}|^2} \tag{5.1}$$

In the Figs. 5.12 and 5.13 the radiation characteristics of the designed array at three different frequencies: 23, 28, and 29 GHz are illustrated. From Fig. 5.12
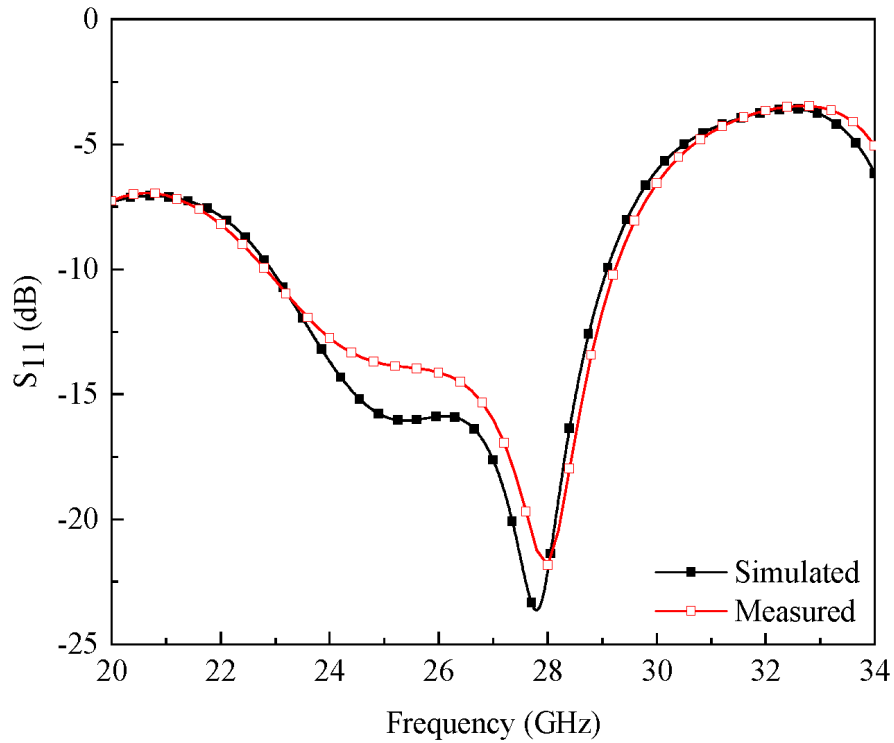
FIGURE 5.9: S_{11} properties of the proposed array.

for E plane, one can observe that the proposed array exhibits a typical eight-shaped radiated pattern for the frequency bands mentioned above. For H plane, shown in Fig. 5.13 highly directive dual-beam radiation properties. In addition, a beamwidth of about 23° is observed for 23 GHz, while for 28 GHz and 29 GHz, it is ≈ 20°. It is observed that the designed array exhibits linear polarization. The 3-D radiation pattern for designed array is shown in the Fig. 5.14.

The distribution of surface currents at the proposed array's operating frequency of 28 GHz is shown in Fig. 5.15. Current seems to flow without congestion anywhere in the feeding network and between the array elements. A uniform amplitude distribution of the surface current led to achieving high gain and smaller beamwidth, which can clearly be observed from the results of Figs. 5.11(a) and 5.12(b).
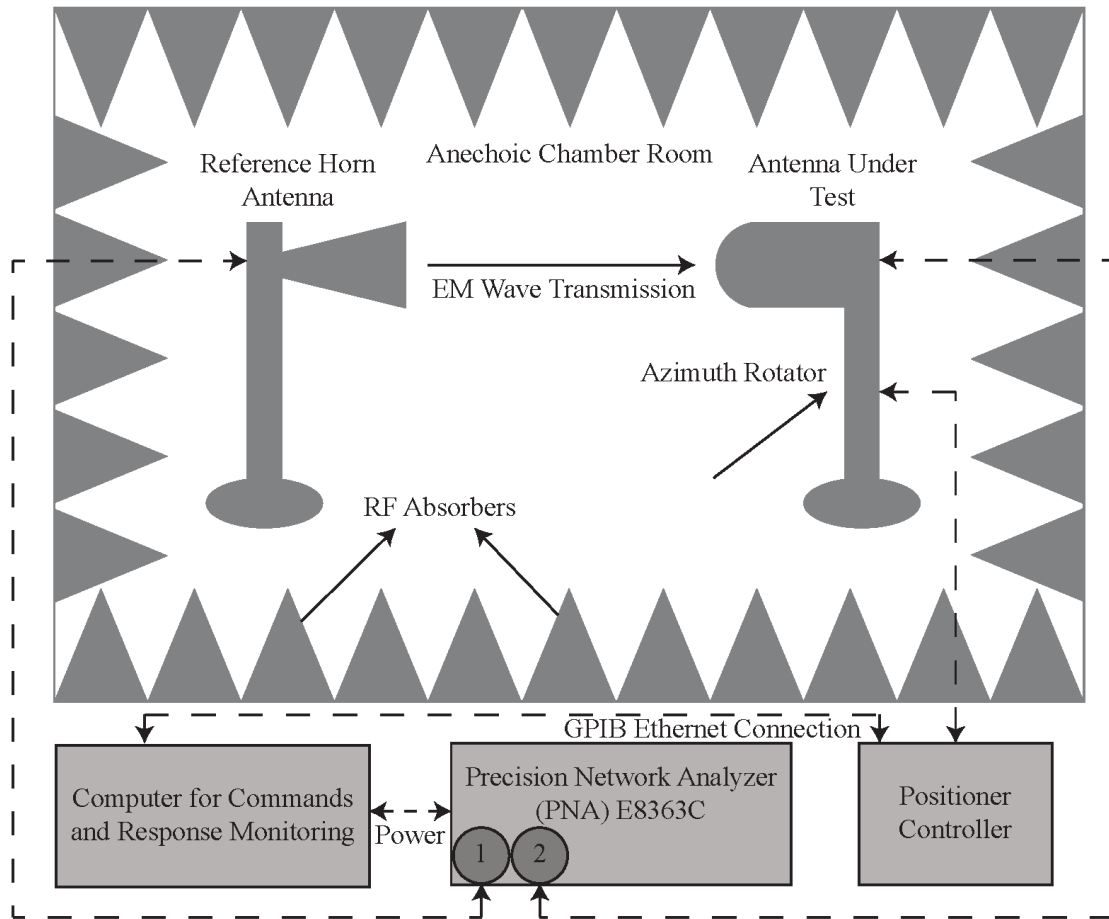
FIGURE 5.10: Block representation of far-field measurement setup [126].

TABLE 5.2: Comparison between proposed array and previously published work.

Ref.	Dimensions		Array Elements	Bandwidth	Efficiency	Gain
	(mm^2)	(λ^2)		(GHz)	(%)	(dBi)
[45]	34.1×10	3.18×0.934	8	27.7	−	10.8
[47]	26×40	2.34×3.6	4	4.92	−	18
[55]	45×20	4.2×1.86	4	10	85	12.15
[56]	40×15	3.73×1.4	4	15.42	83	11.5
[57]	40×19.22	3.73×1.79	4	4.63	85	11.24
[74]	37.6×14.3	3.51×1.33	4	10.51	90	10.7
[59]	32×12	3×1.12	4	3.76	80	10.12
[60]	26.9×18.5	2.51×1.72	4	2.4	90	10.3
[61]	22×20	2.05×1.86	4	3.7	90	10.2
[62]	24×18.5	2.24×1.72	4	3.7	94	11.5
This work	28×17.75	2.61×1.65	4	6.4	95	10.7
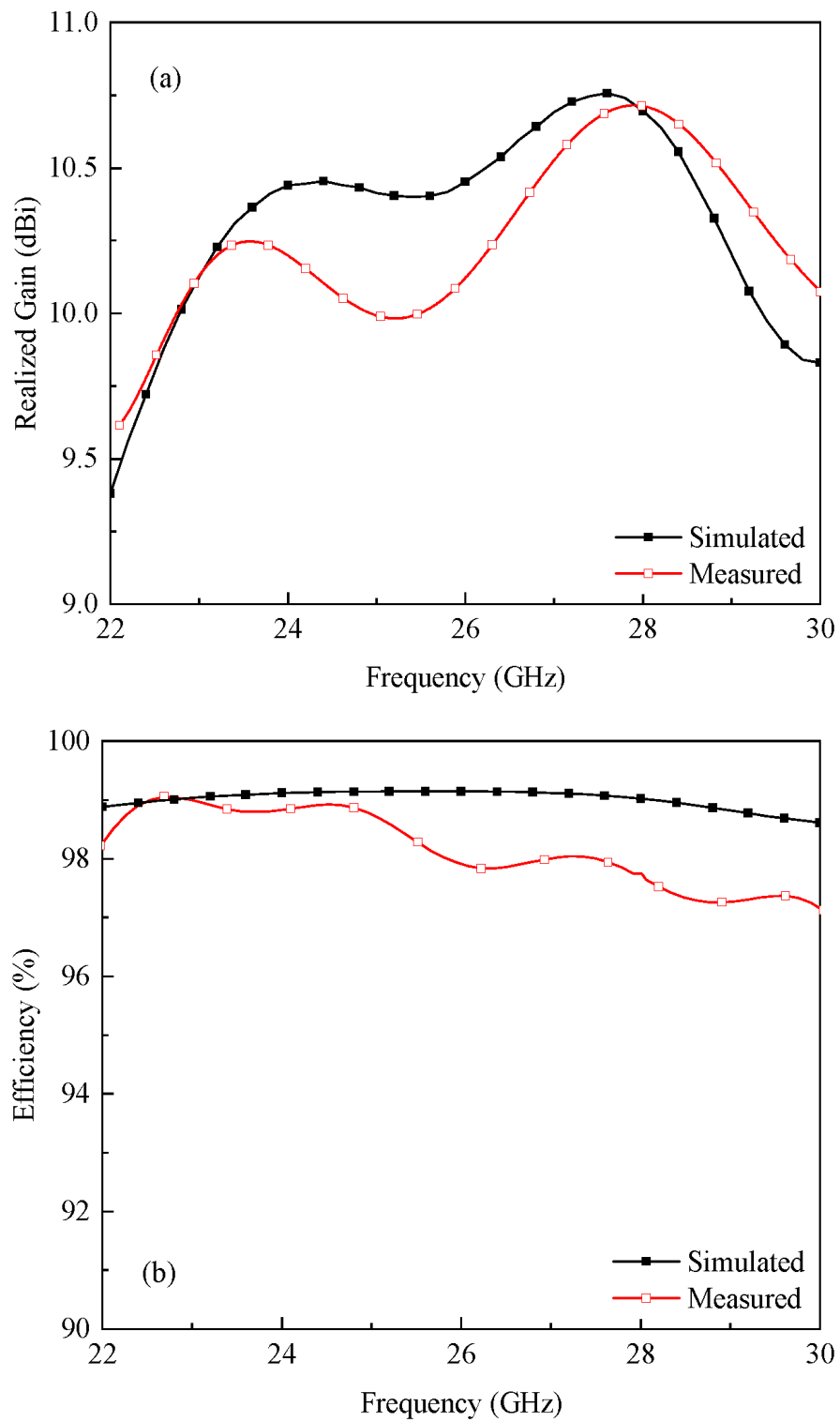
FIGURE 5.11: Simulated and measured (a) realized gain and (b) radiation efficiency of the proposed array.
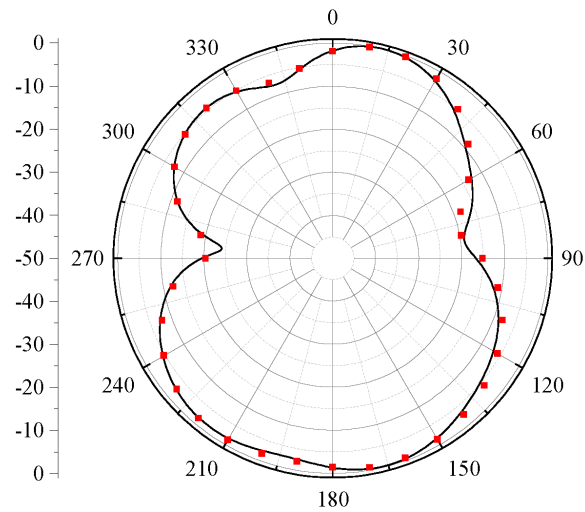
(a)
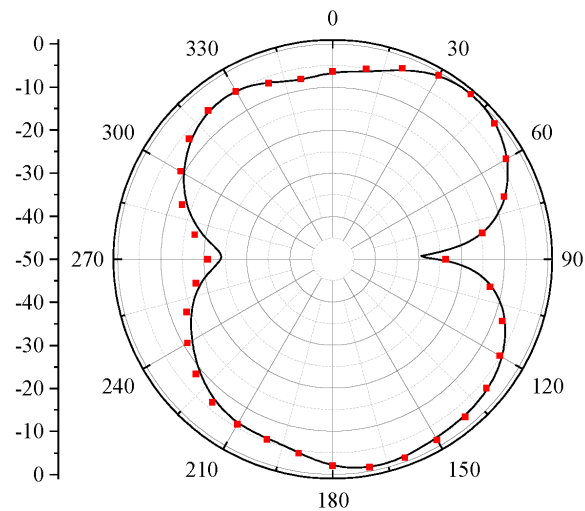
(b)
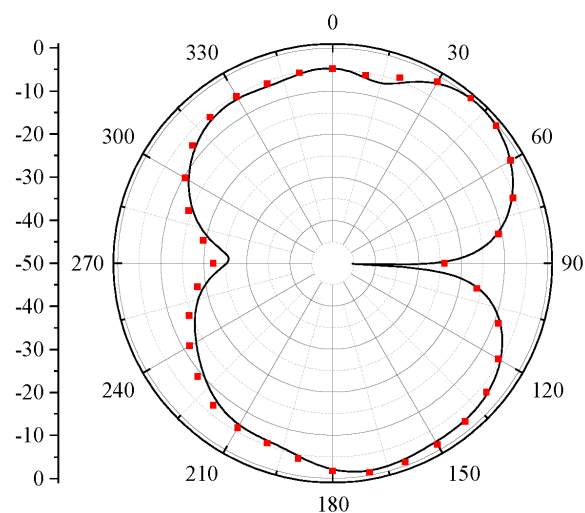
(c)

FIGURE 5.12: Simulated and measured radiation properties of the proposed array for E plane at (a) 23 GHz, (b) 28 GHz, and (c) 29 GHz (− simulated, • measured).
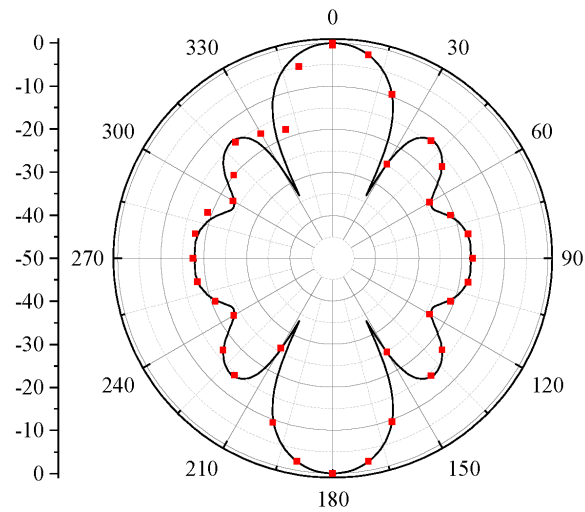
(a)
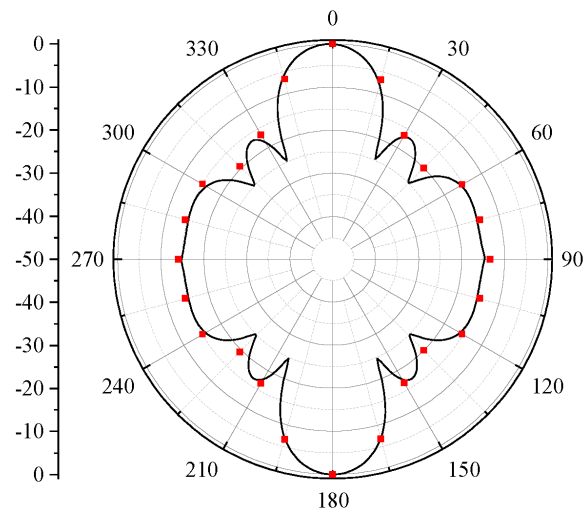
(b)
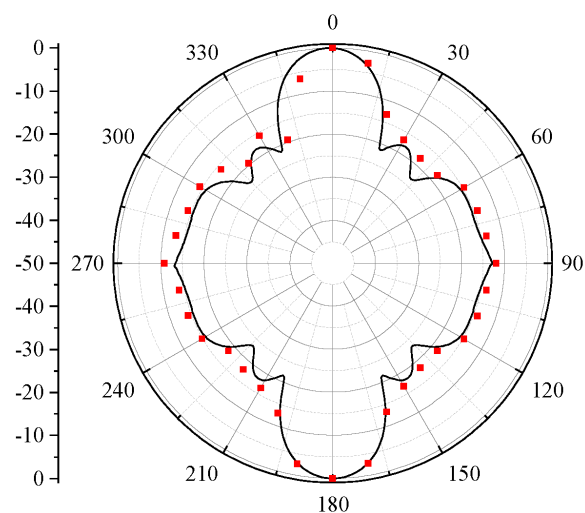
(c)

FIGURE 5.13: Simulated and measured radiation properties of the proposed array for H plane at (a) 23 GHz, (b) 28 GHz, and (c) 29 GHz ($-$ simulated, $\bullet$ measured).

farfield (broadband) [1]
Type   Farfield
Approximation enabled (kR >> 1)
Component   Abs
Output   E-Pattern
Frequency   28.012 GHz
Rad. Effic.   -0.2361 dB
Tot. Effic.   -0.2642 dB
Vmax   0.000 dB
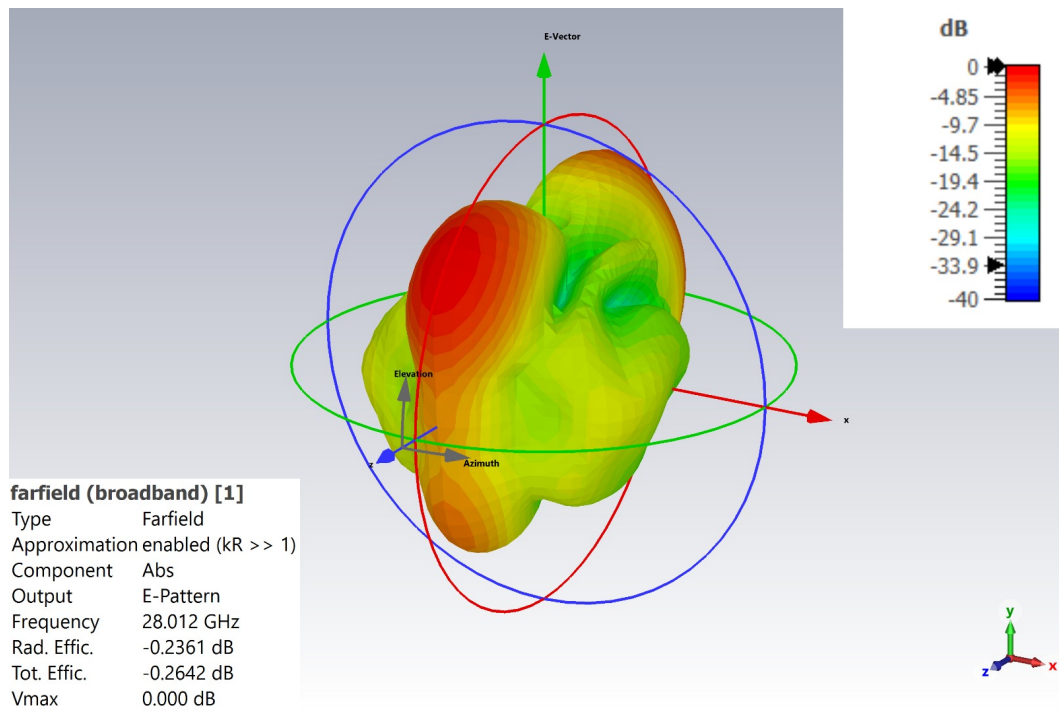
FIGURE 5.14: 3-D Radiation pattern for antenna array.
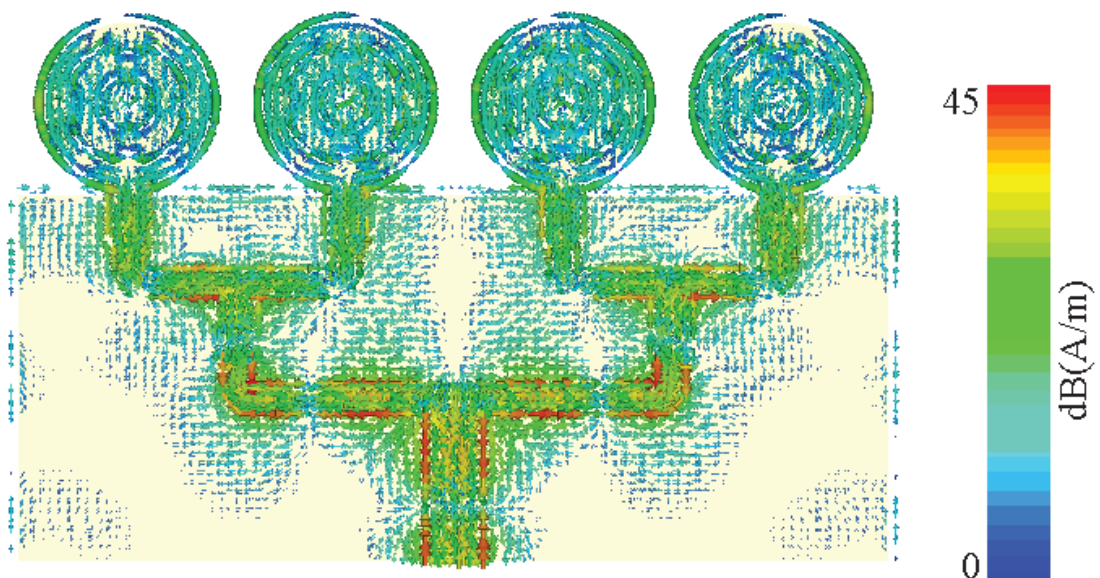
FIGURE 5.15: Surface current distribution for the designed array.

5.4 Comparative Analysis

Table 5.2 presents the comparison made between the designed array and the literature that has been presented previously. The designs that were presented in [47, 55–57, 59, 74] offered large bandwidth or high gain, but their size was much larger than the size of the demonstrated design. On the other hand, the designs that are presented in [60–62] are compact; however, they suffer because of reduced impedance bandwidth. Furthermore, the design presented in [45] offered extremely wide impedance bandwidth on the cost of increased array elements.

5.5 Summary

For use in the 28 GHz frequency band, a 1×4 linear antenna array is designed. The unique element of the array is a notch-loaded partial ground plane and a rhombus-inscribed circular ring fractal patch radiator. The proposed antenna element achieves wide impedance bandwidth, operating in the frequency range of 22.28 to 33 GHz. The antenna array has a 4-way corporate feed network. The designed resonance of the array is found to be satisfactory in the range of interest by both simulations and measurements. In addition to its high radiation efficiency of 95%, this array has a maximum gain of 10.7 dBi. It can also be concluded from the presented antenna array that it could be a potential candidate for future high-speed 5G communication systems.

Chapter 6

High Gain mm-wave Planar Antenna Loaded with Metasurface

6.1 Introduction

In this chapter, an effort has been made to design a compact, high gain, wide-band, and directional planar antenna for mm-wave applications. In continuation to the previous chapters, this chapter enlightens another technique to design planar antennas for 5G communication where the emphasis is to further enhance the impedance bandwidth by incorporating metasurface. The antenna's compact size is achieved by placing the meandered radiating element on a loss-low dielectric substrate. To obtain a wide impedance bandwidth of 22 to 40 GHz, a partial ground plane with parasitic elements is used (these elements are placed on the back-side of the substrate). One of the major objective of the design is to get high gain and directional radiation characteristics, which are achieved by incorporating a wide-band metasurface behind the designed planar antenna. The integration

of metasurface led to achieve the directional radiation performance in the operating bandwidth and an average gain of 6.99 dBi. The complete antenna design procedure along with the results is presented in the upcoming sections.

The demand to connect several devices to the wireless network at once has arisen as a result of the recent advancements in mobile devices and communications technology. In order to achieve this requirement, the Federal Communications Commission (FCC) has currently chosen the bandwidth of 25-70 GHz for the upcoming generations of mobile communication, which is called 5G communication technology. The 5G technology offers faster data speeds, greater dependability, low-power connectivity for millions of devices, and support for cutting-edge innovations like driverless cars, smart cities, and virtual reality. In addition, the 5G communication devices are compact and they require small antennas with better performance. The compactness can be achieved by using a planar configuration, but it suffers due to low gain and radiation efficiency. One of the techniques to achieve high gain is to use frequency selective and metasurface reflectors behind the radiation element. Many researchers have designed different frequency selective surface (FSS) and metasurface-based antennas for high gain 5G communication devices. The targeted specifications of the proposed antenna array are discussed in Table 6.1.

TABLE 6.1: Specification Table.

Variable	Target
Bandwidth	15 GHz
FBW	>35%
Peak gain	10 dBi
Size	8×12×4 mm^3
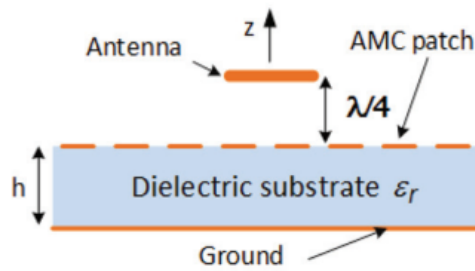
FIGURE 6.1: Illustration of artificial magnetic surface (AMC) used as a meta-surface in microwave patch antenna [128].

6.2 Metasurface-based Planar Antenna

To improve the electrical properties of a patch antenna, metasurfaces are regularly applied. A metasurface offers characteristics that are not available in materials found in nature. These surfaces are specially designed to meet a specific need and their characteristics therefore depends on their design. These artificial materials modify the propagation characteristics of electromagnetic waves by altering the permittivity (ϵ) and/or permeability (μ) of the material. The modified surface could provide high impedance to the incident wave called high impedance surface (HIS). Sometimes it functions as a filter referred to as electromagnetic band gap (EBG) filter, while yet in another design, it might allow specific frequencies to propagate whilst others stop, giving rise to a surafce known as frequency selective surface (FSS) [127]. The ambient of a radiating patch could also be changed by placing it in close proximity to an artificial magnetic conductor (AMC), as shown in 6.1.

The first AMC based metasurface was introduced by Sievenpiper in 1999 [128]. The introduction of AMC in patch antenna solves many issues, especially in wide-band microwave designs. It maximizes radiation to one direction while minimizing the back radiation. The same property has been exploited in the design proposed in this chapter. Before explaining the design of the proposed metasurface-based antenna, the design of the radiating element and metasurface are discussed in detail in the below-mentioned sections.

6.2.1 Meandered Planar Antenna

The design of the proposed wideband planar antenna is illustrated in Fig. 6.2, while the design parameters used to build the antenna are listed in Table 6.2. The antenna is designed on a low-loss and flexible Rogers RT/Duroid 5880 substrate. The thickness of the substrate for the antenna design is chosen to be 0.254 mm. One can note from the design shown in Fig. 6.2(a) that the proposed antenna is composed of a meander-shaped patch radiator fed using a 50Ω microstrip feeding line. The length of the one meandering section is equal to one guided wavelength (λ_g) at 26 GHz, and it can be calculated as:

$$\lambda_g = \frac{c}{f_r\sqrt{\varepsilon_{eff}}} \tag{6.1}$$

where

$$\varepsilon_{reff} = \frac{\varepsilon_r + 1}{2} \tag{6.2}$$

The back side of the antenna is comprised of a partial ground plane (see Fig. 6.2b), which is utilized to achieve wide impedance bandwidth. It is also observed from Fig. 6.2(b) that 3×3 array of parasitic elements is placed right behind the radiating element, whose main purpose is to provide better impedance matching in the operating bandwidth.

TABLE 6.2: Design parameters used for the construction of planar antenna (all dimensions in mm).

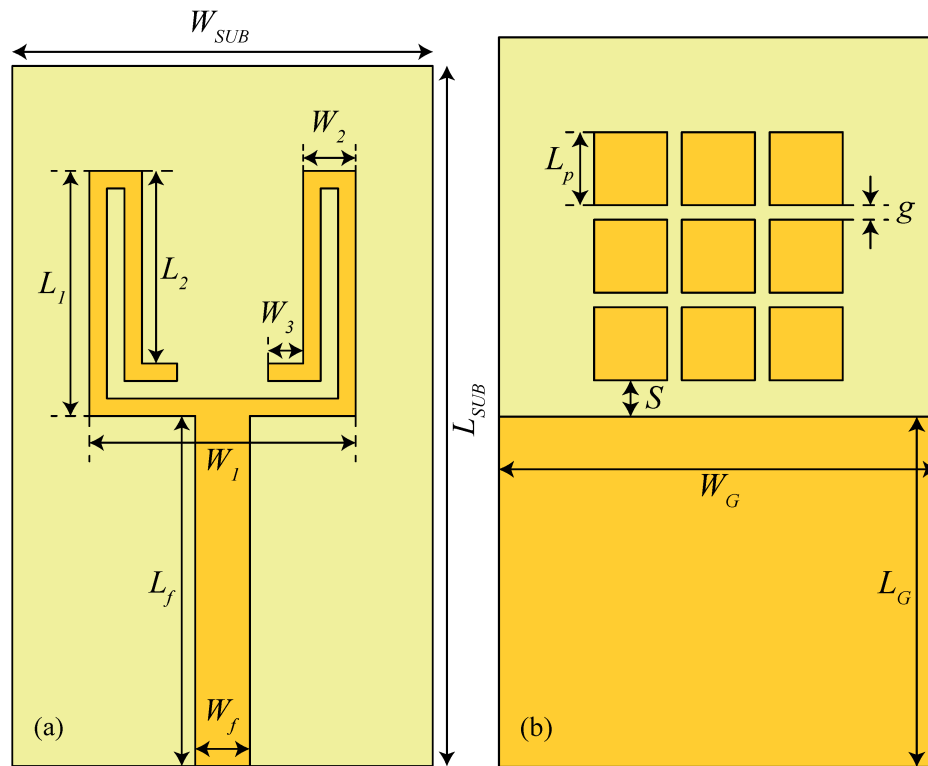| Parameter	Value	Parameter	Value
W_{SUB}	6	L_{SUB}	10
W_f	0.78	L_f	5
W_1	3.8	W_2	0.75
W_3	0.5	L_1	3.5
L_2	2.75	W_G	6
L_G	4.5	S	0.5
L_p	1	g	0.2

FIGURE 6.2: Design of the proposed planar wide-band antenna (a) front-side (b) back-side.
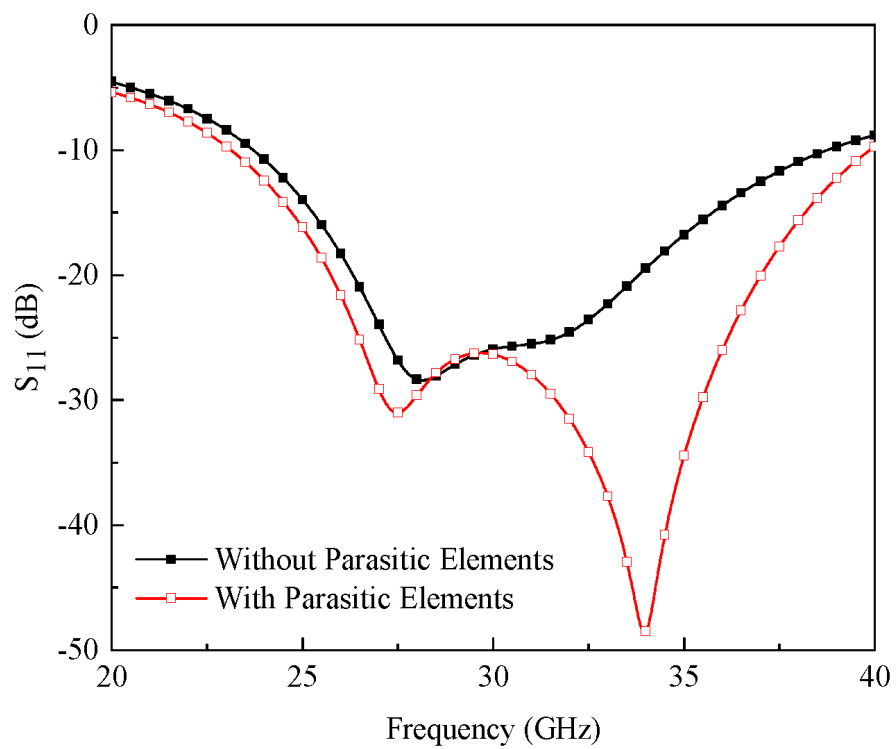
FIGURE 6.3: S_{11} of the proposed planar wide-band antenna without and with parasitic elements.

The effect of parasitic elements on the antenna performance is shown in Fig. 6.3, where the reflection coefficient (S_{11}) response of the proposed antenna is plotted. One can note that without parasitic elements, the antenna offers an impedance bandwidth of 15.02 GHz in the frequency range of 23.72–38.74 GHz, as shown in Fig. 6.3. On the other hand, the use of parasitic elements increased the upper frequency limit of the antenna by 1.12 GHz (see Fig. 6.3) and also increased the lower frequency limit by 580 MHz, as shown in Fig. 6.3. This increase in the frequency limit tends to achieve an impedance bandwidth of 16.72 GHz.

The effect of different parasitic element configurations on the planar antenna S_{11} and realized gain is shown in Fig. 6.4. For 3×3 and 4×3 parasitic arrays, the antenna offers better impedance matching compared to 3×5 and 4×5 arrays, as shown in Fig. 6.4(a). In the case of 4×3 array, a shift in frequency is observed. On the other hand, different arrays have a minor effect on the gain of the antenna (see Fig. 6.4b).

The simulated antenna efficiency and realized gain are shown in Fig. 6.5. As shown in Fig. 6.5(a), the radiation efficiency of the proposed antenna is >95% for the operating frequency range, while the total efficiency fluctuates in the range of 78–97%. On the other hand, the gain of the antenna varies in the range of 4-6.93 dBi in the entire operating range (see Fig. 6.5b).

Figure 6.6 depicts the radiation characteristics of the proposed antenna for both the E and H planes at various frequencies. The results show that the proposed planar antenna has a typical monopole-like radiation pattern for the E plane. In the case of 24 GHz, the E plane main beam is aimed at 210°, indicating that the antenna is radiating backward. The H plane pattern, on the other hand, is noted to be quasi-omnidirectional for frequencies up to 32 GHz, as shown in Fig. 6.6(a-c). This pattern becomes bi-directional at higher frequencies (see Fig. 6.6d). This change in the radiation pattern may be associated with the coupling effect of parasitic elements.

To improve the radiation characteristics of the proposed antenna, a metasurface reflector is designed, whose details are provided in the following sub-section.
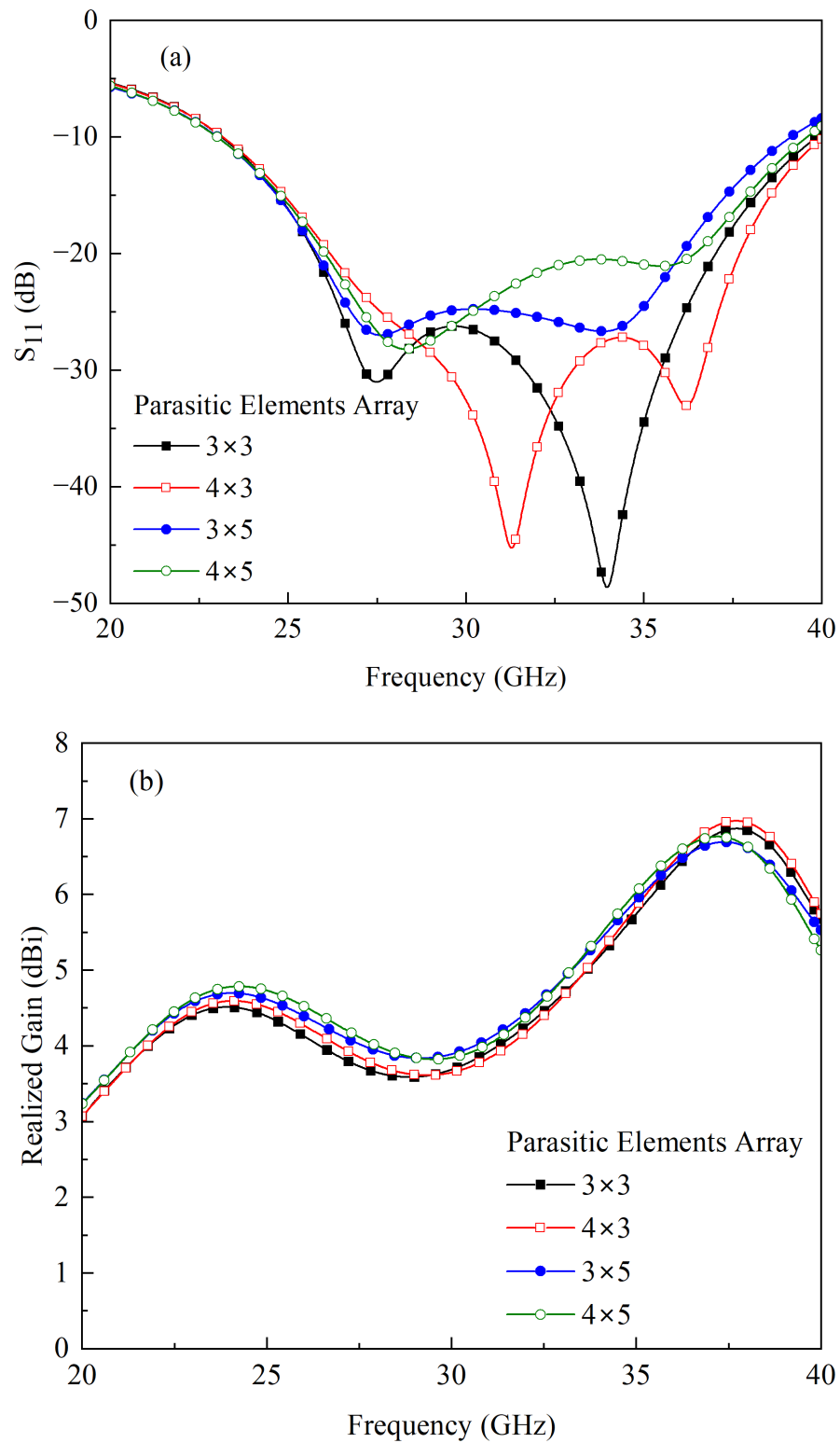
FIGURE 6.4: (a) S_{11} and (b) realized gain of the planar wideband antenna for different parasitic element configurations.
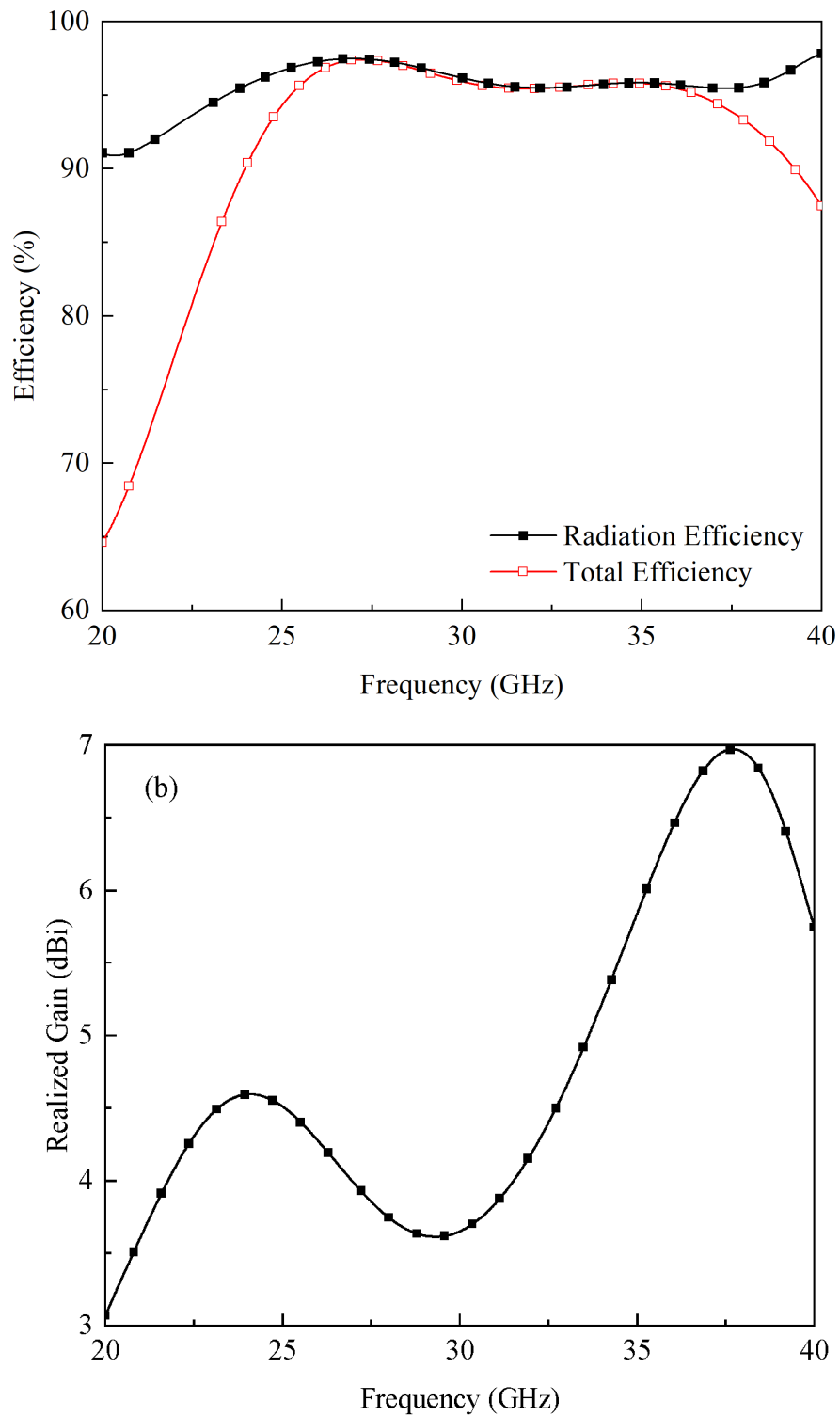
FIGURE 6.5: (a) Radiation efficiency, total efficiency, and (b) realized gain of the proposed planar wide-band antenna.
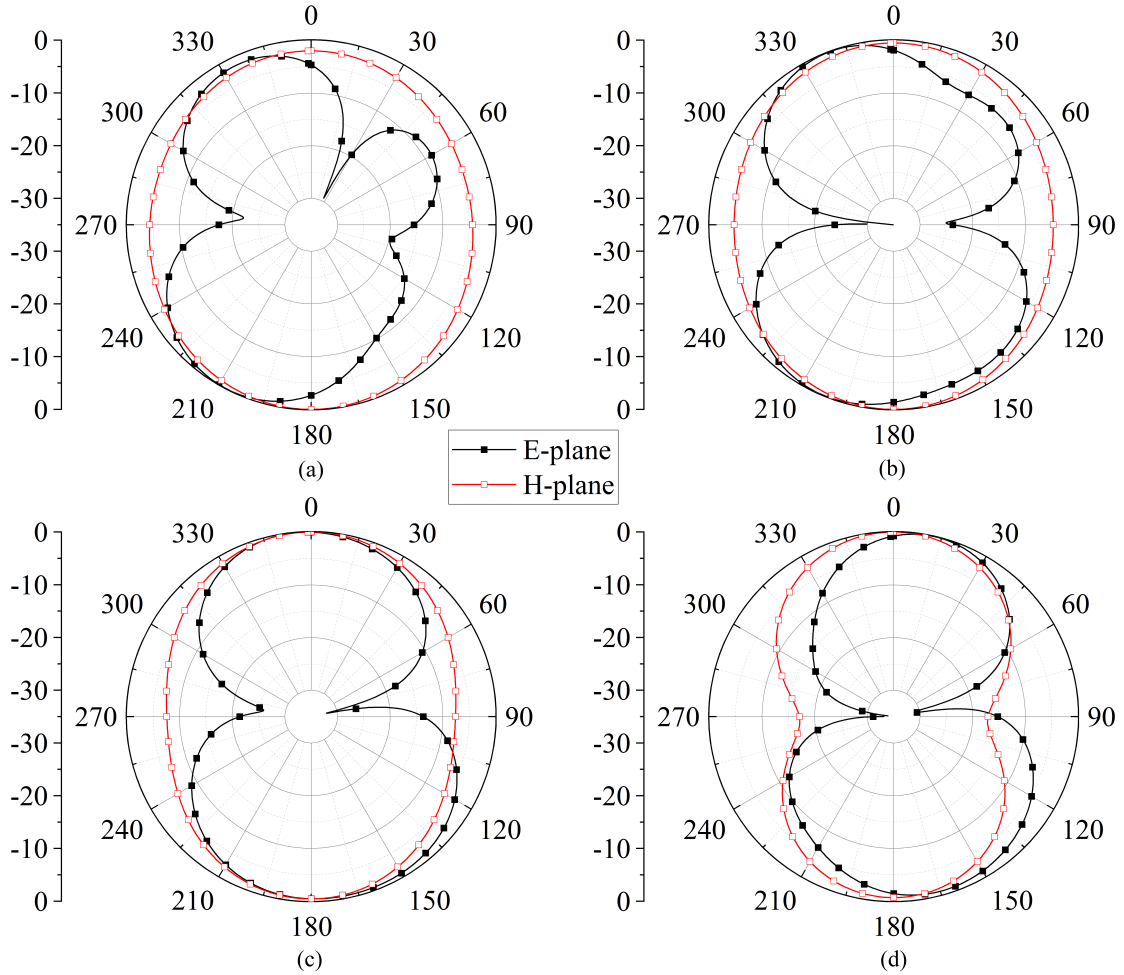
FIGURE 6.6: Radiation characteristics of the proposed planar antenna for (a) 24 GHz (b) 28 GHz (c) 32 GHz (d) 36 GHz.

6.2.2 Metasurface Design

Figure 6.7 shows the front view of the proposed metasurface reflector. It is designed on a low-loss Rogers RT/Duroid 5880 dielectric substrate having a thickness of 1.57 mm. One can observe from the figure that a square split ring resonator (SSRR) along with a circular SRR are used to design the metasurface, while the backside consists of a full ground plane. The other design parameters are as follows: $W_M = 4$, $L_{p1} = 3.5$, $R_{in} = 0.55$, $d_1 = 0.6$, $d_2 = 0.2$, $g_1 = 0.8$, and $g_2 = 0.4$ (all dimensions in mm).

In a SRR, the applied electric field is parallel to the no-split-bearing side and generates electric current on the same side only. On the contrary, when the electric field is applied along a split bearing side, it causes an electric current in the same
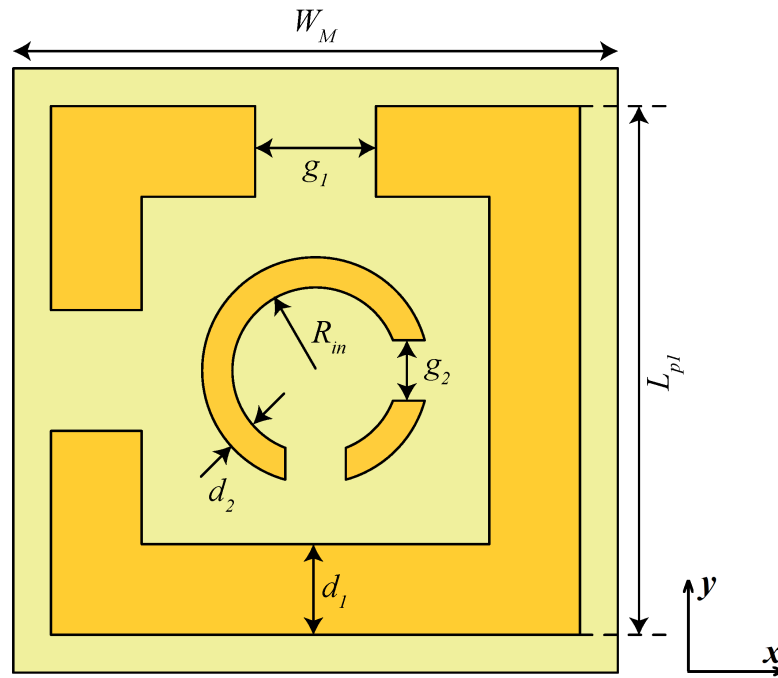
FIGURE 6.7: Proposed metasurface design.
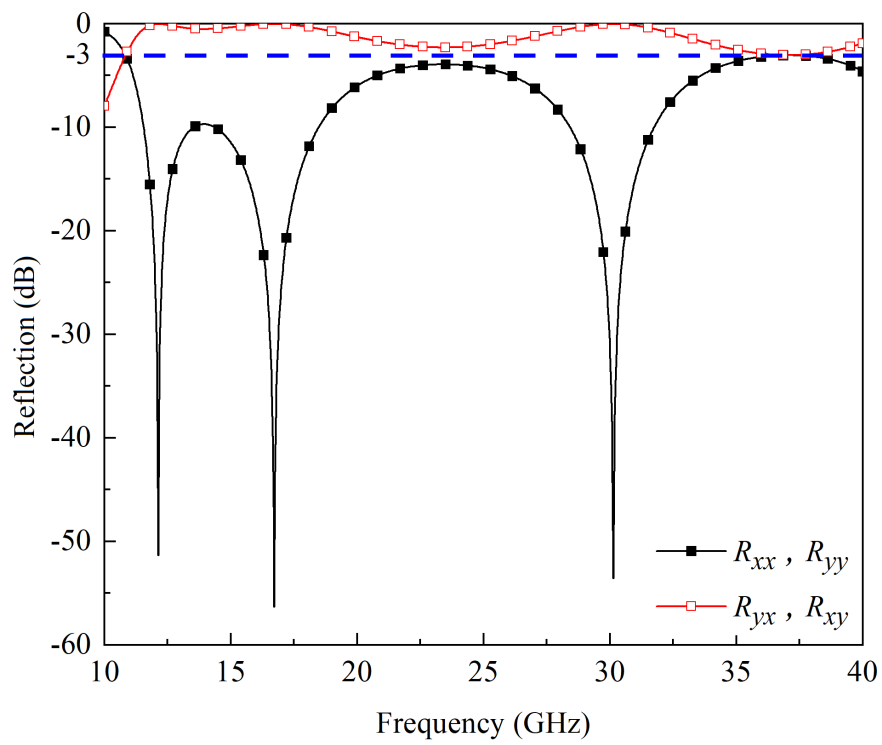
FIGURE 6.8: Reflection coefficient in dB as a function of frequency.
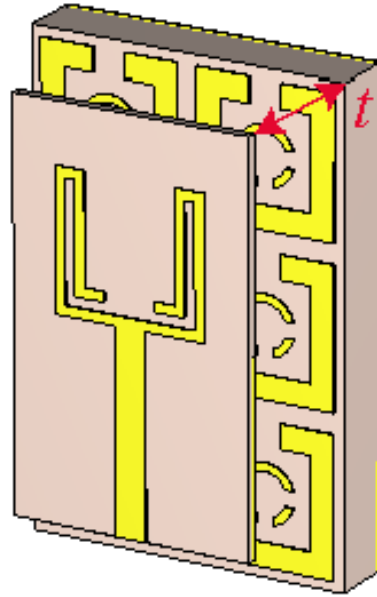
FIGURE 6.9: Configuration of the metasurface integrated planar antenna.
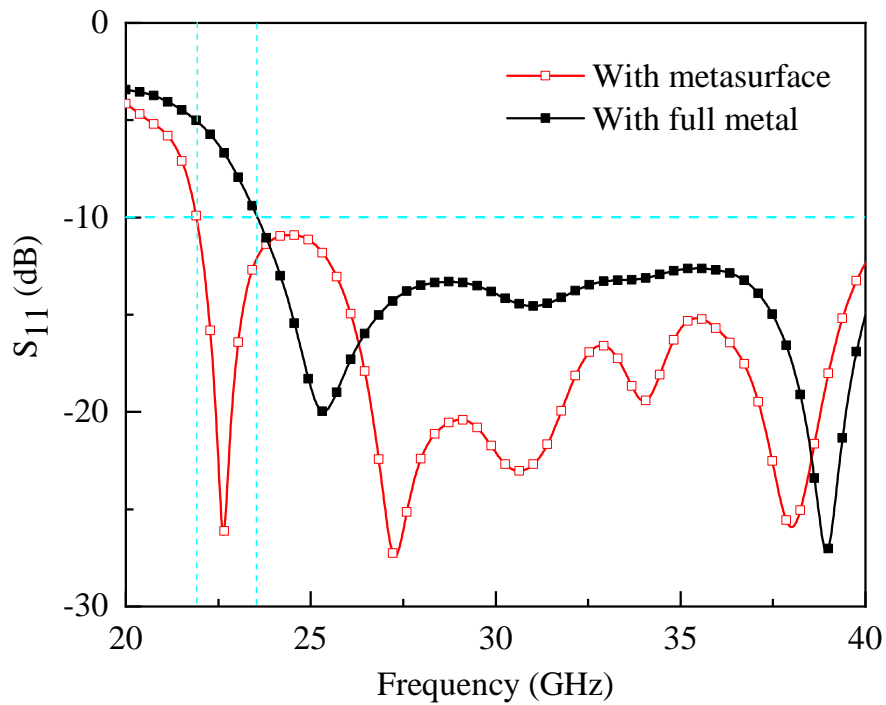
FIGURE 6.10: S_{11} of the planar antenna with metasurface and full metal.

side as well as the perpendicular (no split) side. Using this technique, two gaps are introduced in the adjacent sides of the square SRR, one for each linearly polarized impinging field. The inner circular SRR is used to generate plasmon resonances at higher frequencies, thereby achieving a wider bandwidth.

The metasurface is simulated in CST Microwave Studio by using periodic boundary
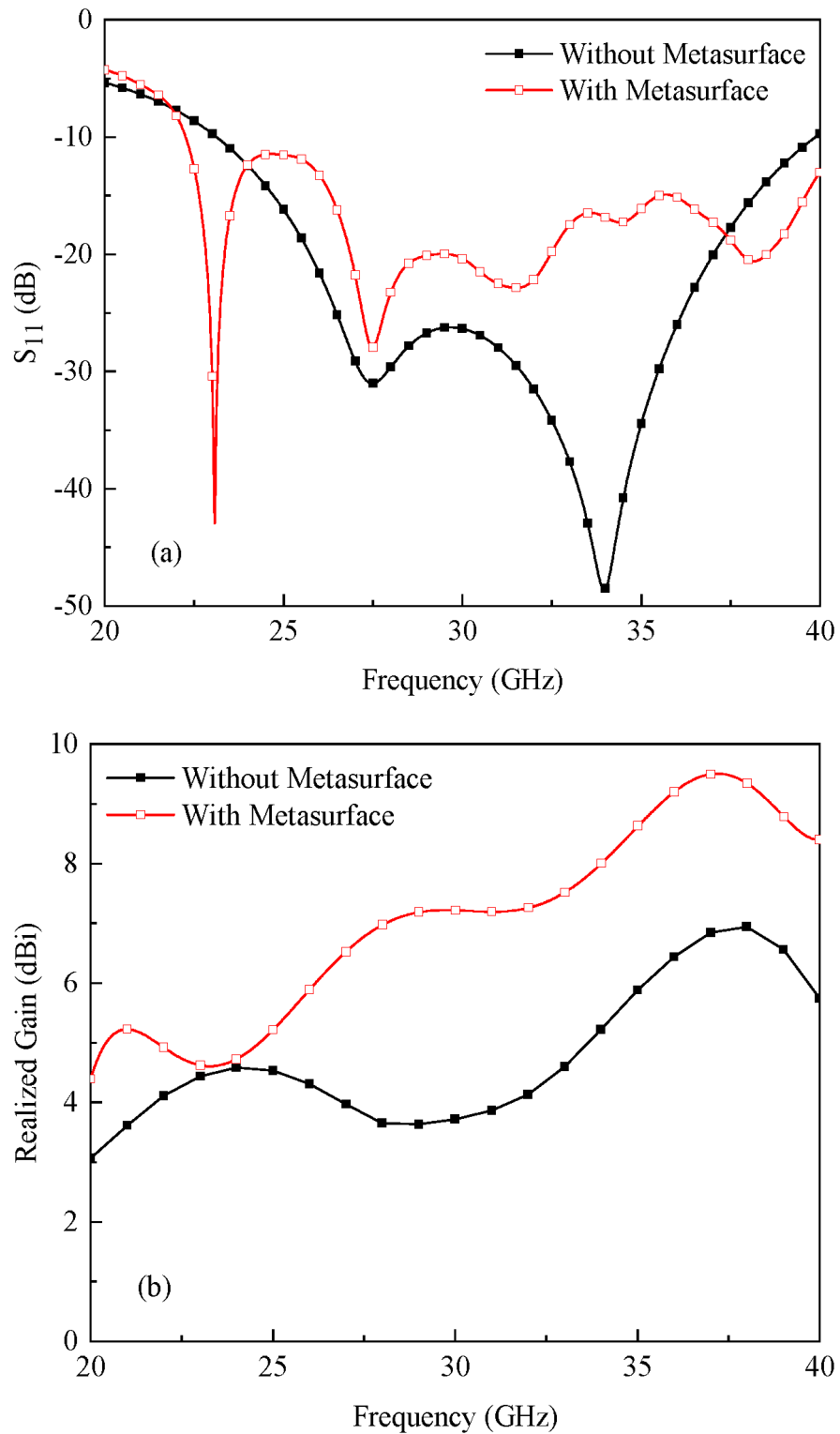
FIGURE 6.11: (a) S_{11} and (b) realized gain of the planar antenna without and with metasurface.
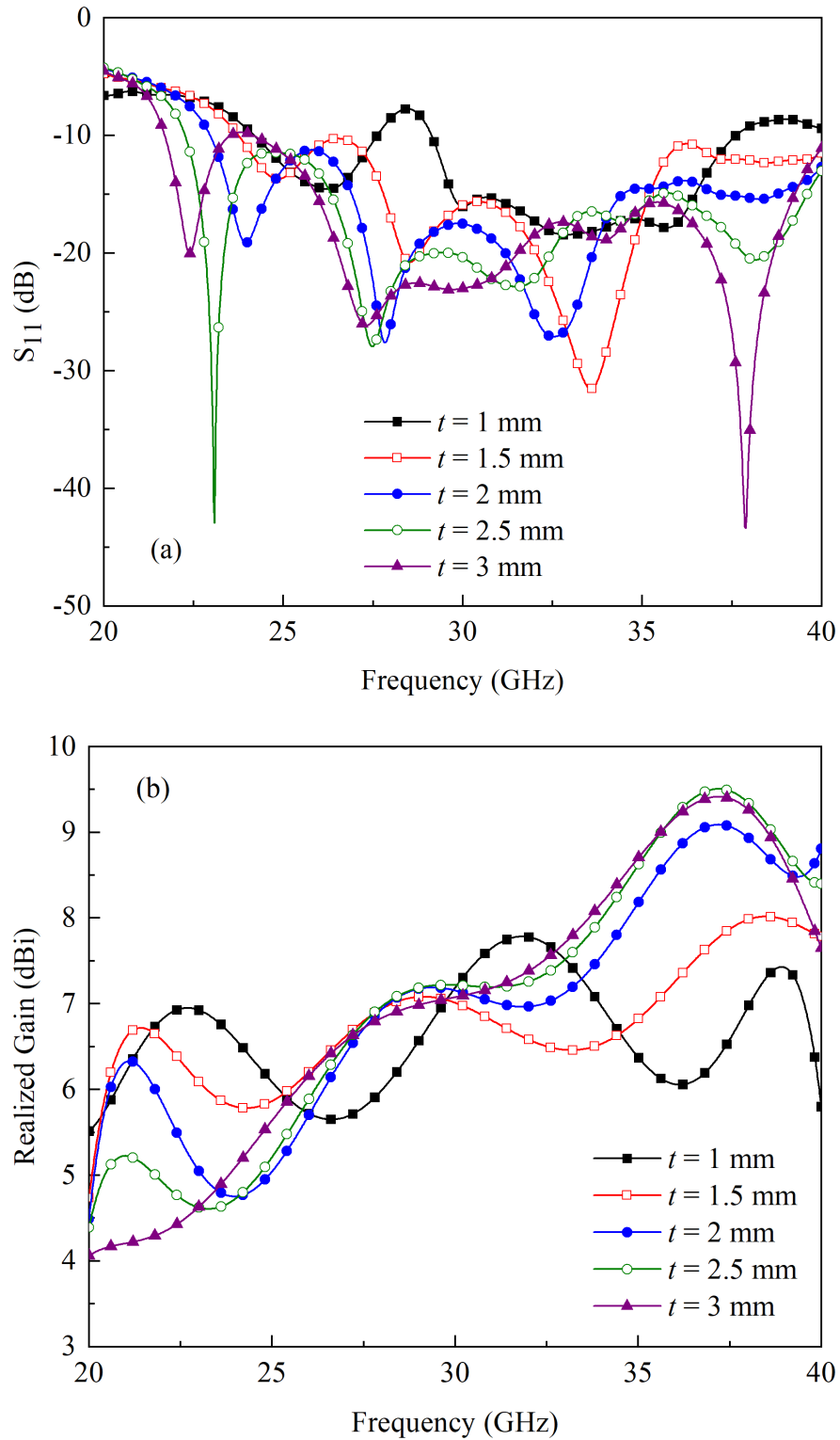
FIGURE 6.12: (a) S_{11} and (b) realized gain of the antenna when the gap between the radiating element and metasurface reflector is changed from 1 to 3 mm.

conditions. Electric and magnetic fields are used in the x- and y- axes, respectively, while floquet port is used in the $+z$-axis. When a x-polarized wave impinges on the
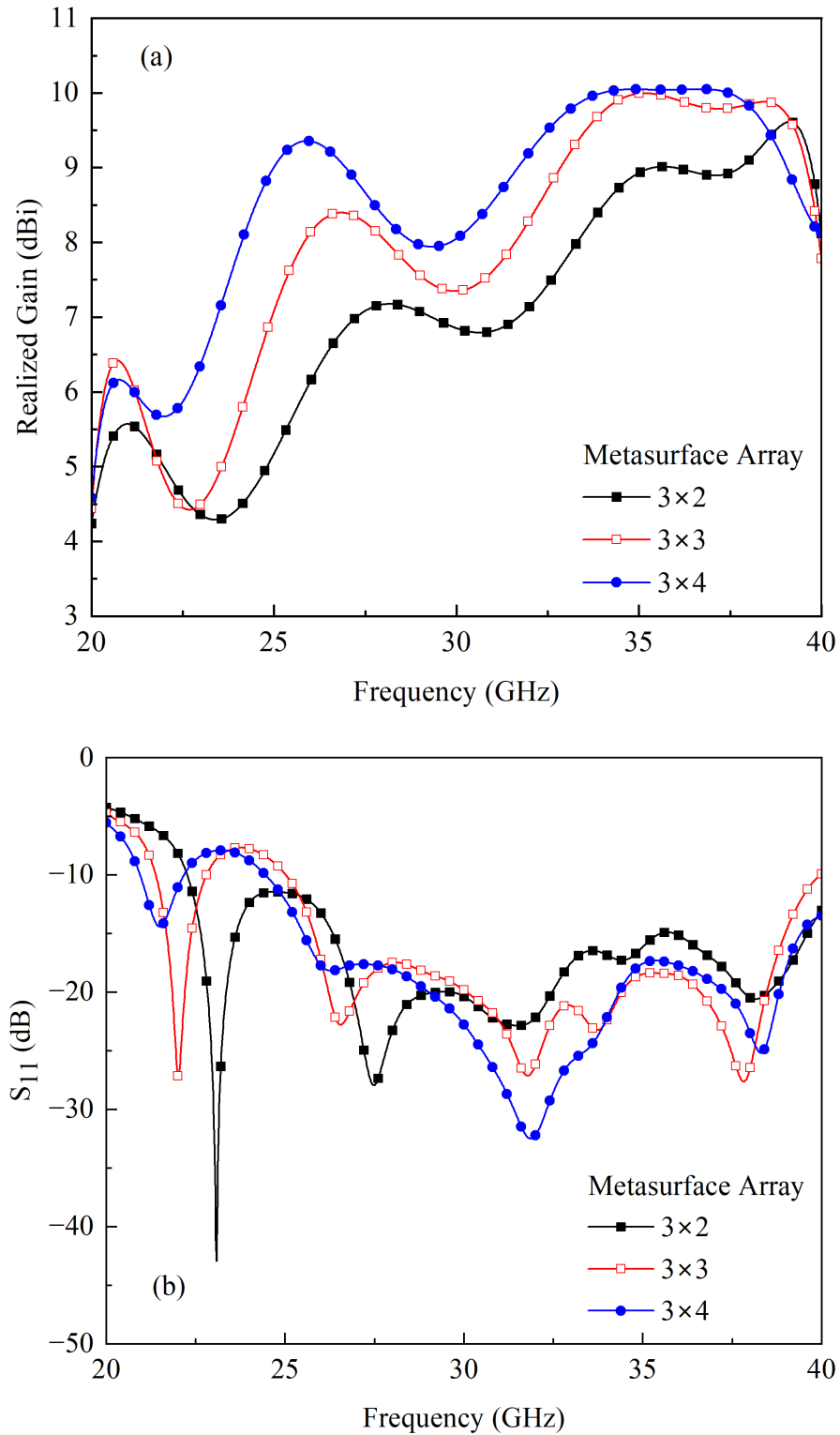
FIGURE 6.13: (a) Realized gain and (b) S_{11} of the planar wideband antenna for different metasurface arrays.

metasurface, it generates two components: co-polarized (R_{xx}) and cross-polarized

(R_{yx}). The mathematical formulation to calculate R_{xx} and R_{yx} is given below:

$$R_{xx} = \frac{|E_{rx}|}{|E_{ix}|}, \quad R_{yx} = \frac{|E_{ry}|}{|E_{ix}|} \tag{6.3}$$

This behavior is same for y-polarized wave. In this case, the corresponding components can be defined as R_{yy} and R_{xy}, respectively. The simulated co- and cross-polarized components of the metasurface are depicted in Fig. 6.8. These components can be represented in terms of reflection and transmission coefficients. It can be observed that the metasurface is operating well from 11 to 35 GHz, according to the -3 dB bandwidth criteria, which covers the operating band of interest [129].

6.2.3 Planar Antenna Integrated with Metasurface

After designing the metasurface, the proposed antenna design presented in subsection 6.2.1 is integrated to achieve high gain and directional radiation characteristics. The configuration of the proposed metasurface integrated planar antenna is shown in Fig. 6.9. When the antenna is located at a specific distance over the metasurface reflector, the metasurface reflects the backward radiation of the antenna to the opposite side. Therefore, two wave components will be added in the same phase, which gives constructive interference and ultimately improves radiation performance. Let's consider that ϕ_t and ϕ_r are the phases of the transmitted and reflected waves, and the complete propagation trip between metasurface reflector is denoted by ϕ_s. Mathematically, these phases can be related as

$$\phi_t = \phi_r + \phi_s \tag{6.4}$$

and

$$\phi_s = 4\pi f \times \frac{t}{c} \tag{6.5}$$

where c is the speed of light, t is the gap between antenna and metasurface, and ϕ_t should be 0 or the integral of 2π [130].

(a)   (b)   (c)   (d)

(e)
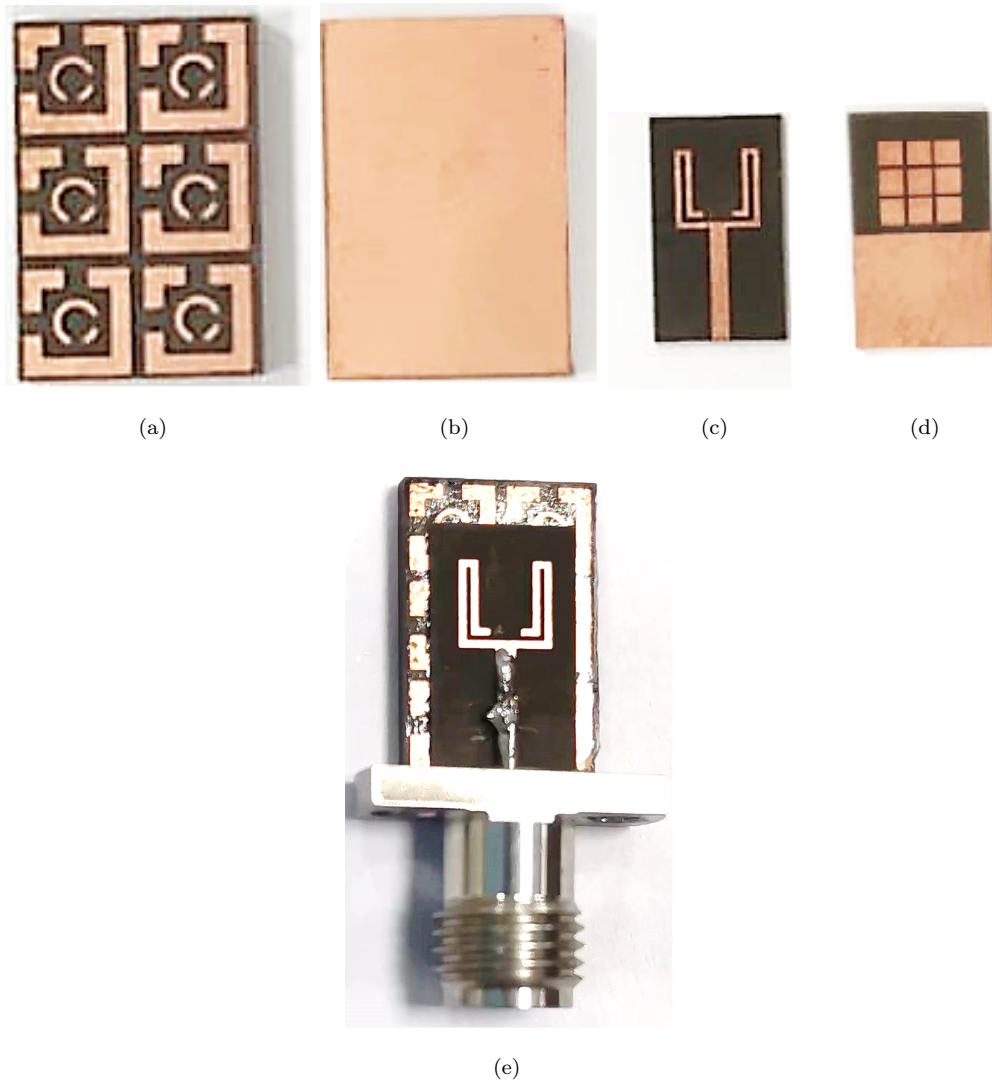
FIGURE 6.14: Fabricated (a-b) Front and back view of metasurface, (c-d) Front and back view of antenna (e) perspective view.

In the proposed design, the metasurface is placed beneath the designed antenna so that it makes the back radiation of the antenna in phase and then enhances the gain. In this scenario, an important factor is the distance between the antenna and the metasurface reflector, which ensures the constructive interference of directly radiated and reflected waves. To estimate the spacing between both of them, the following equation can be used [131]:

$$\phi_{\text{Metasurface}} - 2\beta t = 2n\pi \tag{6.6}$$

where π represents the reflected wave phase from the metasurface layer and β is
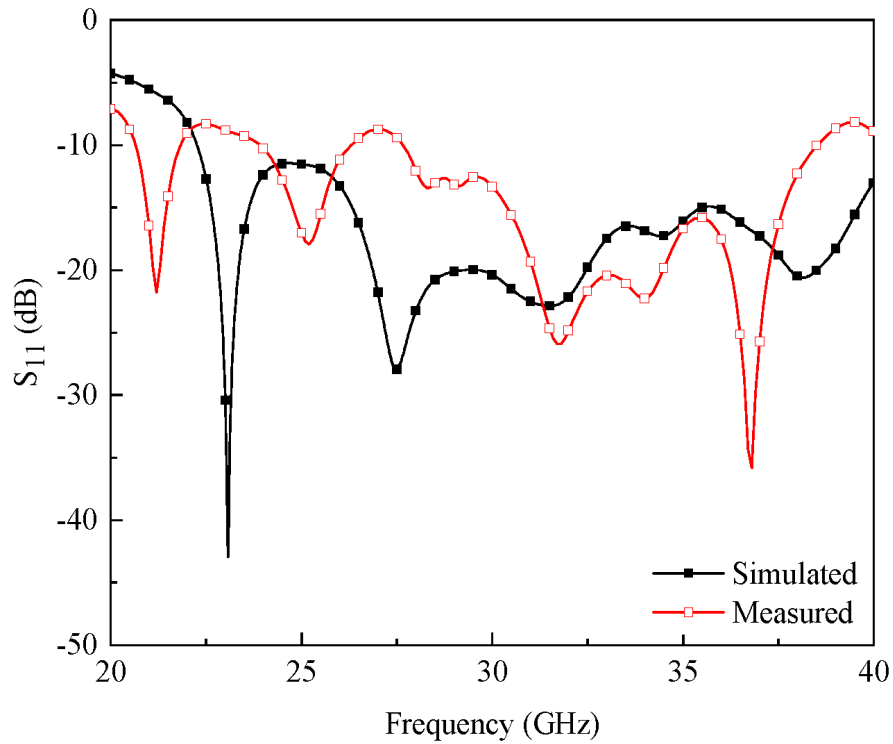
FIGURE 6.15: Simulated and measured S_{11} of the proposed metasurface integrated planar antenna.

the free-space propagation constant, which is equal to $2\pi/\lambda_0$, where λ_0 is the free-space wavelength at 28 GHz. One thing that needs to be noted is that the value of t should be an integer multiple of the wavelength at the center frequency. However, due to the wideband nature of the metasurface, this gap can be optimized to achieve an acceptable gain. Using the aforementioned methodology, the antenna is placed 2.5 mm above a 3×2 array of metasurfaces, which is equal to $\lambda_0/4$.

Fig. 6.10, depicts the simulated reflection coefficient S_{11} characteristics for planar antenna integrated with full metal and metasurface presented above. One can notice from the results of Fig. 6.10 that the integration of metasurface helps to improve the impedance bandwidth of approx 1.22 GHz according to -10 dB bandwidth criteria. The impedance bandwidth with full metal is noted to be 16.5 GHz ranging from 23.5 GHz to 40 GHz, while with metasurface, it is equal to 17.72 GHz, as shown in Fig. 6.10.

Figure 6.11(a) depicts the simulated S_{11} response of the metasurface-based antenna. The figure presents the comparison between the S_{11} characteristics of the
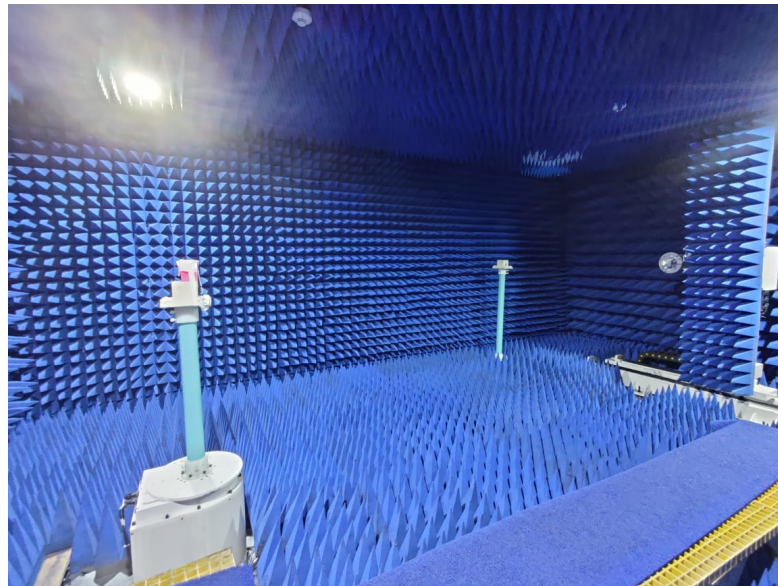
(a)
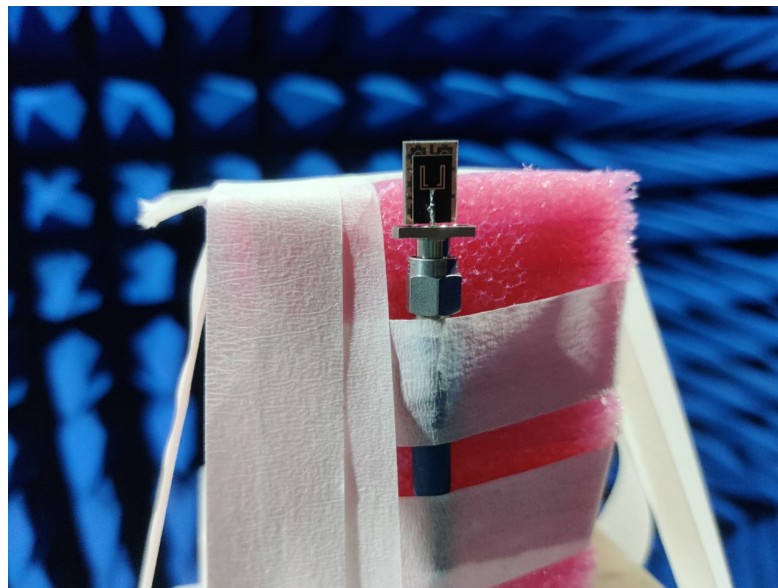
(b)

FIGURE 6.16: (a) Far-field measurement setup (b) Standalone antenna.

antenna without and with a metasurface. It can be clearly observed from the graph in Fig. 6.11(a) that the integration of the metasurface extends the impedance bandwidth of the antenna. The impedance bandwidth without metamaterial is noted to be 16.72 GHz, while with metasurface, it is equal to 17.72 GHz, ranging from 22.28 to 40 GHz, as shown in Fig. 6.11(a). The same kind of enhancement is observed in the antenna gain, as shown in Fig. 6.11(b). The gain of the antenna is increased up to 1.4 dB for the lower frequency bands, while for the higher
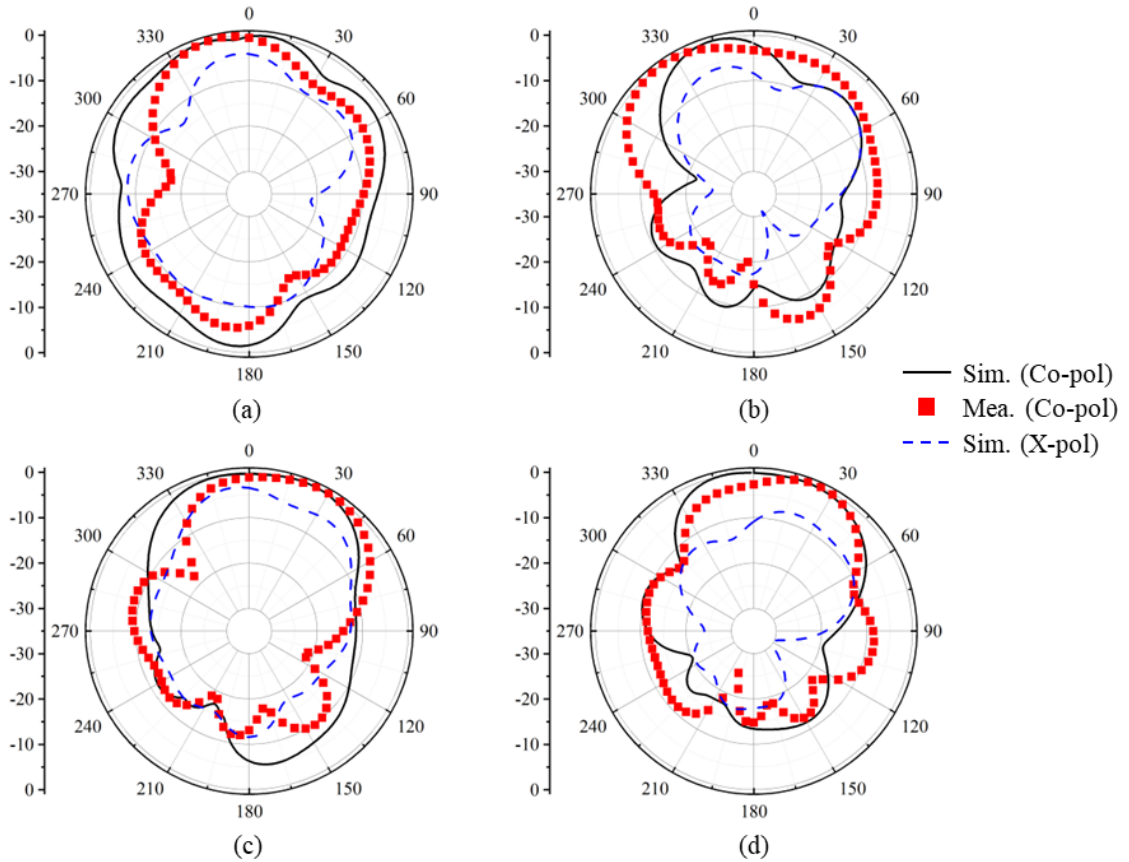
FIGURE 6.17: Simulated and measured far-field radiation characteristics of the proposed antenna for E plane at (a) 24 GHz (b) 28 GHz (c) 32 GHz (d) 36 GHz.

frequency bands, it is enhanced up to 2.5 dB, as shown in Fig. 6.11(b).

To evaluate the antenna's performance, a parametric study is conducted by changing the gap between the antenna and metasurface reflector. The gap is changed from 1 to 3 mm, and the performance is assessed in terms of S_{11} and gain. For $t = 1$ mm, the antenna offers dual-band response ranging from 24.2 to 27.6 GHz and from 29.14 to 37.6 GHz, respectively (see Fig. 6.12a). As the value of t in increased, an increase in the impedance bandwidth is observed, as shown in Fig. 6.12(a). Although the antenna offers a wide bandwidth response for $t = 3$ mm, a mismatch is observed in the frequency range of 23.54-24.14 GHz, as shown in Fig. 6.12(a). On the other hand, for $t = 1$ and 1.5 mm, the gain of the antenna fluactautes in the range of 5.5-8 dBi, as shown in Fig. 6.12(b). As the value of t increased, the gain of the antenna increased linearly (see Fig. 6.12b).
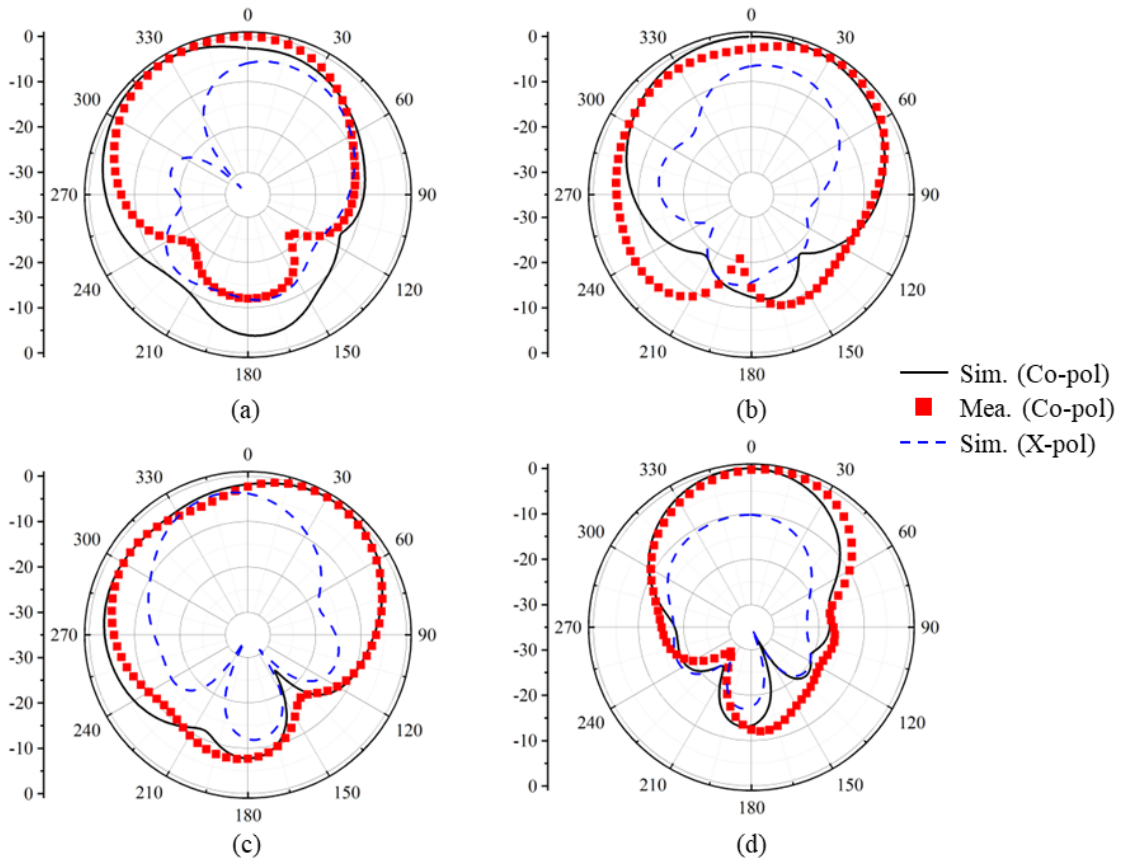
FIGURE 6.18: Simulated and measured far-field radiation characteristics of the proposed antenna for H plane at (a) 24 GHz (b) 28 GHz (c) 32 GHz (d) 36 GHz.

The effect of different metasurface array configurations on the antenna's performance is shown in Fig. 6.13. Although the gain increases with the increase in array size (see Fig. 6.13a), it shifts the lower operating frequency from 22.28 to 26 GHz, ultimately reducing the impedance bandwidth of the antenna, as shown in Fig. 6.13(b). The improvement in bandwidth can be achieved by further increasing the gap between the antenna and the metasurface reflector. This will increase the overall size of the antenna system, which is not useful for compact devices.

6.3   Fabrication and Measurements

The proposed antenna's prototype is fabricated to validate the simulation results. Figure 6.14 shows the fabricated prototype of the antenna and metasurface. The S_{11} characteristics of the antenna are measured using the Power Network Analyzer

(PNA) from Keysight. A piece of rohacell has been used to maintain the gap between designed antenna and metasurface.

The simulated and measured S_{11} of the proposed metasurface-based planar antenna is shown in Fig. 6.15. It is observed from the figure that the antenna offers a simulated impedance bandwidth from 22.28 to 40 GHz (17.72 GHz), while the measured impedance bandwidth is noted to be 15.8 GHz in the frequency range of 23–38.8 GHz, as shown in Fig. 6.15. The discrepancy between the results may be associated with fabrication intolerances, connector or RF cable losses, and scattering environment losses. Despite this, the proposed design is still able to cover the frequency spectrum, which is required for mm-wave communication.

An anechoic chamber is used to characterize the proposed antenna by determining its far-field radiation characteristics. The step-by-step instructions for the technique can be found in Chapter 5 (see Fig. 5.10). Fig. 6.16 depicts the measurement setup that was utilized in the process of determining the characteristics of the proposed antenna.

The far-field radiation properties of the proposed metasurface-based planar antenna for both the E and H planes are shown in Figs. 6.17 and 6.18. From the figure, it can be observed that the proposed antenna exhibits directional radiation characteristics for both planes for the chosen frequency bands. Although the use of a metasurface provides directional characteristics, it also shifts the main beam to different angles. The tilt can be controlled by placing parasitics on the sides of the radiating patch, and beam switching properties can be achieved as demonstrated in [132]. In addition, this beam shift can help achieve beam steering performance by utilizing the array configuration of the proposed design. The simulated cross-polarized (X−pol) components for both planes are also shown in Figs. 6.17 and 6.18. It is observed that for 24, 28, and 32 GHz, the X−pol level is less than −5 dB. As the frequency increases, the X−pol level tends to decrease (< -10 dB). In addition, some discrepancies are observed in the simulated and measured radiation characteristics, which could arise due to the measurement setup losses.

Looking at the data given in Figs. 6.17 and 6.18, it can clearly be seen that the amplitude of X−pol versus Co−Pol at different frequencies of interest is not in complete harmony with the requirements of a linearly polarized antenna. For such an antenna, X−pol should be significantly (< -10 dB) lower than Co−pol. It is an established fact that an antenna cannot be 100% polarized to a single mode for which it has been designed. Orthogonal polarization does exist but it must be as low as possible to improve the transmission and reception of a signal. For the frequencies and angles shown in Figs. 6.17 and 6.18, where the X−pol and Co−pol differences are not at least 10 dB, the proposed design may not be fully effective for these values. Therefore, the design requires further improvements (future work) to reduce X-pol (below -10 dB) compared to Co−pol for the entire band of interest.

The radiation and total efficiency results of the proposed antenna are depicted in Fig. 6.19. As expected, the radiation efficiency of the proposed antenna is noted to be >95% for the operating frequency range, while the total efficiency is observed to be >90%, as shown in Fig. 6.19.

Figure 6.20 illustrates the simulated and measured realized gain of the proposed antenna. One can observe that the simulated gain fluctuates in the range of 4.39–9.5 dBi with an average value of 7 dBi (see Fig. 6.20). On the other hand, the measured gain varies from 4.49 to 9 dBi, as shown in Fig. 6.20. The average measured gain in the operating bandwidth is noted to be 6.99 dBi, which is approximately equal to the simulated value. The 3-D radiation pattern for designed metasurface integrated planar antenna is shown in the Fig. 6.21. From the presented results, it can be concluded that the proposed antenna design can be used in 5G communication devices where wideband response and directional radiation characteristics are required.

Table 6.3 enlists a comparison among proposed and previously presented metasurface-based antenna designs. Although the gain of the antenna is low except [133, 134], it is compact compared to the designs of [133, 135, 136] and simple in nature compared to [136, 137]. In addition, the presented antenna offers a wide impedance
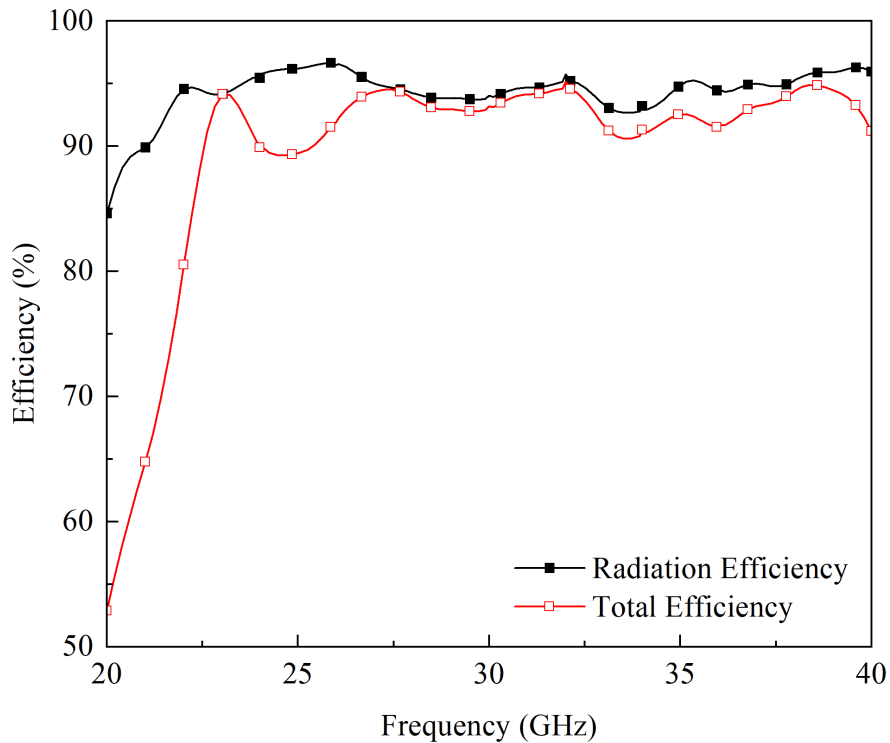
FIGURE 6.19: Radiation and total efficiency of the proposed metasurface integrated planar antenna.

bandwidth and fractional bandwidth (FBW) compared to the designs listed in Table 2.2.

6.4 Summary

A design of a planar wideband antenna is presented for mm-wave 5G communication applications. To ensure compactness, a meander-shaped radiating element is chosen for the design. For enhanced impedance bandwidth, a partial ground plane and parasitic elements are utilized. To achieve high gain and directional radiation characteristics, a metasurface reflector is designed and placed behind the proposed planar antenna. It is observed that the designed metasurface-based antenna is able to operate well in the desired frequency band. The results show that the proposed antenna offers an impedance bandwidth of 15.8 GHz from 23 to 38.8 GHz and exhibits a peak and average gain of 9 dBi and 6.99 dBi in the operating bandwidth, respectively. In addition, the simulated and measured performances
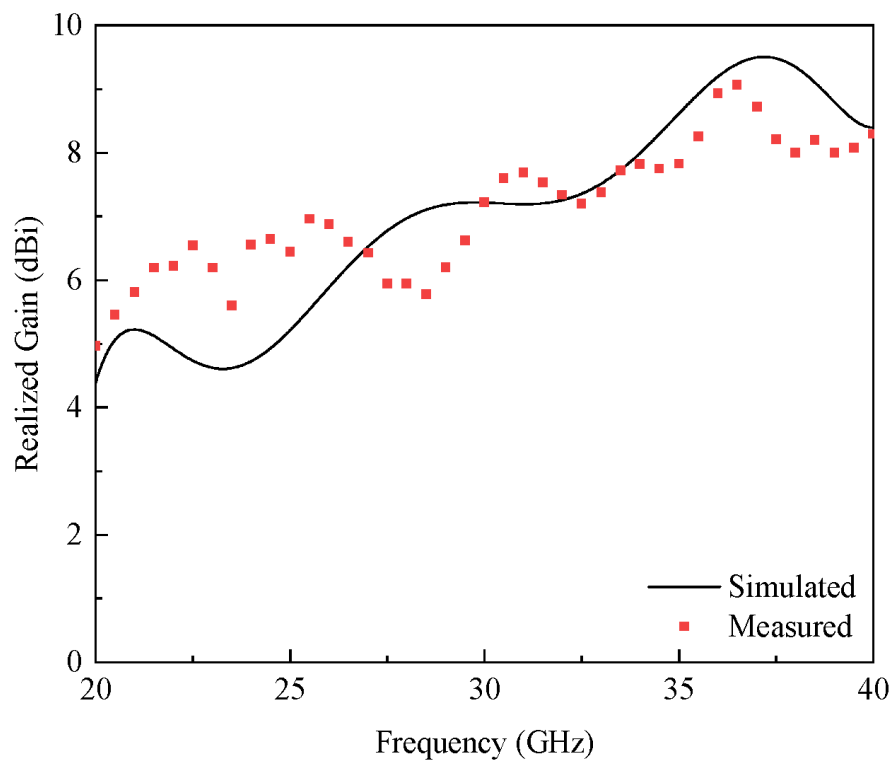
FIGURE 6.20: Simulated and measured realized gain of the proposed metasurface integrated planar antenna.
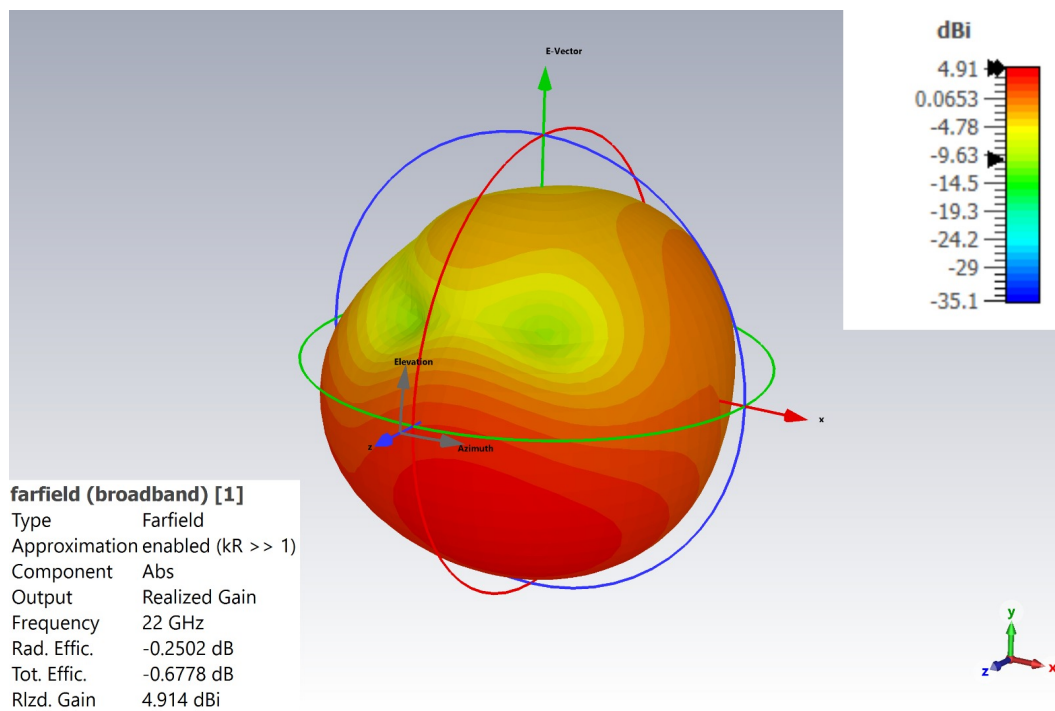
FIGURE 6.21: 3-D Radiation pattern of the proposed metasurface integrated planar antenna.

TABLE 6.3: Comparison among proposed and previously published metasurface integrated planar antennas.

| Ref. | Antenna Type | Dimensions | | Freq. Band | FBW(%) | Peak Gain |
		(mm³)	(λ³)	(GHz)		(dBi)
[138]	CP-patch with metasurface	12×12×1	1.1×1.1×0.093	24-34.1	34.7	11
[135]	MS-based MIMO antenna	30×43×6.8	2.5×3.58×0.565	24.55-26.5	7.63	10.27
[133]	MS-based MIMO antenna	24×24×3.75	2.08×2.08×0.32	23.5-29.4	22.30	7
[137]	CP-patch with 3D MS	10×14×1.83	0.95×1.33×0.183	25.3-31.6	22.14	10.4
[134]	AMC-based Bowtie Antenna	30×16×0.8	3.33×2.1×0.088	30-37	21	5.5
[136]	Mu-near-zero MS-based Patch	20×21×7.6	1.76×1.85×0.163	26-27.45	5.42	12.6
[139]	MS antenna with PRGW	13.5×13.5×0.762	1.26×1.26×0.071	24.9-31.7	24	19.2
This Work	MS-based planar antenna	8×12×4.32	0.8×1.2×0.432	23-38.8	51.13	9

of the proposed antenna are well in agreement. From the results, one can conclude that the proposed metasurface-based planar antenna can be a potential candidate for future 5G communication devices.

Chapter 7

Conclusions and Future Recommendations

7.1   Conclusions

5G communication technology will provide consumers with new and distinctive features. It will provide users with access from anywhere and allow them to select the best performance among various technologies. Optimal performance will be determined not only by throughput, but also by the most relevant metrics based on the nature of the service. For this purpose, communication devices must be completely redesigned to meet the needs of 5G technology. This requires the design and validation of next generation antennas that demonstrate properties not demonstrated in previous generation antennas. Furthermore, there is a need to design high-performance antennas that are smaller in size and efficient in performance. By optimizing the antenna design and associated configuration, the desired characteristics for a particular size can be achieved when using a planar antenna. High gain and radiation characteristics can be demonstrated with the help of reflective structures.

Therefore, a simple and compact equilateral triangle slot-loaded rectangular patch antenna for wide-band mm-wave 5G communication systems is described in the

126

first part of the dissertation. The wide-band antenna is built on a low loss substrate. A step-by-step procedure is explained with the results. By moving the location of the feed line relative to the center of the axis, better impedance matching within the operating bandwidth can be achieved and wide-band response within the mm-wave spectrum can be achieved by employing a partial ground plane. Based on the results, it was determined that the planar antenna design has a high impedance bandwidth of 16.86 GHz between 22.28 GHz and 39.14 GHz. Moreover, the maximum gain and antenna efficiency of the planar antenna design are 6.86 dBi and >85%, respectively. The designed antenna structure is simple and easy to fabricate, making it suitable for implementation in 5G communication devices.

In the second part, two-element patch antenna arrays are presented and designed for mm-wave applications. The arrays are composed of 1×2 semi-ring based patch radiators fed by standard T-junction power dividers. The lower plane of the first network is composed of a faulty ground structure. A rectangular slot is etched into the ground plane to achieve a resonant frequency of 26 GHz. Rectangular slot parameters can be adjusted to achieve the desired frequency response. On the other hand, the second design has a complete ground plane, corresponding to a perfect patch array antenna. According to the presented results, the developed arrays work well from 25.35 to 27.87 GHz (26 GHz frequency band) and 27.5 to 29.25 GHz (28 GHz frequency band), respectively. The first design has a peak gain of 8.75 dBi and antenna efficiency > 85%; the second design has a peak gain of 10.6 dBi and antenna efficiency > 90%. According to the results, the reported antenna arrays are strong contenders for use in 5G mm-wave communication devices.

The third part of the dissertation is devoted to the design of a 1×4 planar antenna array operating in the frequency range of 28 GHz. A single element of the array is designed using fractal geometry and a partially notched ground plane. In order to create the fractal geometry, a rhombus-shaped element is inserted inside a circular-shaped radiating band. The proposed antenna element has a very wide impedance bandwidth, operating from 22.28 to 33 GHz. The 1×4 antenna array is constructed using a conventional four-way feed network. According to observations and calculations, the array resonates adequately in the range of interest and

offers an impedance bandwidth of 6.4 GHz, from 22.28 to 33 GHz. In addition, the maximum gain of the array is 10.7 dBi and its radiation efficiency is 95%. Moreover, the designed array is also fabricated for validation of simulated data. It is noted that the simulated and measured results are in good agreement. It can be concluded that the proposed antenna array has the ability to be a serious contender for next-generation 5G ultra-fast communication networks.

The last section of the dissertation focuses on the design of a simple metasurface reflector-backed planar wide-band antenna suitable for use in mm-wave applications. On the front face of the antenna, there was a meandering radiating element, while the rear side of the antenna was constructed with a partial ground plane and parasitic elements. Due to the partial ground plane, the impedance bandwidth was increased and the parasitic elements were used to further increase the impedance bandwidth and to improve the matching at higher frequency bands. In this design, the influence of parasitic elements on the performance of the antenna was also taken into consideration. It was observed that the use of parasitic elements resulted in a peak gain of 7 dBi in the operating bandwidth and a wide impedance bandwidth of 16.72 GHz. In order to obtain directional radiation characteristics and to further improve the antenna gain, a metasurface array with dimensions of 3×2 was positioned behind a planar antenna. The results led to the conclusion that the metasurface reflector has the potential to achieve a maximum gain of ≈ 9 dBi in the band of interest without causing any disruptions to the impedance bandwidth. The prototype of the novel designed antenna was fabricated and measured. The simulated and measured data were found to concur with one another very closely.

7.2 Future Recommendations

The current study could be expanded into the following areas:

1. Novel antenna element and array designs for mm-wave 5G applications are described in Chapters 3 and 4. These antennas have relatively high efficiency,

but improvements are still possible. In chapter 3 the designed antenna can be realized in an array configuration for high gain applications. For this purpose, there is a need to design a broadband corporate feeding network, which can be used to design an antenna array. On the other hand for the prove of th concept, the array designed and presented in Chapter 4 can be fabricated and tested. Based on the experimental data the design parameters can be further tune to attain improved performance.

2. Circularly polarized antennas and arrays are extremely important research topics for high-gain, wide-band mm-wave applications. Either by designing an antenna with a dielectric resonator or by using SIW technology, circular polarization can be achieved. In addition, antennas and arrays must be efficient in terms of axial ratio and gain. These ideas can be integrated to enhance the established work further.

3. The low manufacturing cost and ease of installation on any surface is driving the growing demand for ink-jet printed conformal antennas. Applications involving mm-waves can benefit from this type of technology which will reduce the cost due to the inherent ease associated with ink-jet technology.

4. Recently, research interest in on-chip antennas has increased. The antenna configurations presented in this dissertation can be scaled with semiconductor technology to meet the industry demands.

5. Due to time constraints, beam steering could not be considered in this dissertation. Since this is an essential factor in the design of an antenna, it is therefore recommended that this research work can be extended to the design of an array capable of sweeping. The development of phased array antenna or lens antenna is necessary to accomplish beam steering, for example, dielectric and metasurface lenses, etc. The lenses not only provide beam direction, but also offer high gain. Thus, it would be a beneficial addition in existing works for industrial applications.

Bibliography

[1] G. Gampala and C. Reddy, "Design of millimeter wave antenna arrays for 5G cellular applications using FEKO," in *2016 IEEE/ACES International Conference on Wireless Information Technology and Systems (ICWITS) and Applied Computational Electromagnetics (ACES)*, pp. 1–2, IEEE, 2016.

[2] G. Intelligence, "Definitive data and analysis for the mobile industry," *GSMAintelligence. com*, 2016.

[3] S. S. Sahoo, M. K. Hota, and K. K. Barik, "5G network a new look into the future: Beyond all generation networks," *American Journal of Systems and Software*, vol. 2, no. 4, pp. 108–112, 2014.

[4] A. F. Molisch, *Wireless communications*, vol. 34. John Wiley & Sons, 2012.

[5] I. Sector, "Requirements related to technical performance for IMT-advanced radio interface(s)," *Report ITU*, pp. 2134–2008, 2008.

[6] I. Poole, "LTE frequency bands and spectrum allocations," *Radio-Electronics. com: Resources and analysis for electronics engineers*, 2015.

[7] S. Parkvall, E. Englund, A. Furuskär, E. Dahlman, T. Jönsson, and A. Paravati, "LTE evolution towards IMT-advanced and commercial network performance," in *2010 IEEE International Conference on Communication Systems*, pp. 151–155, IEEE, 2010.

[8] W. Hong, S.-T. Ko, Y. Lee, and K.-H. Baek, "Multi-polarized antenna array configuration for mmWave 5G mobile terminals," in *2015 International Workshop on Antenna Technology (iWAT)*, pp. 60–61, IEEE, 2015.

[9] T. Kim, I. Bang, and D. K. Sung, "Design criteria on a mm-Wave based small cell with directional antennas," in *2014 IEEE 25th Annual International Symposium on Personal, Indoor, and Mobile Radio Communication (PIMRC)*, pp. 103–107, IEEE, 2014.

[10] Y. Wang, J. Li, L. Huang, Y. Jing, A. Georgakopoulos, and P. Demestichas, "5G mobile: Spectrum broadening to higher-frequency bands to support high data rates," *IEEE Vehicular Technology Magazine*, vol. 9, no. 3, pp. 39–46, 2014.

[11] W. Roh, J.-Y. Seol, J. Park, B. Lee, J. Lee, Y. Kim, J. Cho, K. Cheun, and F. Aryanfar, "Millimeter-wave beamforming as an enabling technology for 5G cellular communications: Theoretical feasibility and prototype results," *IEEE Communications Magazine*, vol. 52, no. 2, pp. 106–113, 2014.

[12] E. Dahlman, G. Mildh, S. Parkvall, J. Peisa, J. Sachs, Y. Selén, and J. Sköld, "5G wireless access: requirements and realization," *IEEE Communications Magazine*, vol. 52, no. 12, pp. 42–47, 2014.

[13] E. Dahlman, G. Mildh, S. Parkvall, J. Peisa, J. Sachs, and Y. Selén, "5G radio access," *Ericsson review*, vol. 6, pp. 2–7, 2014.

[14] A. Osseiran, F. Boccardi, V. Braun, K. Kusume, P. Marsch, M. Maternia, O. Queseth, M. Schellmann, H. Schotten, H. Taoka, *et al.*, "Scenarios for 5G mobile and wireless communications: the vision of the metis project," *IEEE Communications Magazine*, vol. 52, no. 5, pp. 26–35, 2014.

[15] A. I. Sulyman, A. T. Nassar, M. K. Samimi, G. R. MacCartney, T. S. Rappaport, and A. Alsanie, "Radio propagation path loss models for 5g cellular networks in the 28 GHz and 38 GHz millimeter-wave bands," *IEEE Communications Magazine*, vol. 52, no. 9, pp. 78–86, 2014.

[16] R. A. Alhalabi, *High efficiency planar and RFIC-based antennas for millimeter-wave communication systems.* PhD thesis, UC San Diego, 2010.

[17] C. A. Balanis, *Antenna theory: analysis and design.* John Wiley & Sons, USA, 2015.

[18] L. Vishalkumar, K. Sandip, and S. S. Kashyap, "Design of planar microstrip patch antenna for GPS application," *European Journal of Academic Essays*, vol. 2, no. 3, pp. 32–36, 2015.

[19] N. H. M. Adnan, I. M. Rafiqul, and A. Z. Alam, "Effects of inter-element spacing and number of elements on planar array antenna characteristics," *Indonesian Journal of Electrical Engineering and Computer Science (IJEECS)*, vol. 10, no. 1, pp. 230–240, 2018.

[20] N. Meinzer, W. L. Barnes, and I. R. Hooper, "Plasmonic meta-atoms and metasurfaces," *Nature Photonics*, vol. 8, no. 12, pp. 889–898, 2014.

[21] H.-T. Chen, A. J. Taylor, and N. Yu, "A review of metasurfaces: physics and applications," *Reports on Progress in Physics*, vol. 79, no. 7, p. 076401, 2016.

[22] M. Decker, I. Staude, M. Falkner, J. Dominguez, D. N. Neshev, I. Brener, T. Pertsch, and Y. S. Kivshar, "High-efficiency dielectric Huygens' surfaces," *Advanced Optical Materials*, vol. 3, no. 6, pp. 813–820, 2015.

[23] W. Liu, S. Chen, Z. Li, H. Cheng, P. Yu, J. Li, and J. Tian, "Realization of broadband cross-polarization conversion in transmission mode in the terahertz region using a single-layer metasurface," *Optics Letters*, vol. 40, no. 13, pp. 3185–3188, 2015.

[24] N. Yu, F. Aieta, P. Genevet, M. A. Kats, Z. Gaburro, and F. Capasso, "A broadband, background-free quarter-wave plate based on plasmonic metasurfaces," *Nano Letters*, vol. 12, no. 12, pp. 6328–6333, 2012.

[25] K. Konstantinidis, A. P. Feresidis, and P. S. Hall, "Broadband subwavelength profile high-gain antennas based on multi-layer metasurfaces," *IEEE Transactions on Antennas and Propagation*, vol. 63, no. 1, pp. 423–427, 2014.

[26] Z. Wei, Y. Cao, X. Su, Z. Gong, Y. Long, and H. Li, "Highly efficient beam steering with a transparent metasurface," *Optics express*, vol. 21, no. 9, pp. 10739–10745, 2013.

[27] P.-C. Li and E. T. Yu, "Flexible, low-loss, large-area, wide-angle, wavelength-selective plasmonic multilayer metasurface," *Journal of Applied Physics*, vol. 114, no. 13, p. 133104, 2013.

[28] Y. Liu and X. Zhang, "Metamaterials: a new frontier of science and technology," *Chemical Society Reviews*, vol. 40, no. 5, pp. 2494–2507, 2011.

[29] C. R. Simovski, "On electromagnetic characterization and homogenization of nanostructured metamaterials," *Journal of Optics*, vol. 13, no. 1, p. 013001, 2010.

[30] E. F. Kuester, M. A. Mohamed, M. Piket-May, and C. L. Holloway, "Averaged transition conditions for electromagnetic fields at a metafilm," *IEEE Transactions on Antennas and Propagation*, vol. 51, no. 10, pp. 2641–2651, 2003.

[31] Y. Zhao, N. Engheta, and A. Alù, "Homogenization of plasmonic metasurfaces modeled as transmission-line loads," *Metamaterials*, vol. 5, no. 2-3, pp. 90–96, 2011.

[32] G. Valerio, Z. Sipus, A. Grbic, and O. Quevedo-Teruel, "Accurate equivalent-circuit descriptions of thin glide-symmetric corrugated metasurfaces," *IEEE Transactions on Antennas and Propagation*, vol. 65, no. 5, pp. 2695–2700, 2017.

[33] D. L. Sounas, T. Kodera, and C. Caloz, "Electromagnetic modeling of a magnetless nonreciprocal gyrotropic metasurface," *IEEE Transactions on Antennas and Propagation*, vol. 61, no. 1, pp. 221–231, 2012.

[34] S. Sun, K.-Y. Yang, C.-M. Wang, T.-K. Juan, W. T. Chen, C. Y. Liao, Q. He, S. Xiao, W.-T. Kung, G.-Y. Guo, *et al.*, "High-efficiency broadband anomalous reflection by gradient meta-surfaces," *Nano Letters*, vol. 12, no. 12, pp. 6223–6229, 2012.

[35] N. Yu, P. Genevet, M. A. Kats, F. Aieta, J.-P. Tetienne, F. Capasso, and Z. Gaburro, "Light propagation with phase discontinuities: generalized laws of reflection and refraction," *Science*, vol. 334, no. 6054, pp. 333–337, 2011.

[36] C. Pfeiffer, N. K. Emani, A. M. Shaltout, A. Boltasseva, V. M. Shalaev, and A. Grbic, "Efficient light bending with isotropic metamaterial Huygens' surfaces," *Nano Letters*, vol. 14, no. 5, pp. 2491–2497, 2014.

[37] F. Monticone, N. M. Estakhri, and A. Alu, "Full control of nanoscale optical transmission with a composite metascreen," *Physical Review Letters*, vol. 110, no. 20, p. 203903, 2013.

[38] H. Cheng, S. Chen, P. Yu, W. Liu, Z. Li, J. Li, B. Xie, and J. Tian, "Dynamically tunable broadband infrared anomalous refraction based on graphene metasurfaces," *Advanced Optical Materials*, vol. 3, no. 12, pp. 1744–1749, 2015.

[39] A. Belardini, F. Pannone, G. Leahu, M. Larciprete, M. Centini, C. Sibilia, C. Martella, M. Giordano, D. Chiappe, and F. B. de Mongeot, "Asymmetric transmission and anomalous refraction in metal nanowires metasurface," *Journal of the European Optical Society-Rapid Publications*, vol. 7, 2012.

[40] N. Ojaroudiparchin, M. Shen, G. Fr, *et al.*, "Multi-layer 5G mobile phone antenna for multi-user MIMO communications," in *2015 23rd Telecommunications Forum Telfor (TELFOR)*, pp. 559–562, IEEE, 2015.

[41] M. R. Prabhu, J. Arunkumar, A. Rajalingam, and R. Anusuya, "A modified square patch antenna with rhombus slot for high bandwidth," *International Journal of Innovative Technology and Exploring Engineering (IJITEE) ISSN*, pp. 2278–3075, 2019.

[42] B. A. Rahman and S. O. Hasan, "Simulation design of low-profile equilateral triangle microstrip patch antenna operating at 28 ghz," 2022.

[43] O. Darboe, D. B. O. Konditi, and F. Manene, "A 28 ghz rectangular microstrip patch antenna for 5g applications," *International Journal of Engineering Research and Technology*, vol. 12, no. 6, pp. 854–857, 2019.

[44] S.-E. Didi, I. Halkhams, M. Fattah, Y. Balboul, S. Mazer, and M. El Bekkali, "Design of a microstrip antenna patch with a rectangular slot for 5g applications operating at 28 ghz," *TELKOMNIKA (Telecommunication Computing Electronics and Control)*, vol. 20, no. 3, pp. 527–536, 2022.

[45] H. Wang, K. E. Kedze, and I. Park, "A high-gain and wideband series-fed angled printed dipole array antenna," *IEEE Transactions on Antennas and Propagation*, vol. 68, no. 7, pp. 5708–5713, 2020.

[46] L. Malviya and P. Gupta, "Millimeter wave high-gain antenna array for wireless applications," *IETE Journal of Research*, pp. 1–10, 2021.

[47] Y. Q. Guo, Y. M. Pan, and S. Y. Zheng, "Design of series-fed, single-layer, and wideband millimeter-wave microstrip arrays," *IEEE Transactions on Antennas and Propagation*, vol. 68, no. 10, pp. 7017–7026, 2020.

[48] U. Ullah, M. Al-Hasan, S. Koziel, and I. B. Mabrouk, "A series inclined slot-fed circularly polarized antenna for 5G 28 GHz applications," *IEEE Antennas and Wireless Propagation Letters*, vol. 20, no. 3, pp. 351–355, 2021.

[49] Y. Kang, E. Noh, and K. Kim, "Design of traveling-wave series-fed microstrip array with a low sidelobe level," *IEEE Antennas and Wireless Propagation Letters*, vol. 19, no. 8, pp. 1395–1399, 2020.

[50] C.-P. Chao, S.-H. Yang, C.-M. Tung, C.-F. Yang, W.-H. Lin, C.-Y. Chai, and I. Lin, "A series-fed cavity-back patch array antenna for a miniaturized

77 GHz radar module," in *2019 IEEE International Symposium on Antennas and Propagation and USNC-URSI Radio Science Meeting*, pp. 657–658, IEEE, 2019.

[51] L. Li and J.-B. Yan, "A low-cost and efficient microstrip-fed air-substrate-integrated waveguide slot array," *Electronics*, vol. 10, no. 3, p. 338, 2021.

[52] M. I. Khattak, A. Sohail, U. Khan, Z. Barki, and G. Witjaksono, "Elliptical slot circular patch antenna array with dual band behaviour for future 5G mobile communication networks," *Progress In Electromagnetics Research C*, vol. 89, pp. 133–147, 2019.

[53] M. Khalily, R. Tafazolli, T. Rahman, and M. Kamarudin, "Design of phased arrays of series-fed patch antennas with reduced number of the controllers for 28-GHz mm-wave applications," *IEEE Antennas and wireless propagation letters*, vol. 15, pp. 1305–1308, 2015.

[54] A. M. A. Najafabadi, F. A. Ghani, and I. Tekin, "Low-cost multibeam millimeter-wave array antennas for 5G mobile applications," *IEEE Transactions on Vehicular Technology*, 2022.

[55] H. Ullah and F. A. Tahir, "A broadband wire hexagon antenna array for future 5G communications in 28 GHz band," *Microwave and Optical Technology Letters*, vol. 61, no. 3, pp. 696–701, 2019.

[56] H. Ullah and F. A. Tahir, "Broadband planar antenna array for future 5G communication standards," *IET Microwaves, Antennas & Propagation*, vol. 13, no. 15, pp. 2661–2668, 2019.

[57] H. Ullah and F. A. Tahir, "A wide-band rhombus monopole antenna array for millimeter wave applications," *Microwave and Optical Technology Letters*, vol. 62, no. 5, pp. 2111–2117, 2020.

[58] R. Ullah, S. Ullah, F. Faisal, R. Ullah, D.-y. Choi, A. Ahmad, and B. Kamal, "High-gain Vivaldi antenna with wide bandwidth characteristics for 5G

mobile and Ku-band radar applications," *Electronics*, vol. 10, no. 6, p. 667, 2021.

[59] H. Ullah and F. A. Tahir, "A novel snowflake fractal antenna for dual-beam applications in 28 GHz band," *IEEE Access*, vol. 8, pp. 19873–19879, 2020.

[60] M. M. Kamal, S. Yang, S. H. Kiani, D. A. Sehrai, M. Alibakhshikenari, M. Abdullah, F. Falcone, E. Limiti, and M. Munir, "A novel hook-shaped antenna operating at 28 GHz for future 5G mmwave applications," *Electronics*, vol. 10, no. 6, p. 673, 2021.

[61] M. M. Kamal, S. Yang, S. H. Kiani, M. R. Anjum, M. Alibakhshikenari, Z. A. Arain, A. A. Jamali, A. Lalbakhsh, and E. Limiti, "Donut-shaped mmWave printed antenna array for 5G technology," *Electronics*, vol. 10, no. 12, p. 1415, 2021.

[62] S. H. Kiani, X. C. Ren, A. Bashir, A. Rafiq, M. R. Anjum, M. M. Kamal, B. U. Din, and F. Muhammad, "Square-framed T shape mmwave antenna array at 28 GHz for future 5G devices," *International Journal of Antennas and Propagation*, vol. 2021, pp. 1–9, 2021.

[63] C.-X. Mao, M. Khalily, P. Xiao, T. W. Brown, and S. Gao, "Planar sub-millimeter-wave array antenna with enhanced gain and reduced sidelobes for 5G broadcast applications," *IEEE Transactions on Antennas and Propagation*, vol. 67, no. 1, pp. 160–168, 2018.

[64] M. E. Munir, A. G. Al Harbi, S. H. Kiani, M. Marey, N. O. Parchin, J. Khan, H. Mostafa, J. Iqbal, M. A. Khan, C. H. See, *et al.*, "A new mm-Wave antenna array with wideband characteristics for next generation communication systems," *Electronics*, vol. 11, no. 10, p. 1560, 2022.

[65] J. Xu, W. Hong, Z. H. Jiang, H. Zhang, and K. Wu, "Low-profile wideband vertically folded slotted circular patch array for Ka-band applications," *IEEE Transactions on Antennas and Propagation*, vol. 68, no. 9, pp. 6844–6849, 2020.

[66] D. Liu and R. Sirdeshmukh, "A patch array antenna for 60 GHz package applications," in *2008 IEEE Antennas and Propagation Society International Symposium*, pp. 1–4, IEEE, 2008.

[67] T. S. Mneesy, R. K. Hamad, A. I. Zaki, and W. A. Ali, "A novel high gain monopole antenna array for 60 GHz millimeter-wave communications," *Applied Sciences*, vol. 10, no. 13, p. 4546, 2020.

[68] J. Jiang and B. Feng, "Chinese-characters Jin-shaped patch antenna array for 5G millimeter wave communications," in *2021 Cross Strait Radio Science and Wireless Technology Conference (CSRSWTC)*, pp. 251–253, IEEE, 2021.

[69] Y.-J. Kim, Y.-B. Kim, and H. L. Lee, "mmWave high gain planar H-shaped shorted ring antenna array," *Sensors*, vol. 20, no. 18, p. 5168, 2020.

[70] B. Hammu-Mohamed, Á. Palomares-Caballero, C. Segura-Gómez, F. G. Ruiz, and P. Padilla, "SIW cavity-backed antenna array based on double slots for mmWave communications," *Applied Sciences*, vol. 11, no. 11, p. 4824, 2021.

[71] S. Zhu, H. Liu, Z. Chen, and P. Wen, "A compact gain-enhanced vivaldi antenna array with suppressed mutual coupling for 5G mmwave application," *IEEE Antennas and Wireless Propagation Letters*, vol. 17, no. 5, pp. 776–779, 2018.

[72] P. Ramanujam, M. Ponnusamy, and K. Ramanujam, "A compact wide-bandwidth antipodal vivaldi antenna array with suppressed mutual coupling for 5G mm-wave applications," *AEU-International Journal of Electronics and Communications*, vol. 133, p. 153668, 2021.

[73] A. S. Dixit, S. Kumar, S. Urooj, and A. Malibari, "A highly compact antipodal Vivaldi antenna array for 5G millimeter wave applications," *Sensors*, vol. 21, no. 7, p. 2360, 2021.

[74] H. Ullah and F. A. Tahir, "A high gain and wideband narrow-beam antenna for 5G millimeter-wave applications," *IEEE Access*, vol. 8, pp. 29430–29434, 2020.

[75] B. T. Mohamed and H. Ammor, "A 16-elements corporate-series feed rectangular patch antenna array at 28 GHz for future 5G applications," in *2019 International Conference on Wireless Technologies, Embedded and Intelligent Systems (WITS)*, pp. 1–4, IEEE, 2019.

[76] V. Harini, M. Sairam, and R. Madhu, "16-element CPW series fed millimeter-wave hexagonal array antenna for 5G femtocell applications," *International Journal of Microwave and Wireless Technologies*, vol. 14, no. 8, pp. 955–969, 2022.

[77] Z. Wang and Z. Huang, "A microwave/millimeter wave dual-band shared aperture patch antenna array," *IEEE Access*, vol. 8, pp. 218585–218591, 2020.

[78] H. Jin, G. Q. Luo, W. Wang, W. Che, and K.-S. Chin, "Integration design of millimeter-wave filtering patch antenna array with SIW four-way anti-phase filtering power divider," *IEEE Access*, vol. 7, pp. 49804–49812, 2019.

[79] J. P. Gianvittorio and Y. Rahmat-Samii, "Fractal antennas: A novel antenna miniaturization technique, and applications," *IEEE Antennas and Propagation Magazine*, vol. 44, no. 1, pp. 20–36, 2002.

[80] L. Lizzi, F. Viani, E. Zeni, and A. Massa, "A DVBH/GSM/UMTS planar antenna for multimode wireless devices," *IEEE Antennas and Wireless Propagation Letters*, vol. 8, pp. 568–571, 2009.

[81] D. D. Krishna, M. Gopikrishna, C. Aanandan, P. Mohanan, and K. Vasudevan, "Compact wideband Koch fractal printed slot antenna," *IET Microwaves, Antennas & Propagation*, vol. 3, no. 5, pp. 782–789, 2009.

[82] R. Azaro, F. Viani, L. Lizzi, E. Zeni, and A. Massa, "A monopolar quad-band antenna based on a Hilbert self-affine prefractal geometry," *IEEE Antennas and Wireless Propagation Letters*, vol. 8, pp. 177–180, 2009.

[83] C. Puente-Baliarda, J. Romeu, R. Pous, and A. Cardama, "On the behavior of the Sierpinski multiband fractal antenna," *IEEE Transactions on Antennas and Propagation*, vol. 46, no. 4, pp. 517–524, 1998.

[84] H. Orazi and H. Soleimani, "Miniaturisation of the triangular patch antenna by the novel dual-reverse-arrow fractal," *IET Microwaves, Antennas & Propagation*, vol. 9, no. 7, pp. 627–633, 2014.

[85] A. Farswan, A. K. Gautam, B. K. Kanaujia, and K. Rambabu, "Design of Koch fractal circularly polarized antenna for handheld UHF RFID reader applications," *IEEE Transactions on Antennas and Propagation*, vol. 64, no. 2, pp. 771–775, 2015.

[86] C. Caloz and T. Itoh, *Electromagnetic metamaterials: transmission line theory and microwave applications.* John Wiley & Sons, 2005.

[87] R. Marqués, F. Martin, and M. Sorolla, *Metamaterials with negative parameters: theory, design, and microwave applications*, vol. 183. John Wiley & Sons, 2011.

[88] L.-M. Si, W. Zhu, and H.-J. Sun, "A compact, planar, and CPW-fed metamaterial-inspired dual-band antenna," *IEEE Antennas and Wireless Propagation Letters*, vol. 12, pp. 305–308, 2013.

[89] W. Wahba, M. A. Abdalla, A. A. N. Mohamed, and A. Allam, "A uniplanar microstrip CSRR metamaterial antenna," in *2014 IEEE Antennas and Propagation Society International Symposium (APSURSI)*, pp. 545–546, IEEE, 2014.

[90] M. Islam, M. T. Islam, M. Samsuzzaman, and M. R. I. Faruque, "Compact metamaterial antenna for UWB applications," *Electronics Letters*, vol. 51, no. 16, pp. 1222–1224, 2015.

[91] M. Islam, M. Samsuzzaman, M. Islam, and S. Kibria, "Experimental breast phantom imaging with metamaterial-inspired nine-antenna sensor array," *Sensors*, vol. 18, no. 12, pp. 1–19, 2018.

[92] G. Breed, "An introduction to defected ground structures in microstrip circuits," *High Frequency Electronics*, vol. 7, pp. 50–54, 2008.

[93] L. H. Weng, Y.-C. Guo, X.-W. Shi, and X.-Q. Chen, "An overview on defected ground structure," *Progress In Electromagnetics Research*, vol. 7, pp. 173–189, 2008.

[94] B. A. Munk, *Frequency selective surfaces: theory and design.* John Wiley & Sons, 2005.

[95] A. Pirhadi, H. Bahrami, and J. Nasri, "Wideband high directive aperture coupled microstrip antenna design by using a FSS superstrate layer," *IEEE Transactions on Antennas and Propagation*, vol. 60, no. 4, pp. 2101–2106, 2012.

[96] A. Hosseini, F. Capolino, and F. De Flaviis, "Gain enhancement of a V-band antenna using a Fabry-Pérot cavity with a self-sustained all-metal cap with FSS," *IEEE Transactions on Antennas and Propagation*, vol. 63, no. 3, pp. 909–921, 2014.

[97] Z. Chen and Y. P. Zhang, "FR4 PCB grid array antenna for millimeter-wave 5G mobile communications," in *2013 IEEE MTT-S International Microwave Workshop Series on RF and Wireless Technologies for Biomedical and Healthcare Applications (IMWS-BIO)*, pp. 1–3, IEEE, 2013.

[98] P. Cabrol and P. Pietraski, "60 GHz patch antenna array on low cost liquid-crystal polymer (LCP) substrate," in *2014 IEEE Long Island Systems, Applications and Technology Conference (LISAT)*, pp. 1–6, IEEE, 2014.

[99] N. Ashraf, H. Vettikalladi, and M. A. Alkanhal, "A DR loaded substrate integrated waveguide antenna for 60 GHz high speed wireless communication

systems," *International Journal of Antennas and Propagation*, vol. 2014, 2014.

[100] W. Hong, K. Baek, Y. Lee, and Y. G. Kim, "Design and analysis of a low-profile 28 GHz beam steering antenna solution for future 5G cellular applications," in *2014 IEEE MTT-S International Microwave Symposium (IMS)*, pp. 1–4, IEEE, 2014.

[101] O. M. Haraz, A. Elboushi, S. A. Alshebeili, and A.-R. Sebak, "Dense dielectric patch array antenna with improved radiation characteristics using EBG ground structure and dielectric superstrate for future 5G cellular networks," *IEEE Access*, vol. 2, pp. 909–913, 2014.

[102] S. I. Orakwue, R. Ngah, T. Rahman, and H. M. Al-Khafaji, "A steerable 28 GHz array antenna using branch line coupler," in *2015 1st International Conference on Telematics and Future Generation Networks (TAFGEN)*, pp. 76–78, IEEE, 2015.

[103] I. Maina, T. A. Rahman, and M. Khalily, "Bandwidth enhanced and sidelobes level reduced radial line slot array antenna at 28 GHz for 5G next generation mobile communication," *ARPN Journal of Engineering and Applied Sciences*, vol. 10, pp. 5752–5757, 2015.

[104] W. Zhai, V. Miraftab, and M. Repeta, "Broadband antenna array with low cost PCB substrate for 5G millimeter wave applications," in *2015 Global Symposium on Millimeter Waves (GSMM)*, pp. 1–3, IEEE, 2015.

[105] O. Haraz, M. M. M. Ali, A. Elboushi, and A.-R. Sebak, "Four-element dual-band printed slot antenna array for the future 5G mobile communication networks," in *2015 IEEE International Symposium on Antennas and Propagation & USNC/URSI National Radio Science Meeting*, pp. 1–2, IEEE, 2015.

[106] O. M. Haraz, M. M. Ashraf, and S. Alshebili, "8× 8 patch antenna array with polarization and space diversity for future 5G cellular applications," in *2015*

International Conference on Information and Communication Technology Research (ICTRC), pp. 258–261, IEEE, 2015.

[107] M. Khalily, R. Tafazolli, T. Rahman, and M. Kamarudin, "Design of phased arrays of series-fed patch antennas with reduced number of the controllers for 28-GHz mm-wave applications," *IEEE Antennas and Wireless Propagation Letters*, vol. 15, pp. 1305–1308, 2016.

[108] S. F. Jilani and A. Alomainy, "A multiband millimeter-wave 2-D array based on enhanced Franklin antenna for 5G wireless systems," *IEEE Antennas and Wireless Propagation Letters*, vol. 16, pp. 2983–2986, 2017.

[109] M. Khalily, R. Tafazolli, P. Xiao, and A. A. Kishk, "Broadband mm-Wave microstrip array antenna with improved radiation characteristics for different 5G applications," 2018.

[110] Y. Niu, Y. Li, D. Jin, L. Su, and A. V. Vasilakos, "A survey of millimeter wave communications (mmWave) for 5G: opportunities and challenges," *Wireless Networks*, vol. 21, no. 8, pp. 2657–2676, 2015.

[111] T. S. Rappaport, S. Sun, R. Mayzus, H. Zhao, Y. Azar, K. Wang, G. N. Wong, J. K. Schulz, M. Samimi, and F. Gutierrez, "Millimeter wave mobile communications for 5G cellular: It will work!," *IEEE Access*, vol. 1, pp. 335–349, 2013.

[112] P. N. Choubey, W. Hong, Z.-C. Hao, P. Chen, T.-V. Duong, and J. Mei, "A wideband dual-mode SIW cavity-backed triangular-complimentary-split-ring-slot (TCSRS) antenna," *IEEE Transactions on Antennas and Propagation*, vol. 64, no. 6, pp. 2541–2545, 2016.

[113] Z. U. Khan, Q. H. Abbasi, A. Belenguer, T. H. Loh, and A. Alomainy, "Empty substrate integrated waveguide slot antenna array for 5G applications," in *2018 IEEE MTT-S International Microwave Workshop Series on 5G Hardware and System Technologies (IMWS-5G)*, pp. 1–3, IEEE, 2018.

[114] D. A. Sehrai, M. Abdullah, A. Altaf, S. H. Kiani, F. Muhammad, M. Tufail, M. Irfan, A. Glowacz, and S. Rahman, "A novel high gain wideband MIMO antenna for 5G millimeter wave applications," *Electronics*, vol. 9, no. 6, p. 1031, 2020.

[115] A. R. Sabek, A. A. Ibrahim, and W. A. Ali, "Dual-band millimeter wave microstrip patch antenna with stubresonators for 28/38 ghz applications," in *Journal of Physics: Conference Series*, vol. 2128, p. 012006, IOP Publishing, 2021.

[116] H. M. Marzouk, M. I. Ahmed, and A. H. A. Shaalan, "Novel dual-band 28/38 ghz mimo antennas for 5g mobile applications," *Progress In Electromagnetics Research C*, vol. 93, pp. 103–117, 2019.

[117] V. G. Prachi and S. Vijay, "A novel design of compact 28 ghz printed wideband antenna for 5g applications," *International Journal of Innovative Technology and Exploring Engineering (IJITEE)*, vol. 9, no. 3, pp. 3696–3700, 2020.

[118] M. Rinne and O. Tirkkonen, "LTE, the radio technology path towards 4G," *Computer Communications*, vol. 33, no. 16, pp. 1894–1906, 2010.

[119] C. Zhang, S. L. Ariyavisitakul, and M. Tao, "LTE-advanced and 4G wireless communications [Guest Editorial]," *IEEE Communications Magazine*, vol. 50, no. 2, pp. 102–103, 2012.

[120] J. Thompson, X. Ge, H.-C. Wu, R. Irmer, H. Jiang, G. Fettweis, and S. Alamouti, "5G wireless communication systems: Prospects and challenges [Guest Editorial]," *IEEE Communications Magazine*, vol. 52, no. 2, pp. 62–64, 2014.

[121] C.-X. Wang, F. Haider, X. Gao, X.-H. You, Y. Yang, D. Yuan, H. M. Aggoune, H. Haas, S. Fletcher, and E. Hepsaydir, "Cellular architecture and key technologies for 5G wireless communication networks," *IEEE Communications Magazine*, vol. 52, no. 2, pp. 122–130, 2014.

[122] Z. Pi and F. Khan, "An introduction to millimeter-wave mobile broadband systems," *IEEE Communications Magazine*, vol. 49, no. 6, pp. 101–107, 2011.

[123] Z. Qingling and J. Li, "Rain attenuation in millimeter wave ranges," in *2006 7th International Symposium on Antennas, Propagation & EM Theory*, pp. 1–4, IEEE, 2006.

[124] S.-E. Didi, I. Halkhams, A. Es-Saqy, M. Fattah, and Y. Balboul, "New microstrip patch antenna array design at 28 ghz millimeter-wave for fifth-generation application," *Int. J. Electr. Comput. Eng*, vol. 13, no. 4, p. 4184, 2023.

[125] G. Kumar and K. P. Ray, *Broadband microstrip antennas*. Artech House, 2003.

[126] S. H. Kiani, A. G. Alharbi, S. Khan, M. Marey, H. Mostafa, and M. A. Khan, "Wideband three loop element antenna array for future 5g mmwave devices," *IEEE Access*, vol. 10, pp. 22472–22479, 2022.

[127] W. J. Krzysztofik and T. N. Cao, "Metamaterials in application to improve antenna parameters," *Metamaterials and Metasurfaces*, 2018.

[128] D. Sievenpiper, L. Zhang, R. Broas, N. Alexopolous, and E. Yablonovitch, "High-impedance electromagnetic surfaces with a forbidden frequency band," *IEEE Transactions on Microwave Theory and Techniques*, vol. 47, no. 11, pp. 2059–2074, 1999.

[129] I. Hossain, M. T. Islam, H. Alsaif, A. G. Alharbi, N. B. M. Sahar, and M. Samsuzzaman, "An angular stable triple-band anisotropic cross-polarization conversion metasurface," *Results in Physics*, vol. 37, p. 105564, 2022.

[130] P. Das and K. Mandal, "Modelling of ultra-wide stop-band frequency-selective surface to enhance the gain of a UWB antenna," *IET Microwaves, Antennas & Propagation*, vol. 13, no. 3, pp. 269–277, 2019.

[131] Y. Yuan, X. Xi, and Y. Zhao, "Compact UWB FSS reflector for antenna gain enhancement," *IET Microwaves, Antennas & Propagation*, vol. 13, no. 10, pp. 1749–1755, 2019.

[132] H. Zahra, M. Hussain, S. I. Naqvi, S. M. Abbas, and S. Mukhopadhyay, "A simple monopole antenna with a switchable beam for 5G millimeter-wave communication systems," *Electronics*, vol. 10, no. 22, p. 2870, 2021.

[133] D. A. Sehrai, M. Asif, W. A. Shah, J. Khan, I. Ullah, M. Ibrar, S. Jan, M. Alibakhshikenari, F. Falcone, and E. Limiti, "Metasurface-based wideband MIMO antenna for 5G millimeter-wave systems," *IEEE Access*, vol. 9, pp. 125348–125357, 2021.

[134] A. A. Althuwayb, "MTM- and SIW-inspired bowtie antenna loaded with AMC for 5G mm-wave applications," *International Journal of Antennas and Propagation*, vol. 2021, 2021.

[135] S. Tariq, S. I. Naqvi, N. Hussain, and Y. Amin, "A metasurface-based MIMO antenna for 5G millimeter-wave applications," *IEEE Access*, vol. 9, pp. 51805–51817, 2021.

[136] I. H. Abdelaziem, A. A. Ibrahim, and M. A. Abdalla, "A high gain antenna utilizing Mu-near-zero metasurface structures for 5G applications," *International Journal of Microwave and Wireless Technologies*, pp. 1–9, 2022.

[137] B. Ferreira-Gomes, O. N. Oliveira Jr, and J. R. Mejía-Salazar, "Chiral dielectric metasurfaces for highly integrated, broadband circularly polarized antenna," *Sensors*, vol. 21, no. 6, p. 2071, 2021.

[138] N. Hussain, M.-J. Jeong, A. Abbas, T.-J. Kim, and N. Kim, "A metasurface-based low-profile wideband circularly polarized patch antenna for 5G millimeter-wave systems," *IEEE Access*, vol. 8, pp. 22127–22135, 2020.

[139] H. Yi, Y. Mu, J. Han, and L. Li, "Broadband millimeter-wave metasurface antenna array with printed ridge gap waveguide for high front-to-back ratio," *Journal of Information and Intelligence*, 2022.